Universidade Federal de Juiz de Fora

Instituto de Ciências Biológicas

Programa de Pós-Graduação em Biodiversidade e Conservação da Natureza

Spatial and seasonal variability of diffusive carbon flux in contrasting reservoirs: magnitudes and contribution of the aquatic surface and exposed sediment

(*Variabilidade espacial e sazonal dos fluxos difusivos de carbono em reservatórios contrastantes: magnitudes e contribuição da superfície aquática e do sedimento exposto*)

José Reinaldo Paranaíba Vilela Alves Teixeira

Tese apresentada ao Programa de Pós-Graduação em Biodiversidade e Conservação da Natureza do Instituto de Ciências Biológicas da Universidade Federal de Juiz de Fora, como parte dos requisitos para a obtenção do título de Doutor em Comportamento, Ecologia e Sistemática.

Orientador: Nathan O. Barros

Juiz de Fora – Minas Gerais

2021

Universidade Federal de Juiz de Fora

Instituto de Ciências Biológicas

Programa de Pós-Graduação em Biodiversidade e Conservação da Natureza

Spatial and seasonal variability of diffusive carbon flux in contrasting reservoirs: magnitudes and contribution of the aquatic surface and exposed sediment

(*Variabilidade espacial e sazonal dos fluxos difusivos de carbono em reservatórios contrastantes: magnitudes e contribuição da superfície aquática e do sedimento exposto*)

José Reinaldo Paranaíba Vilela Alves Teixeira

Tese apresentada ao Programa de Pós-Graduação em Biodiversidade e Conservação da Natureza do Instituto de Ciências Biológicas da Universidade Federal de Juiz de Fora, como parte dos requisitos para a obtenção do título de Doutor em Comportamento, Ecologia e Sistemática.

Tese defendida em _____ de _____ de 2021

Banca examinadora:

_____

Dr. Pedro Maia Barbosa

_____

Prof. Dr. Alex Enrich-Prast

_____

Profa. Dra. Simone Jaqueline Cardoso

_____

Prof. Dr. André Megali Amado

FICHA CATALOGRÁFICA

Ficha catalográfica elaborada através do programa de geração
automática da Biblioteca Universitária da UFJF,
com os dados fornecidos pelo(a) autor(a)

Paranaíba Vilela Alves Teixeira, José Reinaldo .
Spatial and seasonal variability of diffusive carbon flux in contrasting reservoirs: magnitudes and contribution of the aquatic surface and exposed sediment : variabilidade espacial e sazonal dos fluxos difusivos de carbono em reservatórios contrastantes: magnitudes e contribuição da superfície aquática e do sedimento exposto / José Reinaldo Paranaíba Vilela Alves Teixeira. -- 2021.
228 p. : il.

Orientador: Nathan Oliveira Barros
Coorientador: Sebastian Sobek
Tese (doutorado) - Universidade Federal de Juiz de Fora, Instituto de Ciências Biológicas. Programa de Pós-Graduação em Ecologia, 2021.

1. Biogeoquímica. 2. Reservatórios. 3. Gases de Efeito Estufa. I. Oliveira Barros, Nathan , orient. II. Sobek, Sebastian, coorient. III. Título.

Orientador:

Dr. Nathan O. Barros

Co-orientador:

Dr. Sebastian Sobek

Que a humanidade acorde todos os

dias em busca de um planeta melhor

Dedico esta tese aos meus

pais, familiares, e amigos

Agradecimentos

Obrigado aos meus pais Israel e Maria José. A conquista de hoje é reflexo do passado, do carinho, da preocupação, e do amor que continuo a receber desde o dia em que nasci. Aos meus irmãos Adriana e Aislan que foram, são, e serão meus mestres na arte de viver a vida, sempre com uma pitada de adrenalina, mas também de respeito. Muito obrigado família, tios e tias, primos e primas!

Muito obrigado Nathan! Por ter me oferecido a grande oportunidade de me juntar a você e ao LEA no início de 2015. O profissional que eu me sinto hoje é graças a você que muito me ensinou como funciona esse jogo chamado ciência. Muito obrigado por acreditar em mim, por todas as outras oportunidades que surgiram durante estes últimos anos, e por sempre incentivar o meu aprimoramento.

Gratidão aos meus grandes amigos e amigas, Carlos Henrique (Caique), Diego Raymundo, Ícaro Barbosa, Iollanda Ivanov, Jéssica Vilas-Boas, Marcos Flávio, Mariella Amadeu, e Werner Vieira.

Gratidão também ao grupo LEA! Obrigado a todos pelos momentos de convivência e troca de aprendizagens. Obrigado Fábio Roland, Gladson Marques, Ingrid Campos, Ive Muzitano, Layla Fonseca, Emília Brovini, Jonas, Nathalia Resende, Natália Mendonça, Vitor, Joyce, Patrícia, Wesley, Sheila, Laís, Lucas, Anelise, Gabriela, Lígia, Ana Luiza, Thaiane, e Suênia.

Muito obrigado André Megali, Rafael Almeida, Raquel Mendonça e Simone Cardoso pelos ensinamentos, apoio, oportunidades, e por sempre estarem disponíveis quando precisei. Muito do que sei e sou hoje eu devo a vocês.

I especial thanks to Sebastian and Anna Sobek. You will undoubtedly be in my memories for everything you have done for me over the past few years, especially the year I lived in Sweden. This period was the turning point not only in my professional life but also in my personal life. I hope you know that in Brazil you have a big fan!

Thank you very much Sarian Kosten, for being involved and contributing significantly to my research. I learned a lot from you, and your teachings will always be with me, wherever I am.

Thank you very much Annika Linkhorst. You are a great friend that Limnology gave me. With you I had great moments of learning and fun. Thank you very much for everything you did for me during my time in Sweden. Sharing the office with you was fundamental for my well-being and professional improvement.

Muito obrigado Gabrielle Quadra! Ter você ao meu lado só me trouxe felicidades, sucessos, e aprendizados. Você, todos os dias, me ensina a viver a vida de forma única, e me inspira a ser uma pessoa cada vez melhor. Muito obrigado também por me apresentar e me permitir cuidar daquele que hoje considero como um filho – Leprechaun!

Agradeço a equipe do Programa de Pós-Graduação em Biodiversidade e Conservação da Natureza, Priscila e Rosi. Muito obrigado por todo suporte de excelência que me foi oferecido durantes estes últimos anos.

Muito obrigado aos professores Pedro Maia Barbosa, Alex Enrich-Prast, Simone Jaqueline Cardoso, e André Megali Amado, por aceitarem o convite para participar da banca de defesa da presente tese. Tenho certeza que seus esforços serão de grande valor para o aprimoramento da mesma.

Muito obrigado a CAPES pela bolsa de estudos concedida durante estes 4 anos de estudos. Este apoio foi peça chave para a conclusão da presente tese.

List of symbols and abbreviations

< – Lower

> – Higher

°C – degree Celsius

µg – micrograms

µS – MicroSiemens

AIC – Akaike Information Criterion

Al – Aluminum

atm – atmosphere or atmospheric

BOD – Biological Oxygen Demand

C – Carbon

C_2H_2 – Acetylene

CAPES – Coordenação de Aperfeiçoamento de Pessoal de Nível Superior

Cd – Cadmium

CDU – Chapéu D'Úvas

C_{eq} – theoretical atmospheric gas concentration

CH_4 – Methane

cm – centimeter

CNPq – Conselho Nacional de Desenvolvimento Científico e Tecnológico

CO_2 – Carbon dioxide

CO_2-eq – Carbon dioxide equivalent

CUN – Curuá-Una

C_w – dissolved gas concentration

d – day

df – degree of freedom

DNA – Deoxyribonucleic acid

FAO – Food and Agriculture Organization

FAPEMIG – Fundação de Amparo a Pesquisa de Minas Gerais

FC – Floating Chamber

Fe – Iron

F_g – Flux of a gas

FNS – Furnas

FUN – Funil

g – gram

GHG – Greenhouse Gas

GLMM – Generalized Linear Mixed Models

GPS – Global Positioning System

GWP – Global Warming Potential

h – hour

HNO_3 – Nitric acid

Hz – Hertz

IDW – Inverse Distance Weighting

INCT – Instituto Nacional de Ciência e Tecnologia

INMET – Instituto Nacional de Meteorologia

IRGA – Infra-red Gas Analyzer

K – Kelvin

k and k_{FC} – gas exchange velocity

km – kilometer

L – Liter

LD – Limit of Detection

m – meter

m.a.s.l. – meters above the sea level

MCMC – Markov Chain Monte Carlo

mg – milligram

min – minutes

mL – milliliter

mm – millimeter

mmol – millimols

Mn – Manganese

N – Nitrogen

N_2O – Nitrous oxide

NIASSA – Núcleo de Integração Acadêmica para Sustentabilidade Socioambiental

nm – nanometers

OC – Organic Carbon

OM – Organic Matter

P – Phosphorus

p – Statistical significance

pCH_4 – Methane partial pressure

pCO_2 – Carbon dioxide partial pressure

Pg – Petagrams

PVC – Polyvinyl chloride

Q_1 – First quartile

Q_3 – Third quartile

s – second

S – South

S_{Cw} – Sobol index based on dissolved gas concentration measures

SD – Standard Deviation

SE – Standard Error

S_k – Sobol index based on gas exchange velocity measures

Tg – Teragrams

TN – Total Nitrogen

TP – Total Phosphorus

UGGA – Ultra-portable Greenhouse Gas Analyzer

VIF – Variable Inflation Factor

W – West

y – year

Zn – Zinc

List of Figures

Supplementary figures

List of Tables

Supplmentary tables

Contents

Contextualizing the thesis

Historically, the progress of human civilizations has been closely linked to their proximity to aquatic ecosystems (Van Cappellen and Maavara, 2016). The contiguity to aquatic environments made human expansion possible, both spatially and demographically over the landscape. By mastering agricultural techniques under fertile lands, human civilizations were able to experience the increase in the number of individuals. However, the fine line between the exploitation of natural resources and demand became increasingly evident within the social structures that enjoyed this relationship. As a consequence, the demand for resources intensified more and more in order to maintain the current state of settlements as well as their improvements. One of the alternatives adopted by civilizations in order to foster their needs was the storage of water in strategic locations by diverting and damming water bodies.

There have been records of dam construction by human civilizations for at least seven millennia. However, the systematic damming of rivers began to be seriously implemented after the 1930s. In the late 20th century, more than half of the planet's surface water had passed through artificial dams before reaching the oceans (Vörösmarty et al., 1997). Currently, it is estimated that more than 70,000 large dams have already been built around the globe, with the number of large hydroelectric dams projected to almost double by 2030 (Zarfl et al., 2015). Expanding dam construction to deal with droughts and water scarcity as well as to sustain demands in electricity production is a topic that has been much debated around the world (Di Baldassarre et al., 2018). In general, three counterintuitive aspects receive a lot of attention in this intense debate: i) *supply-demand cycles*; ii) *reservoir effects*; and iii) *changes in the natural landscape as well as changes in the prevailing biogeochemical cycles*. Supply and demand cycles refer

to when water availability allows for greater water demand, which can quickly outweigh the initial benefits of reservoir construction (Di Baldassarre et al., 2018). Reservoir effects refer to cases in which over-reliance on reservoirs increases their vulnerability and therefore increases possible impacts from/by droughts (Di Baldassarre et al., 2018). Finally, damming of water bodies substantially modifies the ecosystems functioning at local and even regional scales by changing lotic to lentic environments as well as due to the flooding of zones that are not naturally flooded (Maavara et al., 2015; Wang et al., 2018).

Focusing on this last aspect, when a river is dammed, significant amounts of terrestrially-derived biomass are submerged. In response, a drastic decrease in local gross primary production is expected, as well as an intensification of microbial respiration rates (decomposition of organic matter - OM) that in turn boost greenhouse gas (GHG) emissions, such as carbon dioxide (CO_2), methane (CH_4) and nitrous oxide (N_2O), from the aquatic surface into the atmosphere (Barros et al., 2011; Deemer et al., 2016; St. Louis et al., 2000).

The past decades of research have made it clear that aquatic ecosystems are significant sources of GHG emissions to the atmosphere (Barros et al., 2011; Bastviken et al., 2011; Deemer et al., 2016; DelSontro et al., 2018; Raymond et al., 2013; St. Louis et al., 2000; Stanley et al., 2016). According to recent estimates, about 2.13 Pg of carbon (C) are emitted annually into the atmosphere by continental aquatic ecosystems, of which ~ 2 Pg C y^{-1} evades to the atmosphere in the form of CO_2, and ~ 0.13 Pg C y^{-1} in the form of CH_4 (DelSontro et al., 2018; Raymond et al., 2013; Stanley et al., 2016). Approximately 38% of the annual emissions mentioned above are attributed to reservoirs,

with ~ 80% of these emissions configured as CH_4, 17% as CO_2, and 4% as N_2O (Deemer et al., 2016).

Another important consequence of damming is the increase in the entrapment of terrestrial (allochthone) and aquatic (autochthone) elements in the reservoir sediments (e.g. organic and inorganic carbon, nutrients, trace elements). This phenomenon leads to a subsequent reduction in the transport of these elements downstream of the impoundments, which can trigger ecological disturbances in various ecosystems that are placed after the dam (Friedl and Wüest, 2002; Maavara et al., 2015; Teodoru and Wehrli, 2005; Van Cappellen and Maavara, 2016).

Thus, the sediment represents one of the most important compartments for the accumulation, processing and transfer of elements in aquatic systems (Calmano and Förstner, 1993). Both autochthonous and allochthonous material, when flowing through reservoirs, may be deposited in the different geochemical layers of the sediment (Salomons and Forstner, 1984). The accumulation of elements in the sediment can be interpreted as a "geochemical memory" in which it provides information about the past of aquatic ecosystems, recording, for example, facts about environmental impact episodes (De La Guardia and Garrigues, 1998; Junior et al., 2014). In addition, the elements buried in the sediments are not inert and may return to the water column through different paths, such as resuspension events caused by wind actions, rising of the water level during flooding, dredging, bioturbation, biological transformations (e.g. photosynthesis, food chain transport), physical changes in the chemical properties of the water-sediment interface (e.g. redox, pH) and diffusion (Calmano and Förstner, 1993; Eggleton and Thomas, 2004; Remaili et al., 2016).

Globally, a large share of reservoirs face occasional or seasonal droughts as a result of natural and man-made activities. Naturally, reservoir water level can suffer drastic decreases due to local hydrological aspects, such as the regime of intermittent and ephemeral rivers as a consequence of precipitation patterns within their hydrographic basins. On the other hand, human aspects, such as demand for electricity production, irrigation and public supply, also play a fundamental role in depleting reservoir water levels.

By decreasing reservoir water level, large areas of marginal aquatic sediments become exposed to the atmosphere. Sediment exposure redraws all the biogeochemical processes that routinely affect these locations when submerged. One of the main changes that occur in the surface of exposed sediments is the intensification of OM mineralization. Recent studies have shown that exposed aquatic sediments may represent a substantial source of GHG to the atmosphere (e.g. CO_2 and CH_4) (Almeida et al., 2019; Jin et al., 2016; Keller et al., 2020; Kosten et al., 2018; Marcé et al., 2019; Obrador et al., 2018; Paranaíba et al., 2020; von Schiller et al., 2014) and are explicitly neglected in the current global C emission estimates (Keller et al., 2020; Marcé et al., 2019).

However, when reservoir water level rises, the previously exposed sediments get submerged again. This rewetting phenomenon, well known as "*The Birch Effect*" (Birch, 1958), may favor the release of remaining elements buried in the sediment to the water column due to the physical, chemical and biological processes mentioned above. Although this is a natural process that occurs on a seasonal scale, increasing the frequency of drying and rewetting on aquatic sediments may exacerbate the release of the elements present in sediments to the water column or directly to the atmosphere.

The intensified release of elements and compounds from the sediment to the water column may affect the aquatic ecosystem equilibrium. The release of nutrients, such as nitrogen (N) and phosphorus (P), may support the growth of phytoplankton, consequently increasing the internal production of OM and potentially leading to eutrophication (Josué et al., 2019; Tranvik et al., 2009). Moreover, the exposure to trace elements (e.g. iron, manganese, zinc) can be toxic to various aquatic organisms, in addition for being able to be transferred to other trophic levels by the biomagnification process (Calmano and Förstner, 1993; Quadra et al., 2019; Scott and Sloman, 2004).

In summary, freshwater reservoirs are complex and dynamic environments. Most of the biogeochemical processes that take place within aquatic thresholds are closely connected. Thus, understanding how dam construction modifies environmental flows of water and elements within river basins must be taken into account in planning implementation of long-term eco-hydrological strategies, aiming, thus, the sustainable use of water resources.

Right ahead you will have access to four studies (chapters), of specific character, on the dynamics of GHG emissions, nutrients and trace elements in continental aquatic ecosystems, with focus on man-made reservoirs. In the first chapter, the spatial and seasonal patterns of CO_2 and CH_4 emissions were investigated using high frequency measurement techniques for data collection during different hydrological seasons in four tropical reservoirs. In the second chapter, it was investigated whether CO_2 emissions from exposed sediments of a tropical reservoir varied according to the types of surrounding land cover. In addition, this chapter evaluated the relative importance of CO_2 emissions from exposed sediments, taking into account the magnitude of emission of this gas by the aquatic surface of the same reservoir on seasonal and inter-annual

scales. The third chapter describes a laboratory experiment that investigated possible effects resulting from induced drought followed by a rewetting event on the release of GHG (CO_2 and CH_4), nutrients (N and P) trace elements (Fe, Mn and Zn), and cytogenotoxic effects of the overlying water on cell of onion bulbs (*Allium cepa*). Ultimately, the fourth chapter refers to a study that sought to quantify the CH_4 flux from exposed sediments from different types of continental aquatic systems (e.g. lakes, ponds, reservoirs and streams) spread across different climatic zones of the globe. The study also sought to determine and understand potential drivers of CH_4 emissions from exposed sediments on a global scale. The average CH_4 flux rates of exposed sediments from each type of aquatic system were upscaled to their respective global surface areas to understand whether these emissions represent a significant share of the inland water C budget.

Enjoy the reading.

First chapter: *Hotspots of diffusive CO_2 and CH_4 emission from tropical reservoirs shift through time*

José R. Paranaíba[1,2], Nathan Barros[1], Rafael M. Almeida[3], Annika Linkhorst[2], Raquel Mendonça[1], Roseilson do Vale[4], Fábio Roland[1], Sebastian Sobek[2]

[1] Institute of Biological Science, Federal University of Juiz de Fora, Minas Gerais 36036900, Brazil.

[2] Department of Ecology and Genetics, Limnology, Uppsala University, 75236 Uppsala, Sweden.

[3] Department of Ecology and Evolutionary Biology, Cornell University, 14850, USA.

[4] Department of Atmospheric Science, Federal University of West of Pará, Pará 68040070, Brazil.

Article under review at Journal of Geophysical Research – Biogeosciences

Date: December 26th, 2020

Abstract

Reservoirs are globally significant sources of carbon dioxide (CO_2) and methane (CH_4) to the atmosphere. The patterns of spatial and temporal variability in CO_2 and CH_4 emission from reservoirs are still poorly studied, especially in tropical regions where hydropower is growing rapidly. We performed spatially resolved measurements of dissolved CO_2 and CH_4 surface water concentrations and their gas-exchange coefficients (k) to compute diffusive carbon flux from four contrasting tropical reservoirs across Brazil during different hydrological seasons. Diffusive CO_2 emissions were higher during the dry season than during the rainy season, whereas there were no consistent seasonal patterns for diffusive CH_4 emissions. Our results reveal that the magnitude and the spatial within-reservoir patterns of diffusive CO_2 and CH_4 flux varied strongly among hydrological seasons. River inflow areas were often characterized by high seasonality in diffusive flux. Areas close to the dam generally showed low seasonal variability in diffusive CH_4 flux but high variability in diffusive CO_2 flux. Overall, we found that reservoir areas exhibiting highest emission rates ('hotspots') shifted substantially across hydrological seasons. Estimates of total diffusive carbon emission from the reservoir surfaces differed between hydrological seasons by a factor up to 7 in Chapéu D'Úvas reservoir, up to 13 in Curuá-Una reservoir, up to 4 in Furnas reservoir, and up to 1.8 in Funil reservoir, indicating that spatially-resolved measurements of gas concentrations and k need to be performed at different hydrological seasons in order to constrain annual diffusive carbon emission.

Plain language summary

Reservoirs are key for flood control, water supply, and hydropower generation. However, reservoirs are usually not carbon neutral. Studies worldwide point to reservoirs as important net sources of anthropogenic carbon emission to the atmosphere. Carbon emission from reservoirs derives from the decomposition of organic matter. Although carbon emission from reservoirs has been increasingly studied over the past two decades, most studies do not sufficiently describe emissions across space and time. Our study applies highly-resolved spatial coverage of dissolved CO_2 and CH_4 surface water concentrations and gas exchange coefficients to compute rates of carbon diffusion to the atmosphere across distinct hydrological seasons in four contrasting tropical reservoirs. We found that emissions varied substantially over both space and time. More specifically, we found that reservoir areas exhibiting highest emission rates ('hotspots') shifted substantially between dry and rainy seasons. Overlooking the within-reservoir spatial variability across seasons may result in serious under- or overestimations of total diffusive carbon emission from reservoirs, depending on the time and space that studies focus their sampling on. Our work may support scientists in adopting more comprehensive sampling strategies relevant for better constrained upscaling, and, consequently, help managers and politicians to take more informed policy decisions and management actions.

Introduction

Reservoirs are important components of the global carbon (C) cycle (Cole et al., 2007; Tranvik et al., 2009). While reservoirs emit substantial amounts of carbon dioxide (CO_2) and methane (CH_4) to the atmosphere (Barros et al., 2011; Deemer et al., 2016; Raymond et al., 2013), they also sequester substantial amounts of organic carbon (OC) in their sediments (Dean & Gorham, 1998; Mendonça et al., 2017). The damming of rivers fundamentally modifies the landscape by flooding terrestrial environments (Maavara et al., 2015; Wang et al., 2018). Upon submergence of terrestrial biomass, gross primary production decreases and microbial respiration rates increase, leading to potentially high CO_2 and CH_4 emissions, especially in the first ten years after reservoir construction (Abril et al., 2005; Barros et al., 2011). In addition to the production of CO_2 and CH_4 from flooded material, allochthonous and autochthonous organic matter are also important fuels for CO_2 and CH_4 production in reservoirs, which presumably remain an active source long after reservoir formation (Prairie et al., 2017). A share of the microbially-produced CO_2 and CH_4 is internally consumed (e.g. via microbial CH_4 oxidation or photosynthesis) (Granéli et al., 1996; Heilman & Carlton, 2001; Pacheco et al., 2015), whereas the surplus evades to the atmosphere by diffusion of dissolved gases, by degassing at turbine passage and in the downstream river, by plant-mediated emission, or by ebullition (i.e. gas bubbles emerging from sediment to air) (Abril et al., 2005; Bastviken et al., 2004; Cole & Caraco, 1998; Delsontro et al., 2011; Linkhorst et al., 2020).

CO_2 and CH_4 emission from reservoirs can be highly variable in space due to the heterogeneity of flooded terrestrial habitats, hydrological gradients (e.g. across the longitudinal axis from river to dam), and variability in internal primary production

(Linkhorst et al., 2020; Pacheco et al., 2015; Paranaíba et al., 2018; Teodoru et al., 2012). Moreover, the complex bathymetry and hydrodynamics of reservoirs imply that sedimentation is heterogeneous in space, which also contributes to the spatial variability in emission rates since both CO_2 and CH_4 are produced during organic matter degradation in sediments (Delsontro et al., 2011; Mendonça et al., 2014; Quadra et al., 2020; Sobek et al., 2012). Hence, accurate quantification of greenhouse gas (GHG) emission from reservoirs requires well-resolved spatial coverage to reduce the uncertainties behind the spatial estimates (Deemer et al., 2016; Paranaíba et al., 2018; Teodoru et al., 2012).

In addition to varying in space, reservoir CO_2 and CH_4 fluxes also vary in time, which is related, for instance, to variation in discharge and the load of C and nutrients from the watershed, water depth, and temperature (Abril et al., 2005; Linkhorst et al., 2020; Pacheco et al., 2015). The extent of the reservoir water body, both their depth and surface area, are strongly affected by seasonal shifts in precipitation regimes within the reservoir watersheds, as well as by demands for electricity production and water supply (Pacheco et al., 2015; Roland et al., 2010). In order to generate reliable estimates when upscaling to whole-reservoir emissions, representative measurements across space and time are therefore needed.

The extent to which spatial patterns of CO_2 and CH_4 emission from reservoirs vary among different hydrological seasons is currently insufficiently understood, probably because past studies have largely focused on either investigating variability in space (e.g. Paranaíba et al., 2018; Roland et al., 2010), or variability in time (e.g. Beaulieu et al., 2014; Jacinthe et al., 2012; Kemenes et al., 2011; Wilkinson et al., 2015). While some progress has recently been made concerning the variability in CH_4 ebullition across domains of both space and time (Harrison et al., 2017; Hilgert et al., 2019; Linkhorst et

al., 2020; Natchimuthu et al., 2016; Wik et al., 2016), systematic studies of the variability in diffusive reservoir CO_2 and CH_4 emission across domains of both space and time are lacking or have a low spatial sampling resolution (e.g. Beaulieu et al., 2014; Jacinthe et al., 2012; Serça et al., 2016; Yang et al., 2013). It is therefore not known whether areas with especially high or low diffusive CO_2 and CH_4 emission rates (Paranaíba et al., 2018) are fixed in space over time, and whether their respective magnitude of emission varies over time, and these gaps in knowledge add uncertainty to current estimates of reservoir C emissions. Given that hydrological seasons can act as a dominant control on reservoir C emissions (Beaulieu et al., 2014; Jacinthe et al., 2012; Kemenes et al., 2011), particularly at low latitudes where the differences in key environmental conditions between rainy and dry seasons can be large (e.g. water flow, catchment load, temperature), and considering that the number of reservoirs that are being constructed is growing worldwide (Zarfl et al., 2015), knowing how to best distribute measurement effort between spatial and seasonal coverage is desirable (Linkhorst et al., 2020; Wik et al., 2016).

Here we quantified the diffusive flux of CO_2 and CH_4 from four tropical reservoirs across Brazil, using spatially resolved measurements of dissolved CO_2 and CH_4 concentrations and CO_2 and CH_4 gas-exchange coefficients (k) in hydrologically different seasons, in order to understand: i) the patterns of the spatial changes in diffusive C fluxes across seasons; and ii) how these seasonal changes affect the annual diffusive C emissions in the studied reservoirs. We hypothesized that the diffusive flux of CO_2 and CH_4 is characterized by pronounced variation across both space and seasons, which results in different patterns of within-reservoir spatial variability between seasons.

Methods

Study sites and sampling strategy

Ten sampling campaigns were performed in four tropical reservoirs in Brazil between 2015 and 2017. The reservoirs are located in three different biomes, and are different in size, age, type of flooded soil, trophic state, and type of use. Reservoir and climate characteristics are shown in Table S1. We sampled each reservoir during at least two different hydrological seasons (Figure 1). The term "*season*" here refers to samplings performed at different times of the year, at different hydrological periods (dry and rainy seasons) resulting from the precipitation patterns observed within the reservoirs' watershed (Figure 1). The rainy season in the southeastern region of Brazil, where three of the four studied reservoirs are located (see below: Chapéu D'Úvas, Furnas and Funil), historically occurs between October and March, with the highest temperatures and rainfall expected in January-February. The dry season for this region tends to occur between April and September. Overall, the Brazilian southeast region tends to experience average annual rainfall of 1300 to 1800 mm (Alvares et al., 2014). The rainy period in the Amazon region, where the fourth reservoir studied here is located (Curuá-Una), occurs historically between December and April, with the highest temperatures and rainfall occurring between February and April. The dry season, or a less intense rainfall period, is expected for this region from May to October. In general, the Brazilian Amazon region experiences average annual rainfall from 1900 to 2200 mm (Alvares et al., 2014). Due to constraints beyond our control (short-term weather variability, reservoir operation, logistics), it was not possible to sample equivalent sections of the hydrograph for all four reservoirs. While three reservoirs were sampled during both the dry and rainy seasons, one reservoir was sampled two times during the dry season, yet at consecutive years. In the following, we

describe briefly each reservoir and relate the sampling campaigns to precipitation and water level conditions (Figure 1).

The 12 km^2 oligotrophic Chapéu D'Úvas (CDU) drinking water reservoir, situated in Atlantic Forest biome, was sampled 4 times: Sampling 1 was at the beginning of the rainy season, at falling water level; sampling 2 was during the rainy season, at rising water level; sampling 3 was at the beginning of the dry season with high stagnant water level; sampling 4 was during the dry season with falling water level (Table S2). The 72 km^2 mesotrophic Curuá-Una hydroelectric reservoir, situated in Amazonia biome, was sampled 2 times: Sampling 1 was the beginning of the rainy season, at rising water level; sampling 2 was during the dry season, at falling water level (Table S2). The 1342 km^2 meso-to-eutrophic Furnas hydroelectric reservoir, situated in the Cerrado biome (Brazilian Savannah), was sampled 2 times: Sampling 1 was during the dry season with stagnant water level; sampling 2 was during the rainy season with falling water level (Table S2). The 40 km^2 eutrophic Funil hydroelectric reservoir, situated in the Atlantic forest biome, was sampled 2 times: Sampling 1 was at the end of the dry season in 2016, at falling water level, and sampling 2 was during the middle of the dry season in 2017, at falling water level (Table S2). All measurements were performed during daylight between 9 and 18 h. While the spatial variability in diffusive CO_2 and CH_4 emission in three of these reservoirs has been described for one season in a previous publication (Paranaíba et al., 2018), we present here, for the first time, an analysis of the seasonal difference in the spatial variability in diffusive CO_2 and CH_4 emission in four contrasting tropical reservoirs.

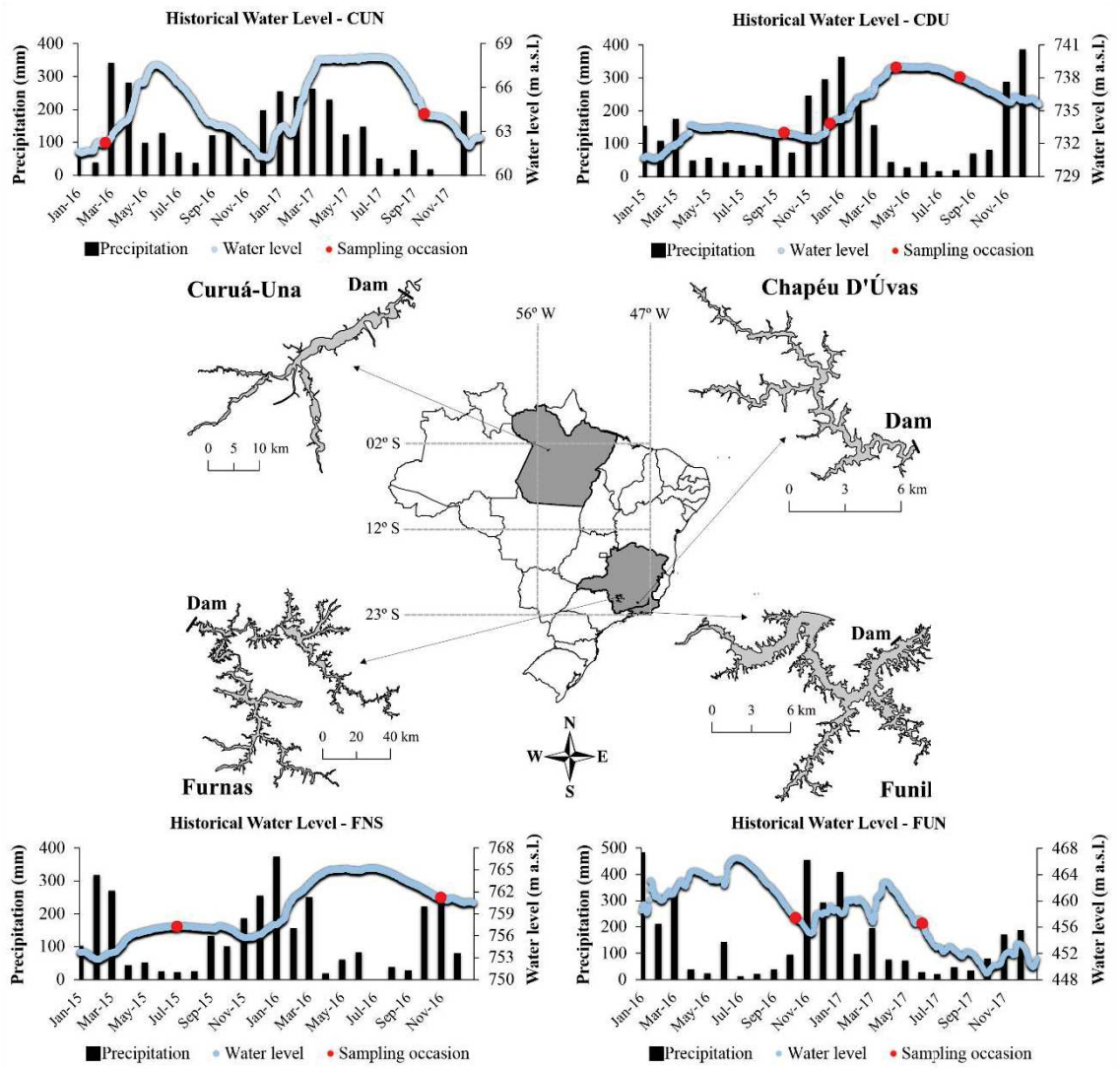

Figure 1: Map of the reservoir locations in Brazil and their respective historical water level (left y-axis) and total monthly precipitation (right y-axis). The red dots represent the sampling campaigns performed in each reservoir. Total monthly precipitation data were acquired from the nearest weather station of each reservoir and are available on the Brazilian National Meteorological Institute website (INMET - http://www.inmet.gov.br/portal/index.php?r=bdmep/bdmep).

CO_2 and CH_4 partial pressure (pCO_2 and pCH_4)

Measurements of pCO_2 and pCH_4 were continuously recorded (1 Hz frequency) using a gas flow equilibration system similar to that described in Gonzalez-Valencia et al. (2014), which was connected to an Ultraportable Greenhouse Gas Analyzer (UGGA, Los Gatos Research; for more details, see Paranaíba et al., 2018). The inlet of the online equilibration system was mounted to a boat, and water from ~0.5 m depth was continuously pumped into the system (3 L min^{-1}). The spatial variability in pCO_2 and pCH_4 was investigated performing shore-to-shore transects throughout each of the reservoirs by navigating at an average speed of 7 km h^{-1} (Figure 2). The boat was stopped approximately every hour for discrete measurements of pCO_2 and pCH_4: 30 mL of surface water (~0.05 m depth) and 10 mL of atmospheric air were collected with 60 mL polyethylene syringes in triplicates to measure pCO_2 and pCH_4 according to the headspace equilibration technique (Cole & Caraco, 1998). After shaking vigorously for 1 minute, the headspace was transferred to a 10 mL polyethylene syringe, and at the end of each sampling day, the discrete samples were manually injected into the UGGA (for details about manual injections, see Paranaíba et al., 2018). These discrete measurements of pCO_2 and pCH_4 were used to determine the equilibration efficiency of the online equilibration system (Figure S1), and also to calculate the gas-exchange coefficient (k; further described below). Average ± standard deviation of the equilibration efficiency for CO_2 and CH_4 was 89% ± 18% and 88% ± 20%, respectively (Figure S1). The response times for the online equilibration system were 3 min for CO_2 and 5 min for CH_4. Geographic coordinates were recorded concomitantly using a USB-GPS (Navilock 6002U with the software Coolterm, version 1.4.7) for the online equilibration measurements, and with a handheld GPS device (Garmin, eTrex 30x) for the discrete measurements.

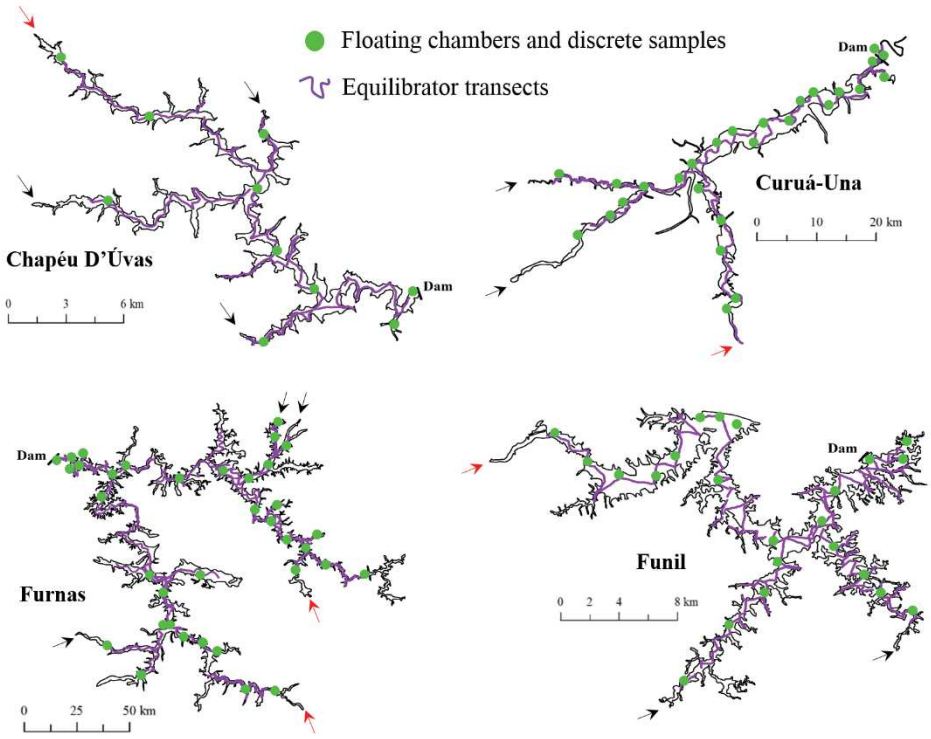

Figure 2: Equilibrator transects (purple lines) and location of floating chamber and discrete sample measurements (green dots) performed during each sampling campaign in Chapéu D'Úvas (CDU), Curuá-Una (CUN), Furnas (FNS), and Funil (FUN). The red arrows indicate where the main contributing rivers are located, with the path from the main river entrance towards the dam corresponding to the main channel, i.e. the relict main river bed. The black arrows indicate where the additional tributaries enter the reservoirs.

Diffusive flux and gas-exchange coefficient (*k* and k_{600}) calculations

At the same sites where discrete samples of CO_2 and CH_4 surface water concentrations were taken (Figure 2), triplicate measurements of CO_2 and CH_4 diffusion were conducted using a transparent acrylic floating chamber (FC; total volume: 17 L, surface area: 0.07 m^2) connected to the UGGA in a closed gas loop. In addition, in the time between each FC deployment, atmospheric concentrations of CO_2 and CH_4 were

measured with the online equilibration system over 1 minute. Changes in CO_2 and CH_4 concentrations within the FC over 5 minutes were monitored in real-time. Measurements with apparent non-linear concentration increase, which is indicative of bubble flux, were immediately aborted and a new measurement was started. Therefore, only linear CO_2 and CH_4 concentration changes during FC measurements, indicative of diffusive flux, were considered (Duchemin et al., 2000; Guérin et al., 2007). We did not observe any flattening of the concentration slope inside the chamber, which would have indicated a weakening of flux due to gas accumulation inside the chambers. In order not to affect photosynthesis and thus natural CO_2 cycling, we used a transparent FC, and the short deployment time minimizes the air temperature change inside the chamber (for details, see Paranaíba et al., 2018).

The gas flux (F_g, mmol m^{-2} d^{-1}) over the air-water interface is driven by the gas concentration difference between air and water, and regulated by the gas exchange velocity (k_g, m d^{-1}), which is specific for each gas and temperature (MacIntyre, 1995):

$$F_g = k_g\,(C_w - C_{eq}) \qquad (1)$$

where C_w (mmol m^{-3}) is the concentration of the given gas in water, and C_{eq} (mmol m^{-3}) is the theoretical concentration of the given gas in water if the water phase was in equilibrium with the atmosphere.

Combining the FC measurements and discrete partial pressure measurements at each site, k (hereafter named as k_{FCg}, m d^{-1}) was then calculated for both CO_2 and CH_4 according to the following equation:

$$k_{FCg} = F_g / (C_w - C_{eq}) \qquad (2)$$

Given that the triplicate FC measurements in each reservoir were taken approximately at the same sites for the different samplings (Figure 2, ~50m apart), we calculated the difference in k_{FC} for CO_2 and CH_4 between seasons. We achieved this by averaging the triplicated k values for each sampling site and then subtracting the minimum k_{FCg} value by the maximum k_{FCg} value (i.e. the range) at each sampling site between seasons.

In order to analyse in how far the gas exchange velocity was driven by wind speed, k_{FC} for CO_2 and CH_4 were normalized to a Schmidt number of 600 (i.e. CO_2 at 20°C), for both CO_2 and CH_4, according to Jähne et al. (1987):

$$k_{600} = k_{FCg,T} \, (600 / Sc_{g,T})^{-n} \qquad (3)$$

where $Sc_{g,T}$ is the Schmidt number for a given gas at a given temperature (Wanninkhof, 1992). We used n = 2/3 for wind speed <3.7 m s^{-1} at 10 m above water level and n = 1/2 for wind speed > 3.7 m s^{-1} at 10 m above water level (Prairie & del Giorgio, 2013).

We measured wind speed at 2 m above the water surface at the same sites where discrete samples were taken, using a portable anemometer (Skymaster Speedtech SM-28, accuracy: 3%). Then, we normalized wind speed measurements to a wind speed at 10 m above the water surface according to Smith (1985).

Water column profile of temperature and dissolved oxygen concentrations

Water temperature and dissolved oxygen concentration profiles were measured using a multiparameter probe (YSI model 6600 V2, Yellow Spring, OH, USA) in different zones of the reservoirs during each sampling campaign. The multiparameter probe was calibrated before each sampling campaign, and the measurements were taken

at every meter from the surface to 15 meters depth, and at every 5 meters from 15 meters depth to the bottom where applicable.

Data analysis

Since FC and discrete pCO_2 and pCH_4 measurements were performed every hour, we used an interpolation algorithm (see below) to produce estimates of k_{FCg} that matched the higher spatial resolution of the online equilibration system. We also spatially interpolated the between-season range in k_{FCg} values that we calculated at each site. Inverse distance weighting (IDW; ArcGIS version 10.3.1, ESRI) was adopted to interpolate dissolved CO_2 and CH_4 concentrations from the online equilibration system and k_{FCg} to non-measured areas. The maps of interpolated CO_2 and CH_4 concentrations (continuous measurement) as well as k_{FCg} of both gases (discrete measurements) were used to calculate the diffusive fluxes according to Equation 1 and to generate maps of diffusive CO_2 and CH_4 fluxes.

To better understand the spatial variability in the diffusive CO_2 and CH_4 flux within and between seasons, the reservoirs were gridded using the Fishnet tool of ArcGIS to create a grid of identical squares (300 x 300 m) over each reservoir's shape. Then, the diffusive flux maps (for each gas and sampling campaign) were combined with the grid layer to extract the mean diffusive flux of all pixels within each grid cell by using the Zonal Statistics as Table function, available in the Spatial Analyst tool of ArcGIS (Figure S2). Of all grid cells in the reservoirs, 48%, 23%, 5%, and 38% presented at least 1 sampling point (continuous measurements) in CDU (mean ± standard deviation: 9 ± 5 sampling points), CUN (5 ± 2 sampling points), FNS (3 ± 1 sampling points), and FUN (6 ± 4 sampling points), respectively. Grid cells with no interpolated data were excluded from the seasonal analysis (CDU: 8-24 of 283 grid cells were excluded; CUN: 93-153 of

1413 grid cells were excluded; FNS: 2448-3112 of 16741 grid cells were excluded; and FUN: 97-111 of 792 grid cells were excluded). Empty grid cells were those in which IDW does not extrapolate beyond measured location, but only interpolates between measurements (e.g. variability in water level resulted in that some areas were covered during one sampling, but not during the other). The number of pixels within grid cells, resulting from IDW interpolation, ranged from 10 to 760 pixels (mean ± standard deviation: 221 ± 177 pixels) in CDU, 12 to 108 pixels (73 ± 71 pixels) in CUN, 9 to 114 pixels (64 ± 25 pixels) in FNS, and 10 to 810 pixels (300 ± 235 pixels) in FUN. Because the grid cells are fixed in space, it was possible to calculate the between-season variability for each grid cell; it was calculated as the range, i.e. for each grid cell, the minimum mean flux was subtracted from the maximum mean flux (Figure S2). Then, all between-season ranges of diffusive flux were plotted in boxplot graphs for each reservoir.

In order to investigate if there are areas within the reservoirs that are characterized by particularly low or high seasonal variability in diffusive CO_2 and/or CH_4 flux, we identified the geographical location where the between-season flux difference was below and above the interquartile range in the boxplots for each reservoir. In addition, to verify whether hotspot zones of diffusive C emission vary in the reservoirs between seasons, we geographically identified the upper quartile containing 25% of the grid cells with the highest diffusive CO_2 and CH_4 fluxes.

In addition to the analyis of interpolated data, we also performed analyses of the measured data. Since the concentration transects as well as the floating chamber measurement locations were not at identical locations for the different sampling campaigns, not all measurements could be matched and the grid cell size had to be increased (from 300 x 300 m to 400 x 400 m). Analyses of the measured data returned

patterns of spatial and temporal distribution (Figures S3-S6) that were similar to the patterns of the interpolated data (Figures 3-6), indicating that the interpolation did not produce artifacts that could affect our conclusions. In the following, we present results based solely on the interpolated data, since it allows us to use all of the measured data (in particular the highly resolved concentration measurements), and allows smaller grid cell sizes, and thus results in a more representative assessment of the reservoirs.

For investigating whether the observed spatial variability in diffusive CO_2 and CH_4 emissions among reservoirs across seasons was driven rather by variability in gas concentration, or rather by variability in gas exchange velocity, a Markov Chain Monte Carlo (MCMC) simulation followed by a variance-based sensitivity analysis was performed to calculate Sobol indices (Sobol, 2001). As the diffusive flux across the air-water interface is regulated by the difference in gas concentration and k (Equation 1), Sobol indices disentangle the variance in flux into fractions which are attributed to the input variables (i.e. gas concentration and k). For MCMC simulations and subsequent Sobol index calculations, we used the mean values of diffusive flux, gas concentration and k_{FCg} extracted from each grid cell, in all reservoirs. We calculated:

i) diffusive flux by fixing k_{FCg} ($Flux|k$) – diffusive CO_2 and CH_4 fluxes were calculated using fixed k_{FCg} values against all grid-extracted gas concentrations in surface water; and

ii) diffusive flux by fixing surface water gas concentration ($Flux|C_w$) – diffusive CO_2 and CH_4 fluxes were calculated using fixed C_w values against all grid-extracted k_{FCg} values.

Averaged and fixed C_{eq} values based on all grid cells in each sampling campaign in each reservoir were used, given that C_{eq} is based on the atmospheric gas concentration and thus is much less variable in space and time when compared to C_w. Subsequently, we separately calculated the average of all fluxes resulting from (i) fixed k_{FCg} and variable C_w, and (ii) fixed C_w and variable k_{FCg}. We, then, calculated the variance of all diffusive fluxes from both scenarios together (Var($Flux|k \cup Flux|C_w$)) and the variance of all averaged diffusive fluxes calculated using fixed k_{FCg} (Var($Flux|k$); calculation i) and using fixed C_w (Var($Flux|C_w$); calculation ii). Finally, the Sobol indices (S_k and S_{Cw}) were calculated dividing Var($Flux|k$) and Var($Flux|C_w$) by Var($Flux|k \cup Flux|C_w$), for each gas and sampling campaign separately. Accordingly, the Sobol indices are values that range from 0 to 1, with higher values meaning larger data variability. High S_k indicates that a large share of the variance in diffusive flux is attributable to high variability in gas concentration C_w (since k_{FCg} was fixed), and high S_{Cw} indicates that a large share of the variance in diffusive flux is attributable to high variability in gas exchange velocity k (since C_w was fixed). The remainder to 1 of $S_k + S_{Cw}$ is attributable to the variance in diffusive flux that is attributable to the interaction between k_{FCg} and C_w .

We calculated the total daily diffusive CO_2 and CH_4 emission per reservoir for each sampling campaign by multiplying the mean gas flux of each grid cell with its grid cell surface area and then summing up the flux values of all grid cells. To achieve this, the daily diffusive CO_2 and CH_4 emission of each sampling campaign was multiplied by the number of days that correspond to each studied hydrological season. Thereby, we assumed that the sampling occasions covered the total seasonal variability, and that the flux during the sampling occasion is representative of a period of 3 months for CDU, 6 months for CUN and FNS, and 12 months for each sampling occasion in FUN; evidently, these assumptions add uncertainty to the annual emission estimate. Accordingly, for

CDU, where four sampling occasions took place, a multiplication factor of 91 was applied, whereas for CUN and FNS, where only two sampling occasions took place, a multiplication factor of 182 was applied. In FUN, which was sampled two times but both times during the dry season, we calculated an annual average assuming that the sampling occasions were each representative for the entire respective year and, therefore, a multiplication factor of 365 was applied, followed by averaging the two annual estimates into an annual average estimate for each gas. Given that our calculations of total diffusive C emission are only based on daytime measurements (between 9 and 18 h), our results may be biased since they do not include any potential diel variations in diffusive C emissions and any specific mixing dynamics happening in the water column during the entire period of each hydrological season represented here (Podgrajsek et al., 2014; Rõõm et al., 2014; Sieczko et al., 2020).

Generalized linear mixed models (GLMM) were applied to assess the differences in the diffusive CO_2 and CH_4 fluxes and gas exchange coefficients between the different spatial variability campaigns, and between the reservoirs. To do so, we used the glmer function in the "*lmer4*" package in R (v. 4.0.2) (R Core Team, 2018). We used the spatial variability campaigns of each reservoir as a fixed factor while the variable "reservoir" was used as random factor to account for the underlying characteristics of each reservoir. We used generalized models because preliminary analyses showed that the distribution of the residuals of the linear mixed models (LMM) followed a logarithmic distribution and, therefore, the gamma family (*link=log*) was applied in the GLMM. A Tukey post-hoc test was applied to compare each possible pair using the glht function as available in the "*multcomp*" package (Hothorn et al., 2008). Graphical analyses were performed using the software JMP (version 14.0.0), statistical analyses and discrete sample calculations

were done using the software R (version 1.1.383), and all maps were created using the software ArcGIS (version 10.3.1, ESRI).

Results and Discussion

Spatial and seasonal variability in pCO_2, pCH_4, k, k_{600}, and diffusive CO_2 and CH_4 fluxes

We observed large variability in pCO_2 and pCH_4 within reservoirs, among reservoirs, and among hydrological seasons (Table 1). The average surface water pCO_2 and pCH_4 were supersaturated with respect to the atmosphere in all reservoirs and all sampling campaigns (Table 1), except for pCO_2 during the late dry season in FUN, a highly eutrophic system (Table S1). For all reservoirs and sampling campaigns together, the average pCO_2 and pCH_4 were 1.6 and 7.4 times higher than atmospheric levels, respectively.

The gas exchange coefficient (k) also varied within reservoirs and among seasons (Tables S3-S6); overall, k ranged from 0.002 to 14 m d^{-1} for CO_2 and from 0.005 to 22 m d^{-1} for CH_4. The mean ± standard deviation of k was 1.1 ± 1.4 m d^{-1} for CO_2 and 4.3 ± 3.5 m d^{-1} for CH_4 in CDU; 1.4 ± 2.5 m d^{-1} for CO_2 and 2.4 ± 1.6 m d^{-1} for CH_4 in CUN; 0.6 ± 0.7 m d^{-1} for CO_2 and 3.0 ± 3.1 m d^{-1} for CH_4 in FNS; and 0.02 ± 0.06 m d^{-1} for CO_2 and 0.07 ± 0.07 m d^{-1} for CH_4 in FUN. While the seasonal variability in k was small in most reservoirs, a few areas in each reservoir were characterized by relatively high seasonal variability (red areas in Figures S7 and S8; Tables S3-S6). Statistical outcomes of the GLMM of k values for CO_2 and CH_4 between seasons and reservoirs are shown in Table S7; within reservoirs: k_{FC}-CO_2 seasonality was significant in all reservoirs except in CUN (z value: -2.6, p = 0.206), whereas k_{FC}-CH_4 seasonality was not significant

between seasons in any reservoir (Table S7). See Table S7 for comparisons between reservoirs. In search for possible drivers controlling gas exchange in all reservoirs across seasons, we plotted the k_{FC} and k_{600} for both CO_2 and CH_4 against the corresponding water temperature and wind speed at the time of sampling, respectively. We found that wind speed was not correlated with k_{600} estimates neither for CO_2 and nor for CH_4 (except for k_{600}-CO_2 in CDU; Figure S9). We also could not observe consistent positive relationships between k_{FC} and water temperature for both CO_2 and CH_4 in all reservoirs (Figure S10). This indicates that neither wind speed, which can affect k at very short time scales (minutes-hours), nor water temperature, which can affect k at diurnal-seasonal time scales, rendered a detectable imprint on the gas exchange velocity in our study. Potentially, the variability in k could be driven by the presumably complex hydrodynamics in these dendritic reservoirs with their multiple tributaries, or by convection-driven turbulence.

As a result of the variability in gas concentration and k, CO_2 and CH_4 diffusive fluxes also varied across both space and time in all reservoirs (Table 1; Figure 3). The average diffusive CO_2 and CH_4 fluxes of our studied reservoirs were within the diffusive CO_2 and CH_4 flux ranges reported by Deemer et al. (2016) for 228 reservoirs worldwide (Figure S11). Overall, diffusive CO_2 emissions from these four reservoirs are in the lower range observed in global reservoirs, whereas CH_4 emissions are in the upper range (Figure S11).

Table 1: Average, standard deviation and range of CO_2 and CH_4 partial pressure (upper table) and diffusive CO_2 and CH_4 flux (bottom table, interpolated values) during the different hydrological seasons in Chapéu D'Úvas (CDU), Curuá-Una (CUN), Furnas (FNS), and Funil (FUN).

Reservoir	pCO_2 (µatm)				pCH_4 (µatm)			
	Rainy season		Dry season		Rainy season		Dry season	
CDU	439 ± 63 (300—773) *(early)*	418 ± 50 (360—703) *(late)*	730 ± 175 (416—1223) *(early)*	665 ± 126 (409—1004) *(late)*	11 ± 9 (2—65) *(early)*	8 ± 5 (1.8—33) *(late)*	27 ± 9 (4.4—55) *(early)*	8 ± 5 (3—30) *(late)*
CUN	664 ± 221 (387—1478)		1171 ± 482 (415—3135)		9 ± 5 (1.8—50)		13 ± 9 (2.2—52)	
FNS	607 ± 265 (262—2536)		400 ± 299 (7—3090)		8 ± 9 (1.8—126)		30 ± 20 (1.8—217)	
			Late dry (2016)	Mid dry (2017)			Late dry (2016)	Mid dry (2017)
FUN			384 ± 127 (240—915)	630 ± 277 (317—1352)			10 ± 9 (3.4—76)	17 ± 18 (3—88)
	CO_2 (diffusive emission mmol m^{-2} d^{-1})				CH_4 (diffusive emission mmol m^{-2} d^{-1})			
	Rainy season		Dry season		Rainy season		Dry season	
CDU	5 ± 6 (-26—24) *(early)*	1.6 ± 2.6 (-0.5—32) *(late)*	7 ± 4.5 (0.002—24) *(early)*	11 ± 6 (0.09—28) *(late)*	1.6 ± 1.7 (0.04—16) *(early)*	2.5 ± 2 (0.02—19) *(late)*	2.5 ± 0.9 (0.3—8.9) *(early)*	1.1 ± 0.5 (0.4—5.2) *(late)*
CUN	8 ± 9 (0.6—83)		92.5 ± 176.6 (3.4—1612)		0.6 ± 0.8 (0.09—7)		0.9 ± 0.7 (0.08—4.3)	
FNS	2.7 ± 5.6 (-4.3—60.6)		7 ± 16 (-36—90)		0.6 ± 0.5 (0.03—8.2)		2.5 ± 2.5 (0.001—21.5)	
			Late dry (2016)	Mid dry (2017)			Late dry (2016)	Mid dry (2017)
FUN			0.03 ± 0.1 (-0.05—1.7)	0.1 ± 0.2 (-0.02—0.9)			0.06 ± 0.2 (0.0002—2.1)	0.08 ± 0.2 (0.002—1.7)

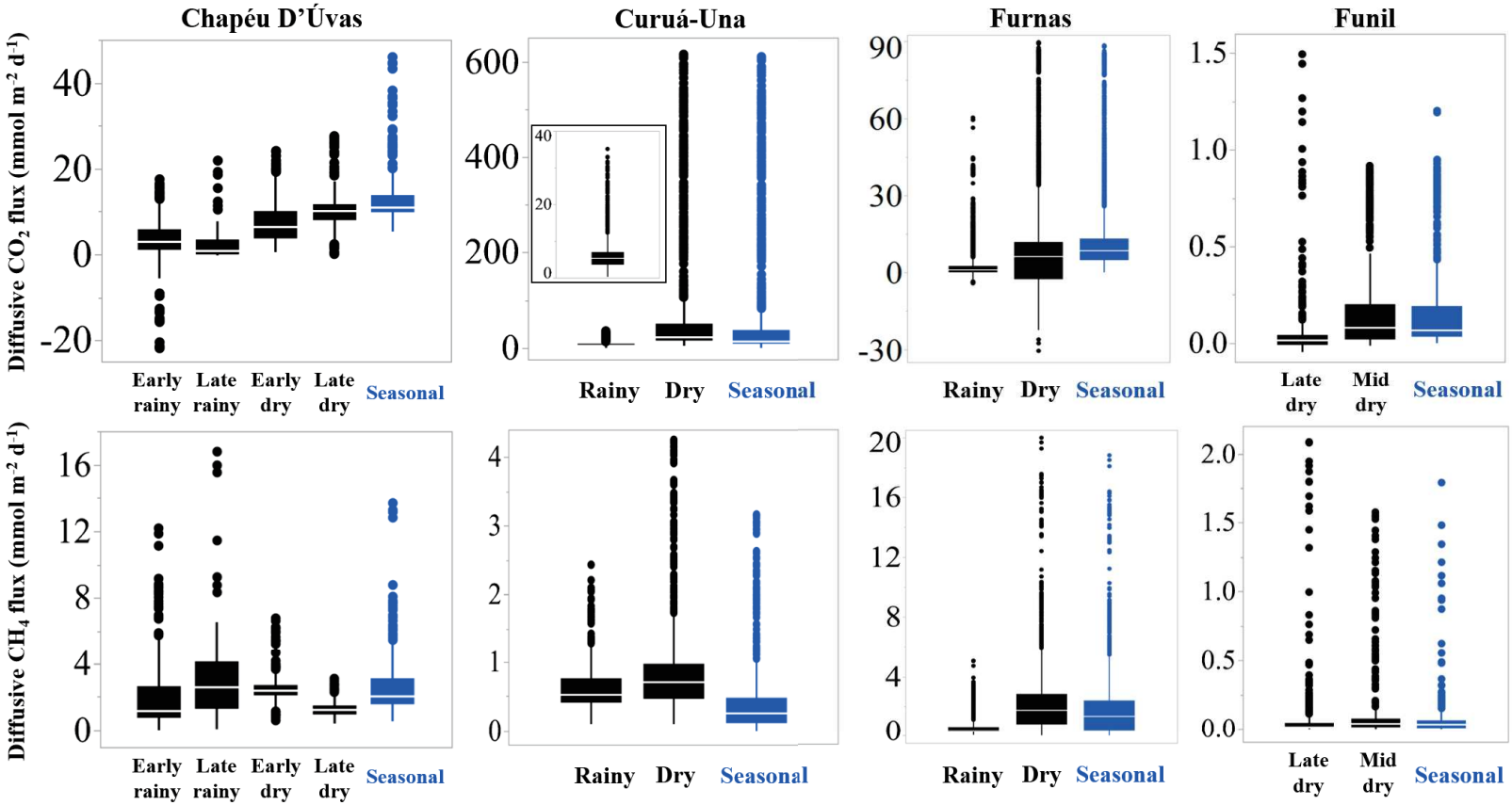

Figure 3: Distribution of the diffusive CO_2 (upper) and CH_4 (bottom) flux in Chapéu D'Úvas (CDU), Curuá-Una (CUN), Furnas (FNS), and Funil (FUN) across different hydrological seasons. The black boxes show the within-reservoir variability at each sampling occasion, represented by the average of all IDW pixels within each grid cell. The blue boxes represent the between-season range calculated for each grid cell.

The variability in diffusive flux of each grid cell between sampling campaigns (blue boxes in Figure 3) was as large as the variability observed between grid cells for every sampling campaign and both gases in all reservoirs (black boxes in Figure 3). This finding adds to previously documented strong within-reservoir variability in diffusive CO_2 and CH_4 fluxes (Paranaíba et al., 2018) by showing that at any given point in space, the variability between sampling occasions can also be as strong as the difference between any two sampling locations.

GLMM analysis revealed statistical differences in the magnitude of diffusive CO_2 and CH_4 fluxes between hydrological seasons in all reservoir except for diffusive CO_2 fluxes in FUN (z value: 2.5, p = 0.238) (Table S8; see also for comparisons between reservoirs). CO_2 emission was higher in the dry season than in the rainy season (Table 1, Figure 3). However, no consistent pattern was visible for CH_4 emission, which was higher during the dry season in CUN and FNS, but higher during the rainy season in CDU (Table 1, Figure 3). For FUN, which was sampled two times during dry seasons, CO_2 and CH_4 emissions were higher during the mid-dry season of 2017 than during the late dry season of 2016, but since the fluxes were very small at both occasions for both gases (Table 1, Figure 3), this difference should be interpreted with caution. It rather seems that sampling FUN two times during dry seasons of consecutive years overall returned similar diffusive emission estimates for both CO_2 and CH_4 (Table 1, Figure 3). Higher C emission rates (for both CO_2 and CH_4) during dry seasons have previously been reported for some tropical hydroelectric reservoirs, in which were related to longer water residence time during dry periods when compared to wet ones (Abril et al., 2005), to non-stratified water columns due to stagnant low air temperatures over the dry period in tropical regions (wintertime) (Pacheco et al., 2015; Roland et al., 2010), and to the increased influence of river inflow areas on the dissolved gas concentrations of a reservoir as a whole (Pacheco

et al., 2015). We also want to emphasize that the seasonal differences reported here refer to the hydrologically different times of the year at which the reservoirs were sampled. We do not use the term "seasonality" to attribute the observed differences in emission to potential drivers that vary at the seasonal scale (e.g. water flow, catchment load, or temperature), and cannot exclude that additional sampling campaigns could identify sources of variability in emission that are not related to seasonal-scale variability in potential drivers of emission.

The daily emission of CO_2 and CH_4 from the reservoir surface via diffusion (exclusive of ebullition or downstream emission) varied largely between reservoirs (Table S9). We describe here the magnitude of seasonal variability by dividing the highest total daily diffusive emission by the lowest total daily diffusive emission for each gas and each reservoir. Accordingly, total daily diffusive C emission varied by a factor of 1.1–13 between seasons in the studied reservoirs (median 5, range 1.8–13 for CO_2; and median 1.9, range 1.1–4 for CH_4) (Table S9), with low between-season variability being observed only for CH_4 emissions in CUN (factor 1.4) and FUN (factor 1.1) (Table S9). The dry season was characterized by the highest daily diffusive CO_2 emission in all reservoirs (total daily diffusive emission ± standard error: 1000 ± 0.5 kg C d^{-1} in CDU, 67600 ± 34.6 kg C d^{-1} in CUN, 86000 ± 12.3 kg C d^{-1} in FNS, and 61 ± 0.04 kg C d^{-1} in FUN (late dry season) (Table 1). The highest daily diffusive CH_4 emission was observed during the end of the rainy season in CDU (240 ± 0.9 kg C d^{-1}), and during the dry season in FNS (26000 ± 3.9 kg C d^{-1}), in CUN (736 ± 0.5 kg C d^{-1}), and FUN (23 ± 0.07 kg C d^{-1}, late dry season) (Table S9).

The Sobol indices showed that the spatial variability in diffusive CO_2 and CH_4 fluxes observed in each hydrological season in the four studied reservoirs was strongly

affected by the variability in the gas exchange velocity (k_{FCg}) between seasons (mean S_{Cw} for all data: 0.56), followed by the variability in surface water gas concentration (mean S_k for all data: 0.26), and by the interaction between the two (mean remainder, 0.19; Table 2). Even though we could not identify consistent relationships between the gas exchange velocity and the suspected drivers wind speed and water temperature (Figures S9 and S10), this finding is in accordance with previous findings of a strong effect of k on reservoir C emission at very short time scales (e.g. at the diel scale; (Deshmukh et al., 2014; Liu et al., 2016)). Our analysis also indicates that gas concentration in concert with the interaction between gas concentration and k contributed almost half of the within-reservoir variability in diffusive flux. Furthermore, the calculation of Sobol indices assumes that the predictor variables are orthogonal, and while this condition was given as indicated in the absence of a relationship between gas concentration and gas exchange velocity (data not shown), it is conceptually evident that gas concentration and gas exchange velocity are not independent. That is, with high k values, dissolved gases from mixed surface waters may rapidly outgas, thereby lowering the C_w concentrations, whereas low k values may allow dissolved gases to build up in the surface waters, thereby leading to high C_w values. Therefore, the high S_{Cw} indices (Table 2), indicating that more than half of the variability in diffusive flux is attributable variability in k_{FCg}, cannot be used to rule out the importance of gas concentration C_w, and of the interaction between C_w and k_{FCg}.

Table 2: Sobol indices (S_k and S_{Cw}) calculated from the Markov Chain Monte Carlo simulations (see section 2.5 Data analysis) for CO_2 and CH_4 in each reservoir: Chapéu D'Úvas (CDU), Curuá-Una (CUN), Furnas (FNS), and Funil (FUN) during the hydrological seasons. The remainder variance (Int.) is attributed to the interaction between S_k and S_{Cw}. Higher Sobol indices, indicating a higher variance, are highlighted in bold. For S_k indices, k_{FCg} values were fixed and C_w values were allowed to vary, and it express therefore the influence of the variability in C_w on the resulting diffusive flux. For S_{Cw} indices, C_w values were fixed and k_{FCg} values were allowed to vary, and it express therefore the influence of the variability in k_{FCg} on the resulting diffusive flux.

Reservoir	Gas	Rainy season						Dry season					
		Early			Late			Early			Late		
		S_k	S_{Cw}	Int.	S_k	S_{Cw}	Int.	S_k	S_{Cw}	Int.	S_k	S_{Cw}	Int.
CDU	CO_2	0.21	**0.57**	0.22	0.17	**0.58**	0.25	0.31	**0.61**	0.08	0.25	**0.69**	0.06
	CH_4	0.18	**0.71**	0.11	0.33	**0.58**	0.09	0.24	**0.74**	0.02	0.09	**0.89**	0.02

Reservoir	Gas	Rainy season			Dry season		
		S_k	S_{Cw}	Int.	S_k	S_{Cw}	Int.
CUN	CO_2	0.36	**0.51**	0.13	**0.71**	0.1	0.19
	CH_4	0.38	**0.52**	0.1	0.25	**0.6**	0.15

Reservoir	Gas	Rainy season			Dry season		
		S_k	S_{Cw}	Int.	S_k	S_{Cw}	Int.
FNS	CO_2	0.11	**0.6**	0.29	0.03	**0.75**	0.22
	CH_4	0.18	**0.71**	0.11	0.17	**0.54**	0.29

Reservoir	Gas	Dry season					
		Late			Mid		
		S_k	S_{Cw}	Int.	S_k	S_{Cw}	Int.
FUN	CO_2	0.04	**0.69**	0.27	0.21	**0.44**	0.35
	CH_4	**0.58**	0.07	0.35	**0.38**	0.2	0.42

Within-reservoir variability in diffusive CO_2 and CH_4 fluxes across seasons

Our results demonstrate that the patterns of spatial within-reservoir variability in diffusive CO_2 and CH_4 emission can be very different between sampling campaigns performed during different hydrological seasons (Table 1 and Figure 4). The within-reservoir hotspots of diffusive gas emission – defined as the upper quartile containing 25% of the grid cells with highest fluxes in a given reservoir – shifted substantially across seasons for both CO_2 and CH_4 in all reservoirs (except for CH_4 in FUN) (Figures 5 and 6).

Mapping the grid cells with the lowest and highest seasonal variability ($<Q_1$ and $>Q_3$) reveals remarkable spatial diffusive flux patterns, which however were not equivalent for CO_2 and CH_4 (Figure 4). Variability in diffusive flux results from the variability in gas concentration (i.e. the net outcome of all processes that either add or remove the gas from the water) and/or variability in k (i.e. transport across the air-water interface). In the following, we discuss the spatial patterns of seasonal variability in diffusive flux in the light of processes that affect gas concentration as well as gas exchange velocity, even if these two terms of the diffusive flux equation are not entirely independent (e.g. Rocher-Ros et al., 2019).

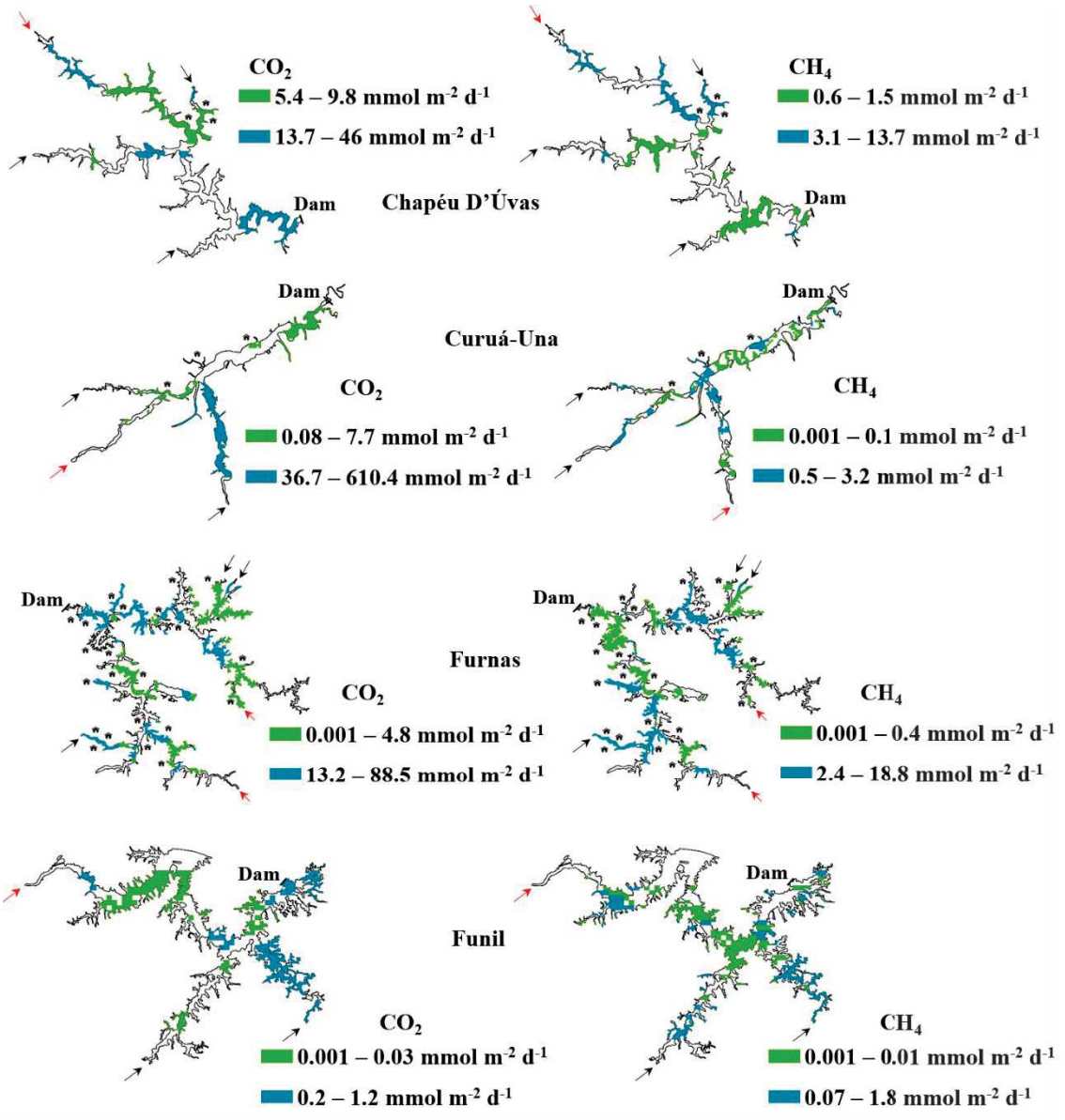

Figure 4: Spatial distribution of the seasonal variability in diffusive CO_2 and CH_4 fluxes in Chapéu D'Úvas (CDU), Curuá-Una (CUN), Furnas (FNS), and Funil (FUN). The green areas had low between-season difference ($<Q_1$ in the distribution of seasonal difference of all grid cells, as shown in the blue boxes in Figure 3), and blue areas had a high seasonal difference ($>Q_3$). Areas without color represent grid cells within the interquartile range of seasonal difference ($>Q_1$ and $<Q_3$). The red arrows indicate where the main contributing rivers are located, with the path from the main river entrance towards the dam corresponding to the main channel, i.e. the relict main river bed. The black arrows

indicate where additional tributaries enter the reservoirs. The black houses represent riverside communities in CDU, CUN, and FNS. There are no riverside communities in the vicinity of FUN.

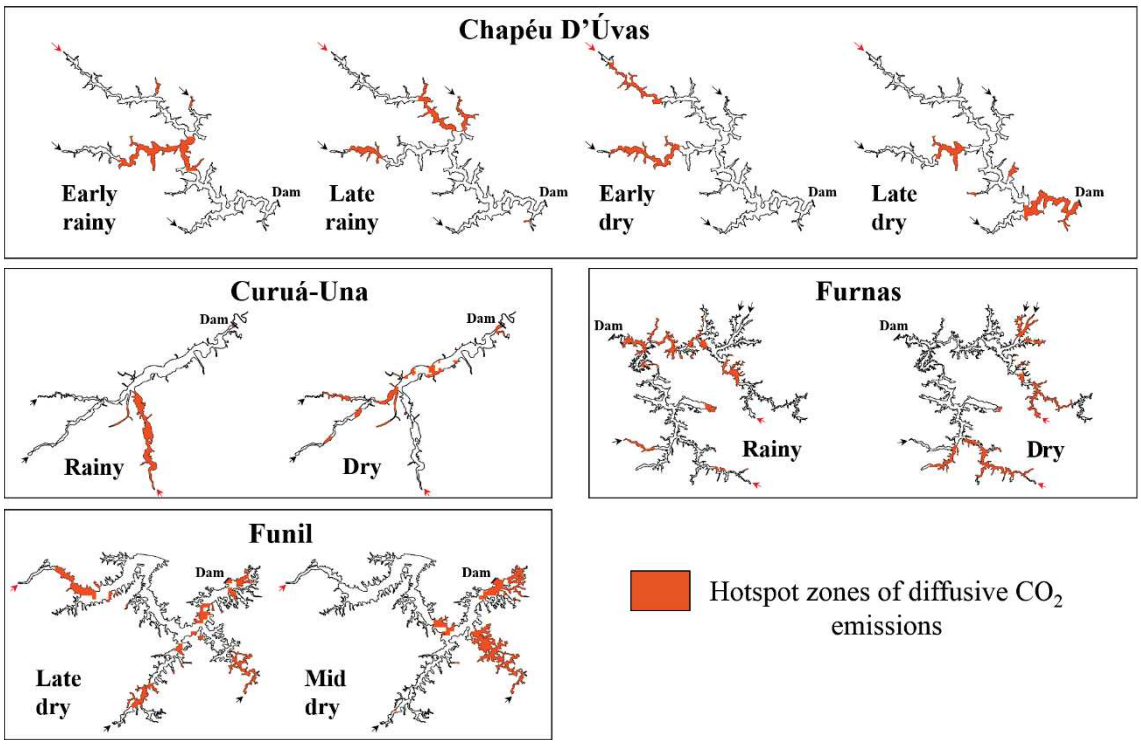

Figure 5: Spatial changes in hotspot zones for diffusive CO_2 emission (orange zones) across different hydrological seasons in Chapéu D'Úvas (CDU), Curuá-Una (CUN), Furnas (FNS), and Funil (FUN). The red arrows indicate where the main contributing rivers are located, with the path from the main river entrance towards the dam corresponding to the main channel, i.e. the relict main river bed. The black arrows indicate where additional tributaries enter the reservoirs. Hotspot zones are defined as the reservoir areas comprising the upper quartile containing 25% of the grid cells with highest diffusive CO_2 fluxes at a given sampling occasion.

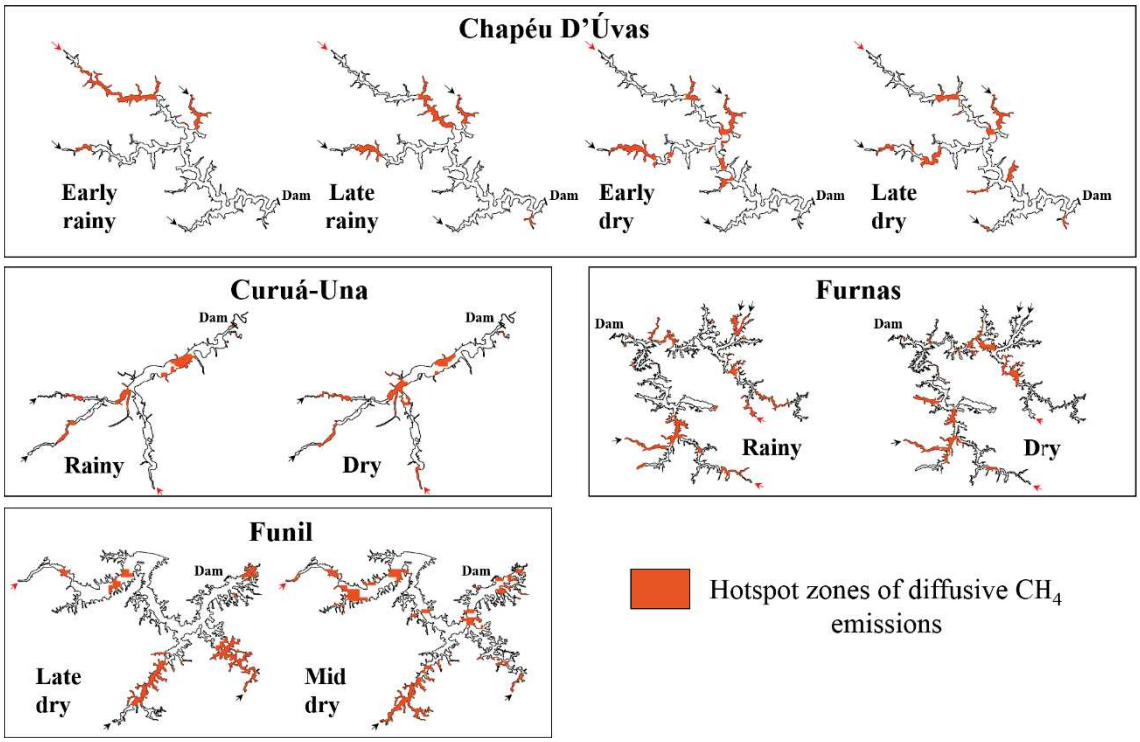

Figure 6: Spatial changes in hotspot zones for diffusive CH_4 emission (orange zones) across different hydrological seasons in Chapéu D'Úvas (CDU), Curuá-Una (CUN), Furnas (FNS), and Funil (FUN). The red arrows indicate where the main contributing rivers are located, with the path from the main river entrance towards the dam corresponding to the main channel, i.e. the relict main river bed. The black arrows indicate where additional tributaries enter the reservoirs. Hotspot zones are defined as the reservoir areas comprising the upper quartile containing 25% of the grid cells with highest diffusive CH_4 fluxes at a given sampling occasion.

The area close to the dam was characterized by high seasonal variability in diffusive CO_2 flux in CDU, FNS, and FUN (but not in CUN), which is probably linked to the fact that the dam area is typically the most lake-like part of a reservoir (deepest, i.e. with longest water residence time), which may favour the growth of phytoplankton and thus allow more biologically-driven CO_2 dynamics (Figure 4). On the other hand, the dam areas of all reservoirs were characterized by low seasonal variability in diffusive CH_4 flux

(Figure 4), which may potentially be explained by the water column being relatively deep close to the dam compared to the rest of the reservoir (depth at dam and mean reservoir depth for CDU, CUN, FNS, and FUN were 30 m and 19 m, 7 m and 6 m, 61 m and 15 m, and 58 m and 22 m, respectively) (Figures S12-S15). A deep water column favours aerobic oxidation of CH_4 during transport from the sediment to the air, and minimizes the mixing of CH_4-rich bottom waters to the surface (Bastviken et al., 2004; McGinnis et al., 2006).

High seasonal variability in the diffusive CH_4 flux was sometimes observed in areas close to riverside communities in CDU and CUN (represented as small black houses in Figure 4), but not for CO_2. Potentially, direct anthropogenic organic matter inputs via untreated sewage in these relatively shallow areas of the reservoirs (CDU: 9 ± 3 m, CUN: 5 ± 2 m) may favour methanogenesis in sediments. Methanogenesis is expected to vary seasonally in relation to temperature changes and sediment inputs (Grasset et al., 2018; Yvon-Durocher et al., 2014), leading to occasional venting to the atmosphere during water column mixing events (Liu et al., 2016). Moreover, total nitrogen (TN) and total phosphorus (TP) concentrations found near these riverside communities in CDU and CUN (mean ± standard deviation of TN in CDU: 810 ± 14 μg L^{-1}, TP in CDU: 23 ± 1 μg L^{-1}, n = 2; TN in CUN: 720 ± 19 μg L^{-1}, TP in CUN: 27 ± 2 μg L^{-1}, n = 3) were higher than the average TN and TP of each reservoir (TN in CDU: 452 ± 273 μg L^{-1}, TP in CDU: 12 ± 9 μg L^{-1}, n = 11; TN in CUN: 661 ± 77 μg L^{-1}, TP in CUN: 19 ± 6 μg L^{-1}, n = 10) (Paranaíba et al., 2018). The occurrence of high TN and TP levels near riverside communities in CDU and CUN may represent another indication that these communities are locally influencing water quality and biogeochemical processes. Even if high nutrient levels can affect the magnitude of CO_2 emission (e.g. Hanson et al., 2003), the variability in CO_2 emission between sampling occasions was apparently not affected. In FNS, which

is much larger in area, depth and total water volume than the other three reservoirs, there was no observable link between nearshore communities and seasonal variability in CO_2 and CH_4 fluxes (Figure 4).

The main channel of FUN and FNS was mostly low in CO_2 flux magnitude and variability (Figure 4), possibly because large open-water areas are more well-mixed and often have a higher gas exchange velocity (Vachon & Prairie, 2013), which spatially homogenizes the diffusive fluxes. Moreover, the influence of the surrounding land ecosystem and the ratio of sediment area to water column depth has a stronger influence in shallow narrow areas than in deep open-water areas (Holgerson & Raymond, 2016; Kortelainen et al., 2006).

In all reservoirs, some areas close to river inflows (as indicated by the arrows in Figure 4) showed high seasonal variability in diffusive CO_2 and CH_4 fluxes. It has been previously shown that river inflow areas may strongly affect the C dynamics in freshwater ecosystems (Delsontro et al., 2011; Pacheco et al., 2015; Paranaíba et al., 2018). The allochthonous inputs of organic matter and nutrients entering the reservoir via river inflows is highly variable depending on weather and human activities in the catchment, which can directly affect the C dynamics in the reservoir (Butman & Raymond, 2011; Pacheco et al., 2015). High water flow from an incoming river also affects the hydrodynamics of the reservoir and can induce resuspension, as well as intermittent vertical and lateral instabilities in the water column. These water column instabilities may contribute to a seasonally occurring lack of thermal stratification (Figures S12-S15) (Winton et al., 2019), increasing the connectivity between the sediments and the atmosphere, thus the diffusive transport of CO_2 and CH_4, which is produced in the sediments and/or water column, to the atmosphere (Abril et al., 2005; Delsontro et al.,

2011; Pacheco et al., 2015; Roland et al., 2010). Moreover, fluctuations in the magnitude of the river water flow may affect water turbulence in inflow areas, such that it could seasonally influence the gas-exchange rates at the air-water interface (Guérin et al., 2007; Long et al., 2015; Paranaíba et al., 2018; Zappa et al., 2007). Accordingly, we observed a strong seasonal difference in *k* in some river inflow areas of the four reservoirs (Figures S7 and S8).

Finally, it is noteworthy that the high seasonal variability in the diffusive CO_2 and CH_4 flux in some areas in the main channel of some of the reservoirs (e.g. in CDU, CUN, and FNS; Figure 4) may also be associated with the local *k* measurements that also varied spatially between seasons in all reservoirs (Figures S7 and S8, and Tables S3-S6) and, thus reflect conditions at the time of sampling. Our *k* values are products of FC measurements over short time intervals (5 minutes), and can, in response to meteorological and hydrological conditions as well as local basin morphology, strongly vary in space and time (Cole & Caraco 1998; Guérin et al., 2007; Zappa et al., 2007; Long et al., 2015; Paranaíba et al., 2018). The small-scale variability in *k* makes it difficult to observe clear patterns at larger scales in space or time (Figures S7 and S8, and Tables S3-S6) (Paranaíba et al., 2018).

Inter-reservoir variability in pCO_2, pCH_4, and diffusive CO_2 and CH_4 fluxes

The highest pCO_2 and areal diffusive CO_2 flux were found in the Amazonian reservoir (CUN, Table 1, Figure 3), and our findings are in accordance with previous results described by other studies on Amazonian inland waters (Belger et al., 2011; Duchemin et al., 2000; Kemenes et al., 2011; Richey et al., 2002). Amazonian freshwater systems are important sources of both CO_2 and CH_4 to the atmosphere, due to their connectivity with wetlands and extensive floodplains and high temperatures throughout

the year (Abril et al., 2013; Almeida et al., 2017; Barbosa et al., 2016; Fearnside & Pueyo, 2012; Melack et al., 2004), even though Deemer et al. (2016) did not find a difference in CH_4 emission between Amazonian and non-Amazonian reservoirs. We found that in CUN, pCH_4 and areal diffusive CH_4 flux were relatively low, similar to an earlier report of low diffusive CH_4 emission in CUN (Duchemin et al., 2000) (Table 1, Figure 3). This low diffusive CH_4 flux in CUN may be linked to microbial CH_4 oxidation in the water column. The entire shallow water column in CUN was well-oxygenated (surface water concentration: 7 ± 0.6 mg L^{-1}; bottom water concentration: 5 ± 1 mg L^{-1}) throughout seasons (Figure S13). In contrast, oxygen-poor bottom water was more common in the water columns of the other reservoirs (Figures S12, S14, and S15). Importantly, CH_4 ebullition, which typically is the main emission pathway of CH_4 emission in shallow waters (Bastviken et al., 2004) and particularly in reservoirs (Deemer et al., 2016), was not measured in this study. High potential for CH_4 ebullition from sediments of CUN has in fact been reported before (Quadra et al., 2020). Accordingly, any assessment of total reservoir CH_4 emission needs to include measurements of CH_4 ebullition, at high spatial resolution and during different hydrological seasons (Grinham et al., 2018; Linkhorst et al., 2020).

The lowest diffusive fluxes of both CO_2 and CH_4 in all four reservoirs was observed in the eutrophic reservoir FUN (Table 1, Figure 3). This was surprising since both diffusive and ebullitive CH_4 emissions tend to increase with productivity (Beaulieu et al., 2019; Deemer et al., 2016), due to the high loads of labile autochthonous organic matter to the generally anoxic sediments. In FUN (Table 1), the average diffusive CH_4 flux was about one order of magnitude lower than in another eutrophic reservoir in the Brazilian semi-arid region (Almeida et al., 2016), but similar to values observed in a eutrophic lake with a similar climate in eastern China (Xiao et al., 2017). Interestingly,

the diffusive CO_2 flux that we observed in both sampling campaigns in FUN (Table 1) was also one to two orders of magnitude lower than reported previously for the same reservoir by Pacheco et al. (2015) and Roland et al. (2010). The pCO_2, however, was within the same order of magnitude as in the above-mentioned studies, indicating that k was comparatively low during our sampling campaigns in FUN. We may attribute such differences in the magnitude of diffusive CO_2 emissions to different meteorological conditions during sampling, methodologies, and sampling coverage. Moreover, this study was focussed on diffusive fluxes and thus did not include ebullition measurements, which together with low k_{FCg} values may explain why CH_4 emission from the highly productive FUN reservoir was low (Table S6, see Tables S3-S5 for the other reservoirs). Also, we did not perform measurements in FUN during the rainy season.

Implications

By combining spatially resolved measurements of CO_2 and CH_4 surface water concentrations and k during different seasons, we show pronounced differences between hydrological seasons in spatial within-reservoir variability in the diffusive CO_2 and CH_4 fluxes of four tropical reservoirs. To the best of our knowledge, we showed for the first time that hotspot areas of diffusive C emission shift substantially between sampling occasions conducted during different hydrological seasons. Ignoring spatial and seasonal within-reservoir variability in gas concentration and k may introduce a serious bias in annual diffusive emission estimates; more specifically, the estimates in our four studied reservoirs differed by a factor of up to 13 for CO_2, and up to a factor of 4 for CH_4. The seasonal and spatial variability patterns of CO_2 and CH_4 diffusion in this study were not consistent within and between reservoirs, which emphasizes the need of spatially resolved sampling campaigns at least during two hydrological seasons to constrain annual

diffusive C emission estimates in tropical reservoirs. However, our analyses addressed diffusive emission only, while in many reservoirs, CH_4 ebullition is the pathway contributing most to CO_2-equivalent emission (Deemer et al., 2016). Accordingly, spatially-resolved ebullition measurements during our 2016 sampling campaigns in CDU (early dry season) and FUN (late dry season) found that CH_4 ebullition made up for 60 and 99% of total CO_2 equivalent emission in CDU and FUN, respectively (Linkhorst et al., submitted). This indicates that sampling effort not only needs to be distributed in space and time, but also between flux pathways. For many reservoirs, more effort on CH_4 ebullition and CH_4 oxidation in mixed layers (Thottathil et al., 2018) than only on diffusive emission measurements will be conducive to constraining greenhouse gas emission.

Acknowledgments. We are grateful to Simone Cardoso, Grigori Chapiro, and Suresh Sethi for their insightful comments on the data analysis. We are also grateful to CESAMA and Eletronorte S/A for their logistical support during our fieldwork in CDU and CUN, respectively.

References

Abril, Gwenaël, Parize, M., Pérez, M. A. P., & Filizola, N. (2013). Wood decomposition in Amazonian hydropower reservoirs: An additional source of greenhouse gases. *Journal of South American Earth Sciences*, *44*, 104–107. https://doi.org/10.1016/j.jsames.2012.11.007

Abril, Gwenäel, Guérin, F., Richard, S., Delmas, R., Galy-Lacaux, C., Gosse, P., et al. (2005). Carbon dioxide and methane emissions and the carbon budget of a 10-year old tropical reservoir (Petit Saut, French Guiana). *Global Biogeochemical Cycles*, *19*(4), 1–16. https://doi.org/10.1029/2005GB002457

Almeida, R. M., Nóbrega, G. N., Junger, P. C., Figueiredo, A. V., Andrade, A. S., de Moura, C. G. B., et al. (2016). High primary production contrasts with intense carbon emission in a eutrophic tropical reservoir. *Frontiers in Microbiology*, *7*(717), 1–13. https://doi.org/10.3389/fmicb.2016.00717

Almeida, R. M., Pacheco, F. S., Barros, N., Rosi, E., & Roland, F. (2017). Extreme floods increase CO2 outgassing from a large Amazonian river. *Limnology and Oceanography*, *62*(3), 989–999. https://doi.org/10.1002/lno.10480

Alvares, C. A., Stape, J. L., Sentelhas, P. C., Gonçalves, J. L. de M., & Sparovek, G. (2014). Koppen's climate classification map for Brazil Clayton. *Meteorologische Zeitschrift*, *22*(6), 711–728. https://doi.org/10.1127/0941-2948/2013/0507

Barbosa, P. M., Melack, J. M., Farjalla, V. F., Amaral, J. H. F., Scofield, V., & Forsberg, B. R. (2016). Diffusive methane fluxes from Negro, Solimões and Madeira rivers and fringing lakes in the Amazon basin. *Limnology and Oceanography*, *61*, 221–

237. https://doi.org/10.1002/lno.10358

Barros, N., Cole, J. J., Tranvik, L. J., Prairie, Y. T., Bastviken, D., Huszar, V. L. M., et al. (2011). Carbon emission from hydroelectric reservoirs linked to reservoir age and latitude. *Nature Geoscience*, *4*(9), 593–596. https://doi.org/10.1038/ngeo1211

Bastviken, D., Cole, J., Pace, M., & Tranvik, L. (2004). Methane emissions from lakes: Dependence of lake characteristics, two regional assessments, and a global estimate. *Global Biogeochemical Cycles*, *18*(4), 1–12. https://doi.org/10.1029/2004GB002238

Beaulieu, J. J., Smolenski, R. L., Nietch, C. T., Townsend-Small, A., & Elovitz, M. S. (2014). High methane emissions from a midlatitude reservoir draining an agricultural watershed. *Environmental Science and Technology*, *48*(19), 11100–11108. https://doi.org/10.1021/es501871g

Beaulieu, J. J., DelSontro, T., & Downing, J. A. (2019). Eutrophication will increase methane emissions from lakes and impoundments during the 21st century. *Nature Communications*, *10*(1), 1–5. https://doi.org/10.1038/s41467-019-09100-5

Belger, L., Forsberg, B. R., & Melack, J. M. (2011). Carbon dioxide and methane emissions from interfluvial wetlands in the upper Negro River basin, Brazil. *Biogeochemistry*, *105*(1), 171–183. https://doi.org/10.1007/s10533-010-9536-0

Butman, D., & Raymond, P. A. (2011). Significant efflux of carbon dioxide from streams and rivers in the United States. *Nature Geoscience*, *4*(12), 839–842. https://doi.org/10.1038/ngeo1294

Cole, J. J., Prairie, Y. T., Caraco, N. F., McDowell, W. H., Tranvik, L. J., Striegl, R. G.,

et al. (2007). Plumbing the global carbon cycle: Integrating inland waters into the terrestrial carbon budget. *Ecosystems*, *10*(1), 171–184. https://doi.org/10.1007/s10021-006-9013-8

Cole, Jonathan J., & Caraco, N. F. (1998). Atmospheric exchange of carbon dioxide in a low-wind oligotrophic lake measured by the addition of SF6. *Limnology and Oceanography*, *43*(4), 647–656. https://doi.org/10.4319/lo.1998.43.4.0647

Dean, W. E., & Gorham, E. (1998). Magnitude and significance of carbon burial in lakes, reservoirs, and peatlands. *Geology*, *26*(6), 535–538. https://doi.org/10.1130/0091-7613(1998)026<0535:MASOCB>2.3.CO;2

Deemer, B. R., Harrison, J. A., Li, S., Beaulieu, J. J., DelSontro, T., Barros, N., et al. (2016). Greenhouse Gas Emissions from Reservoir Water Surfaces: A New Global Synthesis. *BioScience*, *66*(11), 949–964. https://doi.org/https://doi.org/10.1093/biosci/biw117

Delsontro, T., Kunz, M. J., Kempter, T., Wüest, A., Wehrli, B., & Senn, D. B. (2011). Spatial heterogeneity of methane ebullition in a large tropical reservoir. *Environmental Science and Technology*, *45*(23), 9866–9873. https://doi.org/10.1021/es2005545

Deshmukh, C., Serça, D., Delon, C., Tardif, R., Demarty, M., Jarnot, C., et al. (2014). Physical controls on CH4 emissions from a newly flooded subtropical freshwater hydroelectric reservoir : Nam Theun 2. *Biogeosciences*, *11*, 4251–4269. https://doi.org/10.5194/bg-11-4251-2014

Duchemin, E., Lucotte, M., Canuel, R., Queiroz, A. G., Almeida, D. C., Pereira, H. C., &

Dezincourt, J. (2000). Comparison of greenhouse gas emissions from an old tropical reservoir with those from other reservoirs worldwide. *Internationale Vereinigung Für Theoretische Und Angewandte Limnologie: Verhandlungen*, *27*(3), 1391–1395. https://doi.org/10.1080/03680770.1998.11901464

Fearnside, P. M., & Pueyo, S. (2012). Greenhouse-gas emissions from tropical dams. *Nature Climate Change*, *2*(6), 382–384. https://doi.org/10.1038/nclimate1540

Gonzalez-Valencia, R., Magana-Rodriguez, F., Gerardo-Nieto, O., Sepulveda-Jauregui, A., Martinez-Cruz, K., Walter Anthony, K., et al. (2014). In situ measurement of dissolved methane and carbon dioxide in freshwater ecosystems by off-axis integrated cavity output spectroscopy. *Environmental Science and Technology*, *48*(19), 11421–11428. https://doi.org/10.1021/es500987j

Granéli, W., Lindell, M., & Tranvik, L. (1996). Photo-oxidative production of dissolved inorganic carbon in lakes of different humic content. *Limnology and Oceanography*, *41*(4), 698–706. https://doi.org/10.4319/lo.1996.41.4.0698

Grasset, C., Mendonça, R., Villamor Saucedo, G., Bastviken, D., Roland, F., & Sobek, S. (2018). Large but variable methane production in anoxic freshwater sediment upon addition of allochthonous and autochthonous organic matter. *Limnology and Oceanography*, *63*(4), 1488–1501. https://doi.org/10.1002/lno.10786

Grinham, A., Albert, S., Deering, N., Dunbabin, M., Bastviken, D., Sherman, B., et al. (2018). The importance of small artificial water bodies as sources of methane emissions in Queensland, Australia. *Hydrology and Earth System Sciences*, *22*(10), 5281–5298. https://doi.org/10.5194/hess-22-5281-2018

Guérin, F., Abril, G., Serça, D., Delon, C., Richard, S., Delmas, R., et al. (2007). Gas transfer velocities of CO2 and CH4 in a tropical reservoir and its river downstream. *Journal of Marine Systems*, *66*(1–4), 161–172. https://doi.org/10.1016/j.jmarsys.2006.03.019

Hanson, P. C., Bade, D. L., Carpenter, S. R., & Kratz, T. K. (2003). Lake metabolism: Relationships with dissolved organic carbon and phosphorus. *Limnology and Oceanography*, *48*(3), 1112–1119. https://doi.org/10.4319/lo.2003.48.3.1112

Harrison, J. A., Deemer, B. R., Birchfield, M. K., & O'Malley, M. T. (2017). Reservoir Water-Level Drawdowns Accelerate and Amplify Methane Emission. *Environmental Science and Technology*, *51*(3), 1267–1277. https://doi.org/10.1021/acs.est.6b03185

Heilman, M. A., & Carlton, R. G. (2001). Ebullitive release of lacunar gases from floral spikes of Potamogeton angustifolius and Potamogeton amplifolius: Effects on plant aeration and sediment CH4 flux. *Aquatic Botany*, *71*(1), 19–33. https://doi.org/10.1016/S0304-3770(01)00166-8

Hilgert, S., Scapulatempo Fernandes, C. V., & Fuchs, S. (2019). Redistribution of methane emission hot spots under drawdown conditions. *Science of the Total Environment*, *646*, 958–971. https://doi.org/10.1016/j.scitotenv.2018.07.338

Holgerson, M. A., & Raymond, P. A. (2016). Large contribution to inland water CO2 and CH4 emissions from very small ponds. *Nature Geoscience*, *9*(3), 222–226. https://doi.org/10.1038/ngeo2654

Hothorn, T., Bretz, F., & Westfall, P. (2008). Simultaneous inference in general

parametric models. *Biometrical Journal*, *50*(3), 346–363. https://doi.org/10.1002/bimj.200810425

Jacinthe, P. A., Filippelli, G. M., Tedesco, L. P., & Raftis, R. (2012). Carbon storage and greenhouse gases emission from a fluvial reservoir in an agricultural landscape. *Catena*, *94*, 53–63. https://doi.org/10.1016/j.catena.2011.03.012

Jähne, B. J., Münnich, K. O. M., Bösinger, R., Dutzi, A., Huber, W., & Libner, P. (1987). On the Parameters Influencing Air-Water Gas Exchange. *Journal of Geophysical Research*, *92*(C2), 1937–1949. https://doi.org/https://doi.org/10.1029/JC092iC02p01937

Kemenes, A., Forsberg, B. R., & Melack, J. M. (2011). CO2 emissions from a tropical hydroelectric reservoir (Balbina, Brazil). *Journal of Geophysical Research: Biogeosciences*, *116*(3), 1–11. https://doi.org/10.1029/2010JG001465

Kortelainen, P., Rantakari, M., Huttunen, J. T., Mattsson, T., Alm, J., Juutinen, S., et al. (2006). Sediment respiration and lake trophic state are important predictors of large CO2 evasion from small boreal lakes. *Global Change Biology*, *12*(8), 1554–1567. https://doi.org/10.1111/j.1365-2486.2006.01167.x

Linkhorst, A., Hiller, C., DelSontro, T., M. Azevedo, G., Barros, N., Mendonça, R., & Sobek, S. (2020). Comparing methane ebullition variability across space and time in a Brazilian reservoir. *Limnology and Oceanography*, (January), 1–12. https://doi.org/10.1002/lno.11410

Liu, H., Zhang, Q., Katul, G. G., Cole, J. J., Chapin, F. S., & MacIntyre, S. (2016). Large CO2 effluxes at night and during synoptic weather events significantly contribute to

CO2 emissions from a reservoir. *Environmental Research Letters*, *11*(6), 1–8. https://doi.org/10.1088/1748-9326/11/6/064001

Long, H., Vihermaa, L., Waldron, S., Hoey, T., Quemin, S., & Newton, J. (2015). Hydraulics are a first-order control on CO2 efflux from fluvial systems. *Journal of Geophysical Research: Biogeosciences*, *120*, 1912–1922. https://doi.org/10.1002/2015JG002955.

Maavara, T., Parsons, C. T., Ridenour, C., Stojanovic, S., Dürr, H. H., Powley, H. R., & Van Cappellen, P. (2015). Global phosphorus retention by river damming. *Proceedings of the National Academy of Sciences*, *12*(51), 15603–15608. https://doi.org/10.1073/pnas.1511797112

MacIntyre, S. (1995). Trace gas exchange across the air-sea interface in fresh water and coastal marine environments. In *Biogenic trace gases: Measuring emissions from soil and water* (pp. 52–97).

McGinnis, D. F., Greinert, J., Artemov, Y., Beaubien, S. E., & Wüest, A. (2006). Fate of rising methane bubbles in stratified waters: How much methane reaches the atmosphere? *Journal of Geophysical Research: Oceans*, *111*(9), 1–15. https://doi.org/10.1029/2005JC003183

Melack, J. M., Hess, L. L., Gastil, M., Forsberg, B. R., Hamilton, S. K., Lima, I. B. T., & Novo, E. M. L. M. (2004). Regionalization of methane emissions in the Amazon Basin with microwave remote sensing. *Global Change Biology*, *10*(5), 530–544. https://doi.org/10.1111/j.1529-8817.2003.00763.x

Mendonça, R., Kosten, S., Sobek, S., Cole, J. J., Bastos, A. C., Albuquerque, A. L., et al.

(2014). Carbon Sequestration in a Large Hydroelectric Reservoir: An Integrative Seismic Approach. *Ecosystems*, *17*(3), 430–441. https://doi.org/10.1007/s10021-013-9735-3

Mendonça, R., Müller, R. A., Clow, D., Verpoorter, C., Raymond, P., Tranvik, L. J., & Sobek, S. (2017). Organic carbon burial in global lakes and reservoirs. *Nature Communications*, *8*(1), 1–6. https://doi.org/10.1038/s41467-017-01789-6

Natchimuthu, S., Sundgren, I., Gålfalk, M., Klemedtsson, L., Crill, P., Danielsson, Å., & Bastviken, D. (2016). Spatio-temporal variability of lake CH4 fluxes and its influence on annual whole lake emission estimates. *Limnology and Oceanography*, *61*, 13–26. https://doi.org/10.1002/lno.10222

Pacheco, F. S., Soares, M. C. S., Assireu, A. T., Curtarelli, M. P., Abril, G., Stech, J. L., et al. (2015). The effects of river inflow and retention time on the spatial heterogeneity of chlorophyll and water-air CO2 fluxes in a tropical hydropower reservoir. *Biogeosciences*, *12*(1), 147–162. https://doi.org/10.5194/bg-12-147-2015

Paranaíba, J. R., Barros, N., Mendonça, R., Linkhorst, A., Isidorova, A., Roland, F., et al. (2018). Spatially Resolved Measurements of CO2 and CH4 Concentration and Gas-Exchange Velocity Highly Influence Carbon-Emission Estimates of Reservoirs. *Environmental Science and Technology*, *52*(2), 607–615. https://doi.org/10.1021/acs.est.7b05138

Podgrajsek, E., Sahlee, E., & Rutgersson, A. (2014). Diurnal cycle of lake methane flux. *Journal of Geophysical Research: Biogeosciences*, *119*, 236–248. https://doi.org/10.1002/2013JG002327

Prairie, Y. T., & del Giorgio, P. A. (2013). A new pathway of freshwater methane emissions and the putative importance of microbubbles. *Inland Waters*, *3*(3), 311–320. https://doi.org/10.5268/IW-3.3.542

Prairie, Y. T., Alm, J., Beaulieu, J., Barros, N., Battin, T., Cole, J., et al. (2017). Greenhouse Gas Emissions from Freshwater Reservoirs: What Does the Atmosphere See? *Ecosystems*, *21*(5), 1058–1071. https://doi.org/10.1007/s10021-017-0198-9

Quadra, G. R., Sobek, S., Paranaíba, J. R., Isidorova, A., Roland, F., do Vale, R., & Mendonça, R. (2020). High organic carbon burial but high potential for methane ebullition in the sediments of an Amazonian reservoir. *Biogeosciences Discussions*, *17*, 1495–1505. https://doi.org/10.5194/bg-2019-246

R Core Team. (2018). R: A language and environment for statistical computing. Vienna, Austria: R Foundation for Statistical Computing. Retrieved from https://www.r-project.org/

Raymond, P. A., Hartmann, J., Lauerwald, R., Sobek, S., McDonald, C., Hoover, M., et al. (2013). Global carbon dioxide emissions from inland waters. *Nature*, *503*(7476), 355–359. https://doi.org/10.1038/nature12760

Richey, J. E., Melack, J. M., Aufdenkampe, A. K., Ballester, V. M., & Hess, L. L. (2002). Outgassing from Amazonian rivers and wetlands as a large tropical source of atmospheric CO2. *Nature*, *416*(6881), 617–620. https://doi.org/10.1038/416617a

Rocher-Ros, G., Sponseller, R. A., Lidberg, W., Mörth, C., & Giesler, R. (2019). Landscape process domains drive patterns of CO2 evasion from river networks. *Limnology and Oceanography Letters*, *4*, 87–95. https://doi.org/10.1002/lol2.10108

Roland, F., Vidal, L. O., Pacheco, F. S., Barros, N. O., Assireu, A., Ometto, J. P. H. B., et al. (2010). Variability of carbon dioxide flux from tropical (Cerrado) hydroelectric reservoirs. *Aquatic Sciences*, *72*(3), 283–293. https://doi.org/10.1007/s00027-010-0140-0

Rõõm, E. I., Ñges, P., Feldmann, T., Tuvikene, L., Kisand, A., Teearu, H., & Ñges, T. (2014). Years are not brothers: Two-year comparison of greenhouse gas fluxes in large shallow Lake Vrtsjärv, Estonia. *Journal of Hydrology*, *519*, 1594–1606. https://doi.org/10.1016/j.jhydrol.2014.09.011

Serça, D., Deshmukh, C., Pighini, S., Oudone, P., Vongkhamsao, A., Guédant, P., et al. (2016). Nam Theun 2 Reservoir four years after commissioning: significance of drawdown methane emissions and other pathways. *Hydroécologie Appliquée*, *19*, 119–146. https://doi.org/10.1051/hydro/2016001

Sieczko, A. K., Thanh, N., Schenk, J., Pajala, G., Rudberg, D., Sawakuchi, H. O., & Bastviken, D. (2020). Diel variability of methane emissions from lakes. *Proceedings of the National Academy of Sciences*, *117*(35), 21488–21494. https://doi.org/10.1073/pnas.2006024117

Smith, S. V. (1985). Physical, chemical and biological characteristics of CO2 gas flux across the air-water interface. *Plant, Cell & Environment*, *8*(6), 387–398. https://doi.org/10.1111/j.1365-3040.1985.tb01674.x

Sobek, S., Delsontro, T., Wongfun, N., & Wehrli, B. (2012). Extreme organic carbon burial fuels intense methane bubbling in a temperate reservoir. *Geophysical Research Letters*, *39*(1), 2–5. https://doi.org/10.1029/2011GL050144

Sobol, I. M. (2001). Global sensitivity indices for nonlinear mathematical models and their Monte Carlo estimates. *Mathematics and Computers in Simulation*, *55*, 271–280. https://doi.org/10.1016/S0378-4754(00)00270-6

Teodoru, C. R., Bastien, J., Bonneville, M. C., Del Giorgio, P. A., Demarty, M., Garneau, M., et al. (2012). The net carbon footprint of a newly created boreal hydroelectric reservoir. *Global Biogeochemical Cycles*, *26*(2), 1–14. https://doi.org/10.1029/2011GB004187

Thottathil, S. D., Reis, P. C. J., del Giorgio, P. A., & Prairie, Y. T. (2018). The Extent and Regulation of Summer Methane Oxidation in Northern Lakes. *Journal of Geophysical Research: Biogeosciences*, *123*(10), 3216–3230. https://doi.org/10.1029/2018JG004464

Tranvik, L. J., Downing, J. A., Cotner, J. B., Loiselle, S. A., Striegl, R. G., Ballatore, T. J., et al. (2009). Lakes and reservoirs as regulators of carbon cycling and climate. *Limnology and Oceanography*, *54*, 2298–2314. https://doi.org/10.4319/lo.2009.54.6_part_2.2298

Vachon, D., & Prairie, Y. T. (2013). The ecosystem size and shape dependence of gas transfer velocity versus wind speed relationships in lakes. *Canadian Journal of Fisheries and Aquatic Sciences*, *70*(12), 1757–1764. https://doi.org/10.1139/cjfas-2013-0241

Wang, F., Maberly, S. C., Wang, B., & Liang, X. (2018). Effects of dams on riverine biogeochemical cycling and ecology. *Inland Waters*, *8*(2), 130–140. https://doi.org/10.1080/20442041.2018.1469335

Wanninkhof, R. (1992). Relationship Between Wind Speed and Gas Exchange Over the Ocean. *Journal of Geophysical Research*, *97*(92), 7373–7382.

Wik, M., Thornton, B. F., Bastviken, D., Uhlbäck, J., & Crill, P. M. (2016). Biased sampling of methane release from northern lakes: A problem for extrapolation. *Geophysical Research Letters*, *43*, 1256–1262. https://doi.org/10.1002/2015GL066501.Received

Wilkinson, J., Maeck, A., Alshboul, Z., & Lorke, A. (2015). Continuous Seasonal River Ebullition Measurements Linked to Sediment Methane Formation. *Environmental Science and Technology*, *49*(22), 13121–13129. https://doi.org/10.1021/acs.est.5b01525

Winton, R. S., Calamita, E., & Wehrli, B. (2019). Reviews and syntheses: Dams, water quality and tropical reservoir stratification. *Biogeosciences*, *16*(8), 1657–1671. https://doi.org/10.5194/bg-16-1657-2019

Xiao, Q., Zhang, M., Hu, Z., Gao, Y., Hu, C., Liu, C., et al. (2017). Spatial variations of methane emission in a large shallow eutrophic lake in subtropical climate. *Journal of Geophysical Research: Biogeosciences*, *122*(7), 1597–1614. https://doi.org/10.1002/2017JG003805

Yang, J., Liu, J., Hu, X., Li, X., Wang, Y., & Li, H. (2013). Effect of water table level on CO2,CH4 and N2O emissions in a freshwater marsh of Northeast China. *Soil Biology and Biochemistry*, *61*, 52–60. https://doi.org/10.1016/j.soilbio.2013.02.009

Yvon-Durocher, G., Allen, A. P., Bastviken, D., Conrad, R., Gudasz, C., St-Pierre, A., et al. (2014). Methane fluxes show consistent temperature dependence across

microbial to ecosystem scales. *Nature*, *507*(7493), 488–491. https://doi.org/10.1038/nature13164

Zappa, C. J., McGillis, W. R., Raymond, P. A., Edson, J. B., Hintsa, E. J., Zemmelink, H. J., et al. (2007). Environmental turbulent mixing controls on air-water gas exchange in marine and aquatic systems. *Geophysical Research Letters*, *34*(10), 1–6. https://doi.org/10.1029/2006GL028790

Zarfl, C., Lumsdon, A. E., Berlekamp, J., Tydecks, L., & Tockner, K. (2015). A global boom in hydropower dam construction. *Aquatic Sciences*, *77*(1), 161–170. https://doi.org/10.1007/s00027-014-0377-0

Supporting information

Hotspots of diffusive CO_2 and CH_4 emission from tropical reservoirs shift through time

José R. Paranaíba[1,2]✉, Nathan Barros[1], Rafael M. Almeida[3], Annika Linkhorst[2], Raquel Mendonça[1], Roseilson do Vale[4], Fábio Roland[1], Sebastian Sobek[2]

[1] Institute of Biological Science, Federal University of Juiz de Fora, Minas Gerais 36036900, Brazil.

[2] Department of Ecology and Genetics, Limnology, Uppsala University, 75236 Uppsala, Sweden.

[3] Department of Ecology and Evolutionary Biology, Cornell University, 14850, USA.

[4] Department of Atmospheric Science, Federal University of West of Pará, Pará 68040070, Brazil.

Supporting information

26 pages, with 15 figures and 9 tables.

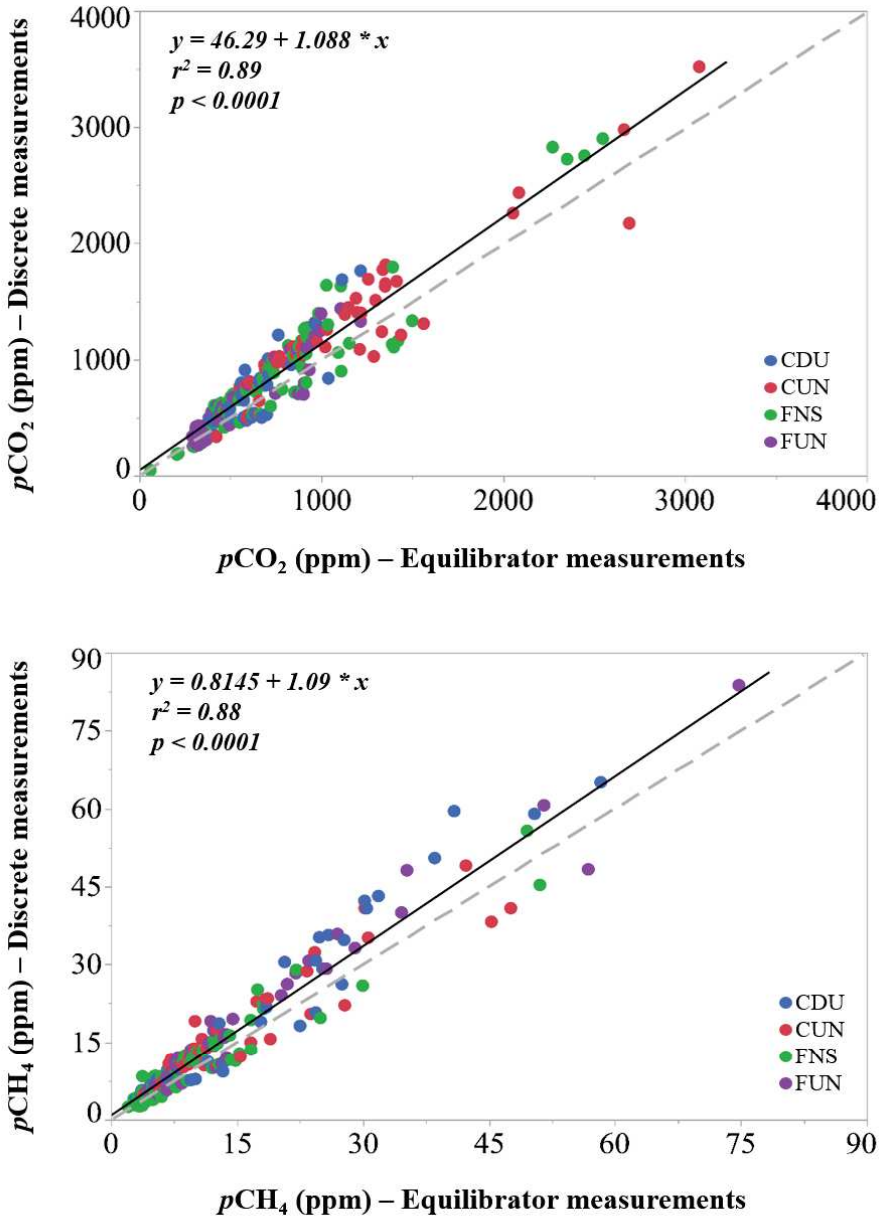

Figure S1: Comparison of the CO_2 (upper) and CH_4 (bottom) partial pressure values measured in surface waters by discrete (y-axis) and continuous measurements (x-axis) in Chapéu D'Úvas (CDU: blue), Curuá-Una (CUN: red), Furnas (FNS: green), and Funil (FUN: purple). The solid black line represents the fit line and the dashed grey line represents the 1:1 line.

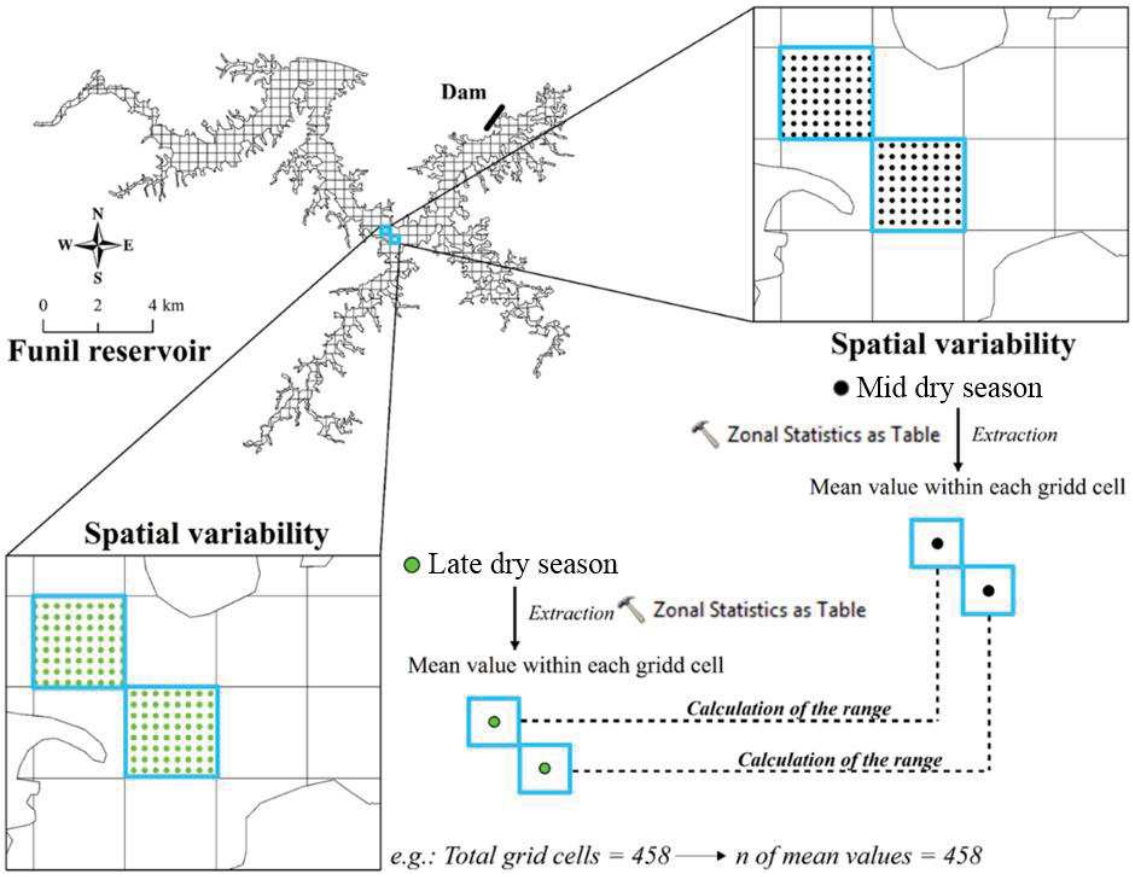

Figure S2: Schematic diagram of the data processing procedure, as described in the section "Data analyses and statistical procedures". Spatially resolved data derived from interpolation (points) are averaged over the grid cell area, and the difference in mean grid cell flux between seasons (green: late dry season; black: mid dry season) is calculated for each grid cell and named as between-season range.

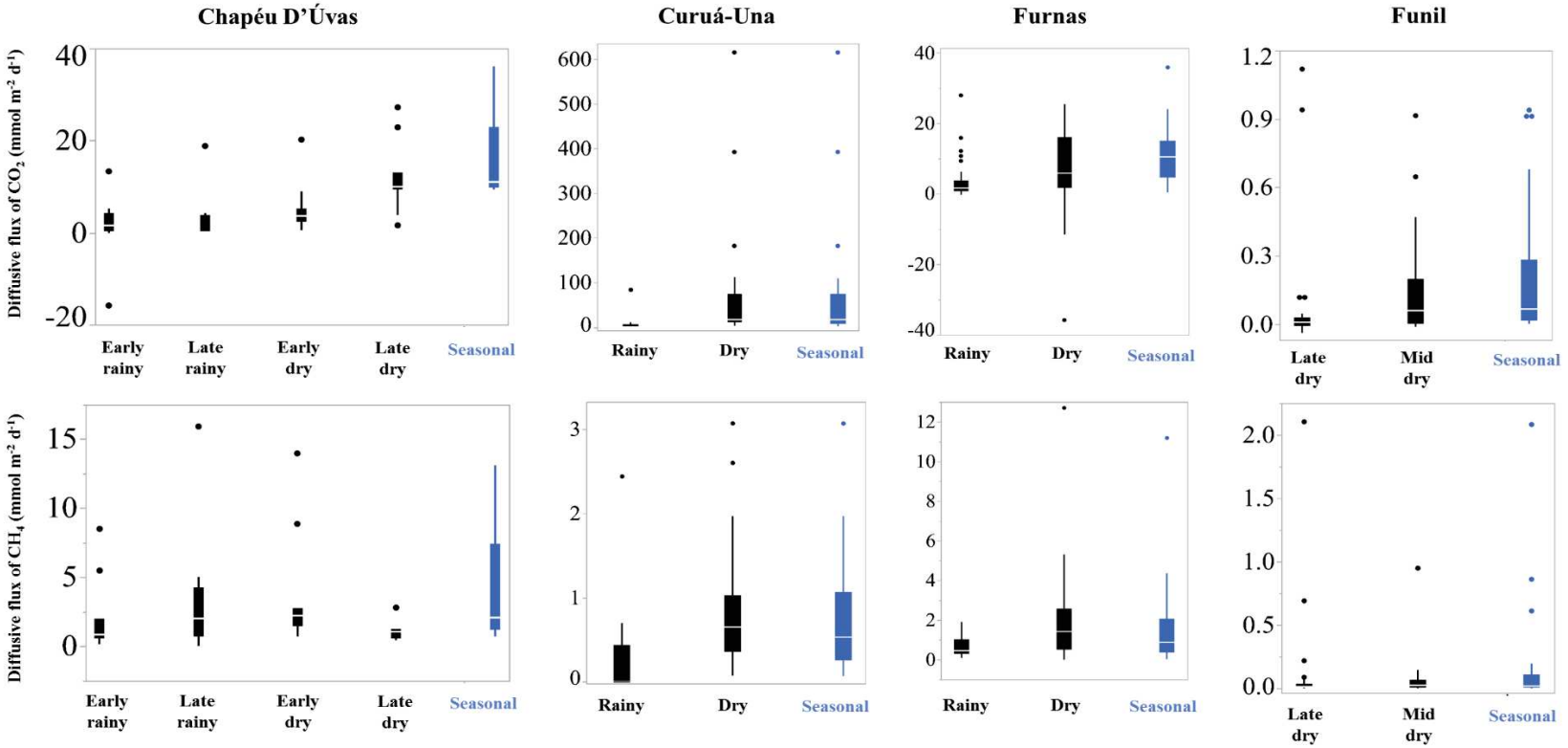

Figure S3: Distribution of direct measurements of the diffusive CO_2 (upper) and CH_4 (bottom) flux in Chapéu D'Úvas (CDU), Curuá-Una (CUN), Furnas (FNS), and Funil (FUN) across different hydrological seasons. The black boxes show the within-reservoir variability at each sampling occasion, represented by data measure in situ and extracted for each grid cell. The blue boxes represent the between-season range calculated for each grid cell. This figure corresponds to Figure 3 of the main manuscript on which it was based on interpolated data.

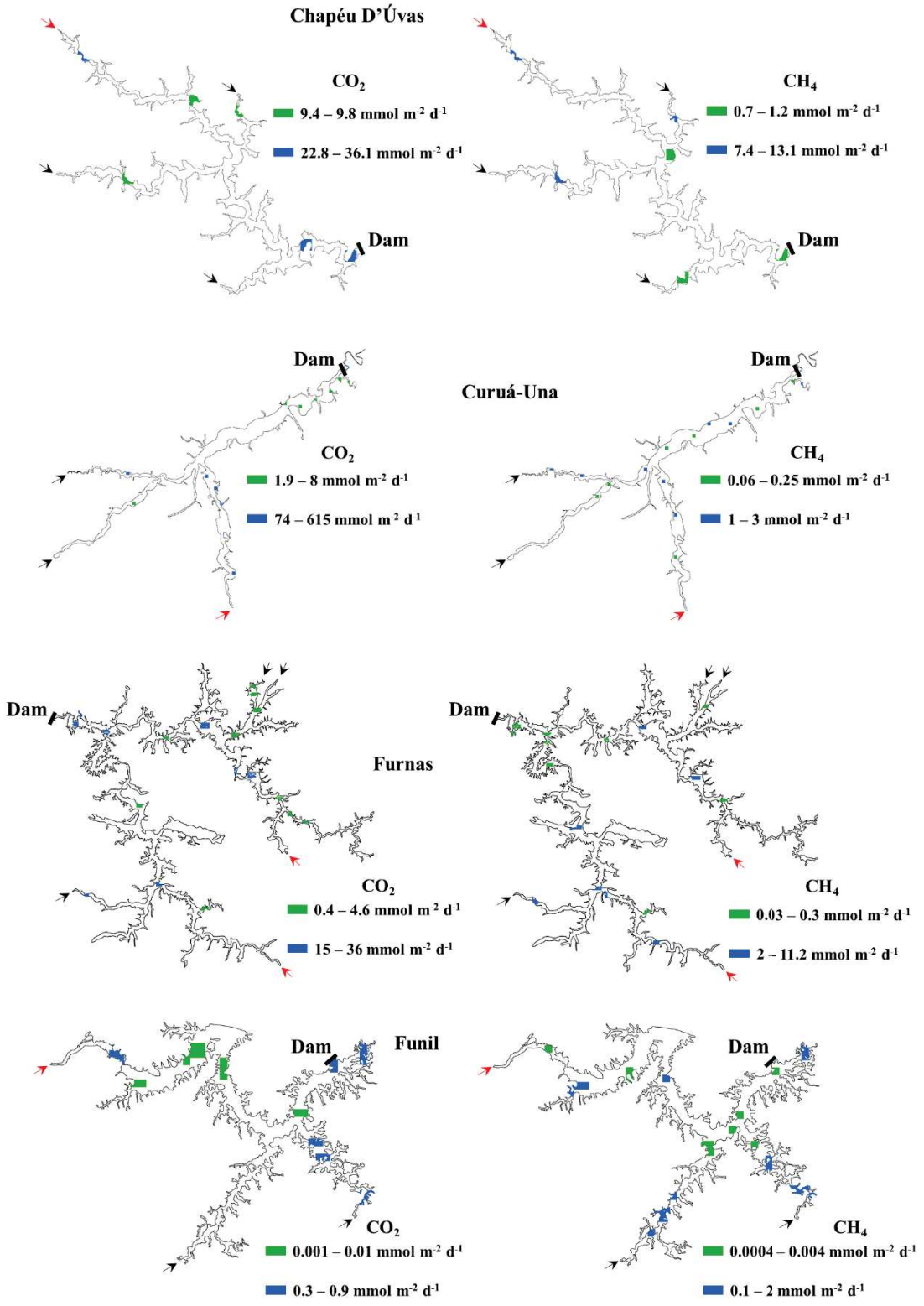

Figure S4: Spatial distribution of the seasonal variability in directly measured diffusive CO_2 and CH_4 fluxes in Chapéu D'Úvas (CDU), Curuá-Una (CUN), Furnas (FNS), and Funil (FUN). The green areas had low between-season difference (<Q_1 in the distribution

of seasonal difference of all grid cells, as shown in the blue boxes in Figure S3), and blue areas had a high seasonal difference (>Q_3). Areas without color represent grid cells within the interquartile range of seasonal difference (>Q_1 and <Q_3). The red arrows indicate where the main rivers forming the reservoirs are located, with the path from the beginning of the river entrance towards the dam corresponding to the location of the relict river bed (i.e. main channel). The black arrows indicate where additional tributaries enter the reservoirs. The black houses represent riverside communities in CDU, CUN, and FNS. There are no riverside communities in the vicinity of FUN. This figure corresponds to Figure 4 of the main manuscript on which it was based on interpolated data.

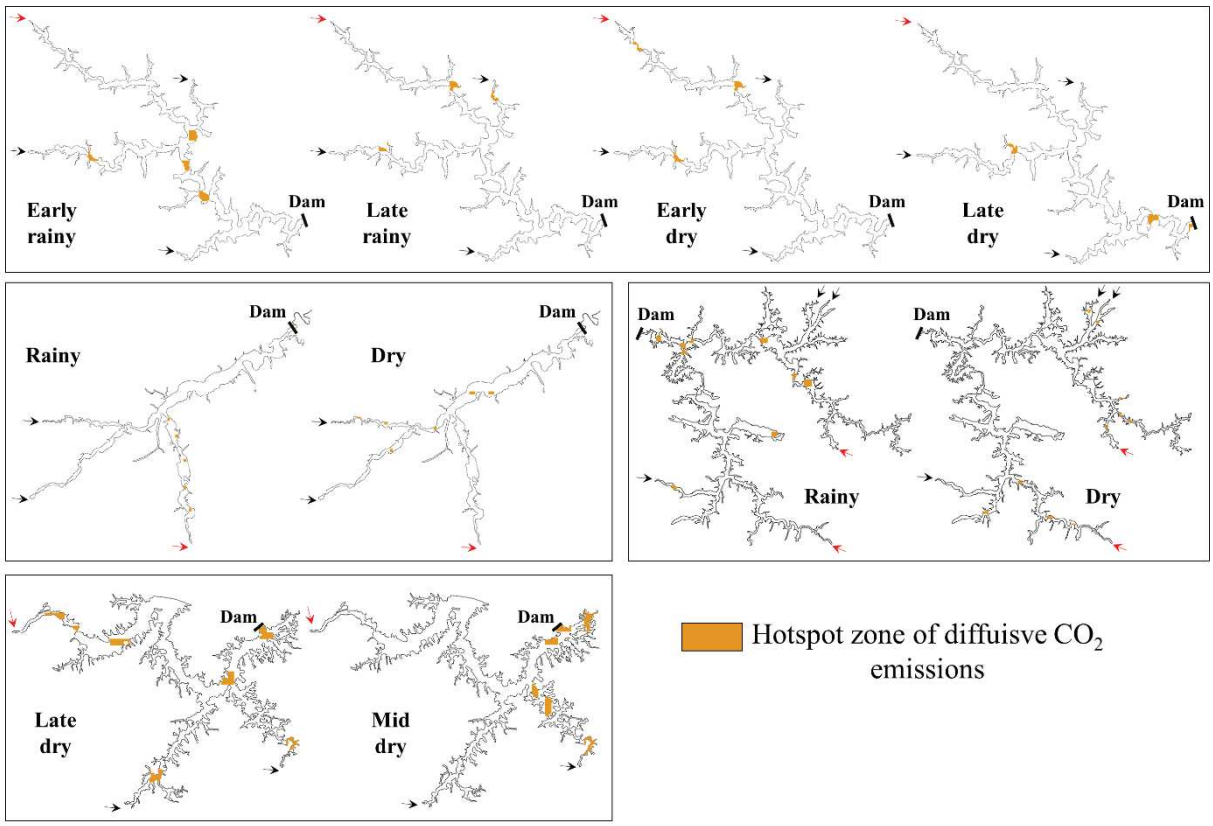

Figure S5: Spatial changes in hotspot zones for directly measured diffusive CO_2 emission (orange zones) across different hydrological seasons in Chapéu D'Úvas (CDU), Curuá-Una (CUN), Furnas (FNS), and Funil (FUN). The red arrows indicate where the main rivers forming the reservoirs are located, with the path from the beginning of the river entrance towards the dam corresponding to the location of the relict river bed (i.e. main channel). The black arrows indicate where additional tributaries enter the reservoirs. Hotspot zones are defined as the reservoir areas comprising the upper quartile containing 25% of the grid cells with highest diffusive CO_2 fluxes at a given sampling occasion. This figure corresponds to Figure 5 of the main manuscript on which it was based on interpolated data.

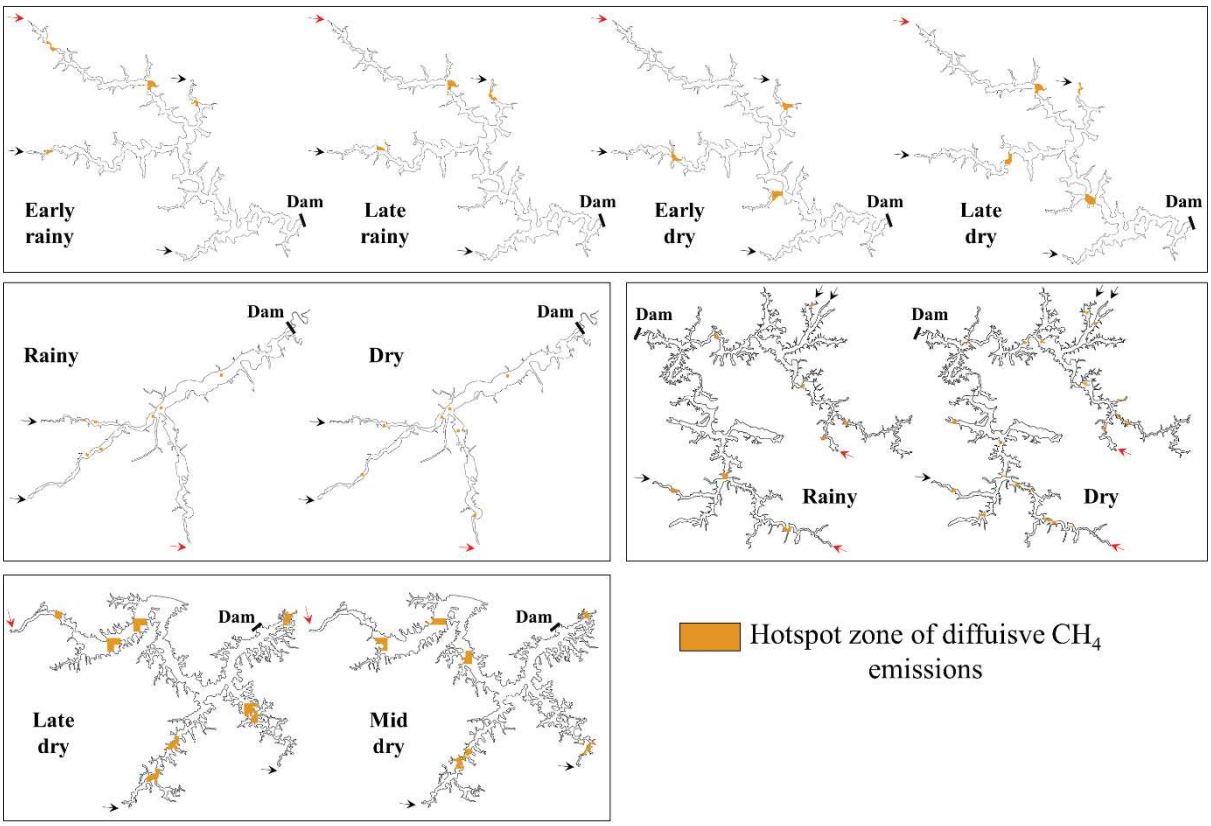

Figure S6: Spatial changes in hotspot zones for directly measured diffusive CH_4 emission (orange zones) across different hydrological seasons in Chapéu D'Úvas (CDU), Curuá-Una (CUN), Furnas (FNS), and Funil (FUN). The red arrows indicate where the main rivers forming the reservoirs are located, with the path from the beginning of the river entrance towards the dam corresponding to the location of the relict river bed (i.e. main channel). The black arrows indicate where additional tributaries enter the reservoirs. Hotspot zones are defined as the reservoir areas comprising the upper quartile containing 25% of the grid cells with highest diffusive CH_4 fluxes at a given sampling occasion. This figure corresponds to Figure 6 of the main manuscript on which it was based on interpolated data.

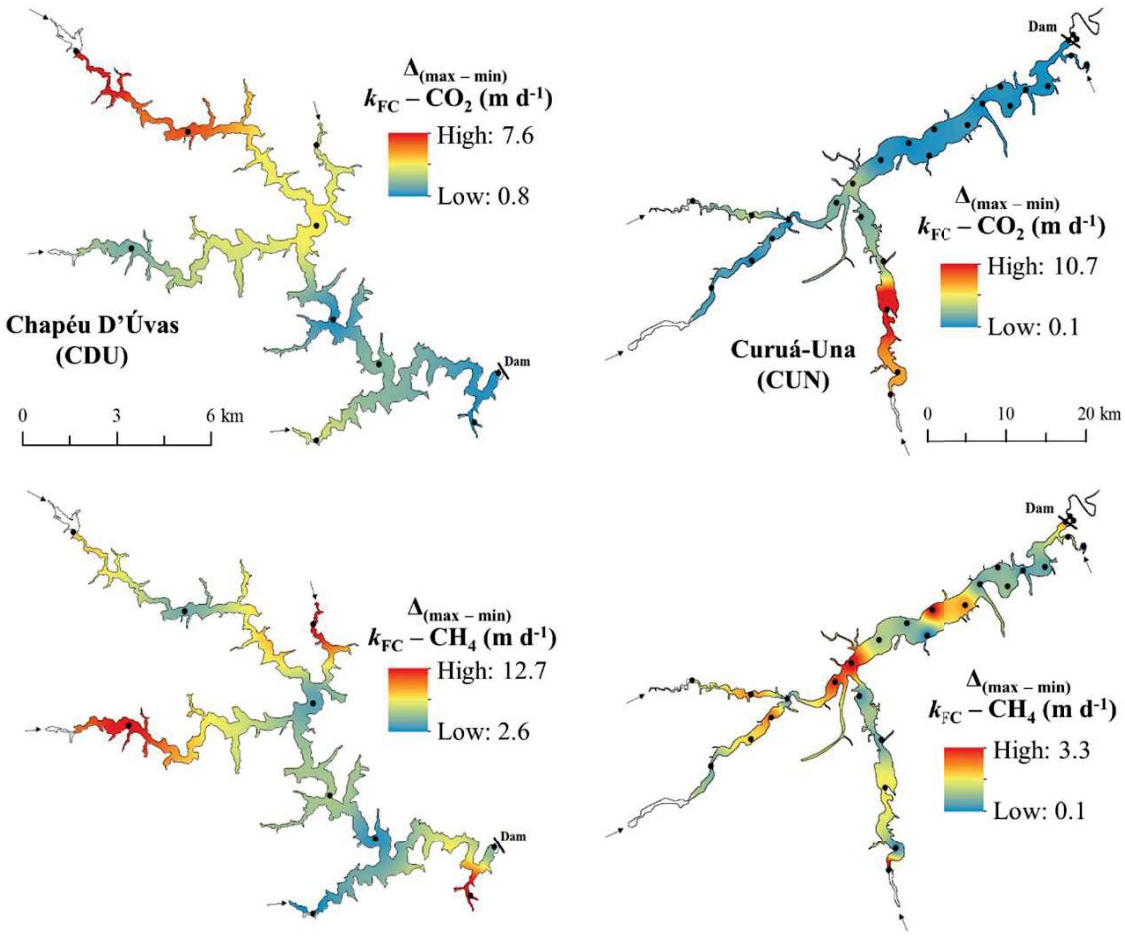

Figure S7: Variability of gas exchange velocity between seasons in Chapéu D'Úvas (CDU) and Curuá-Una (CUN). IDW interpolation of the differences between $k_{FC} - CO_2$ (upper) and $k_{FC} - CH_4$ (bottom) calculated at each sampling site in CDU and CUN across hydrological seasons. The black arrows on the maps indicate major river inflows. Black dots represent the sampling sites of floating chambers and discrete samples.

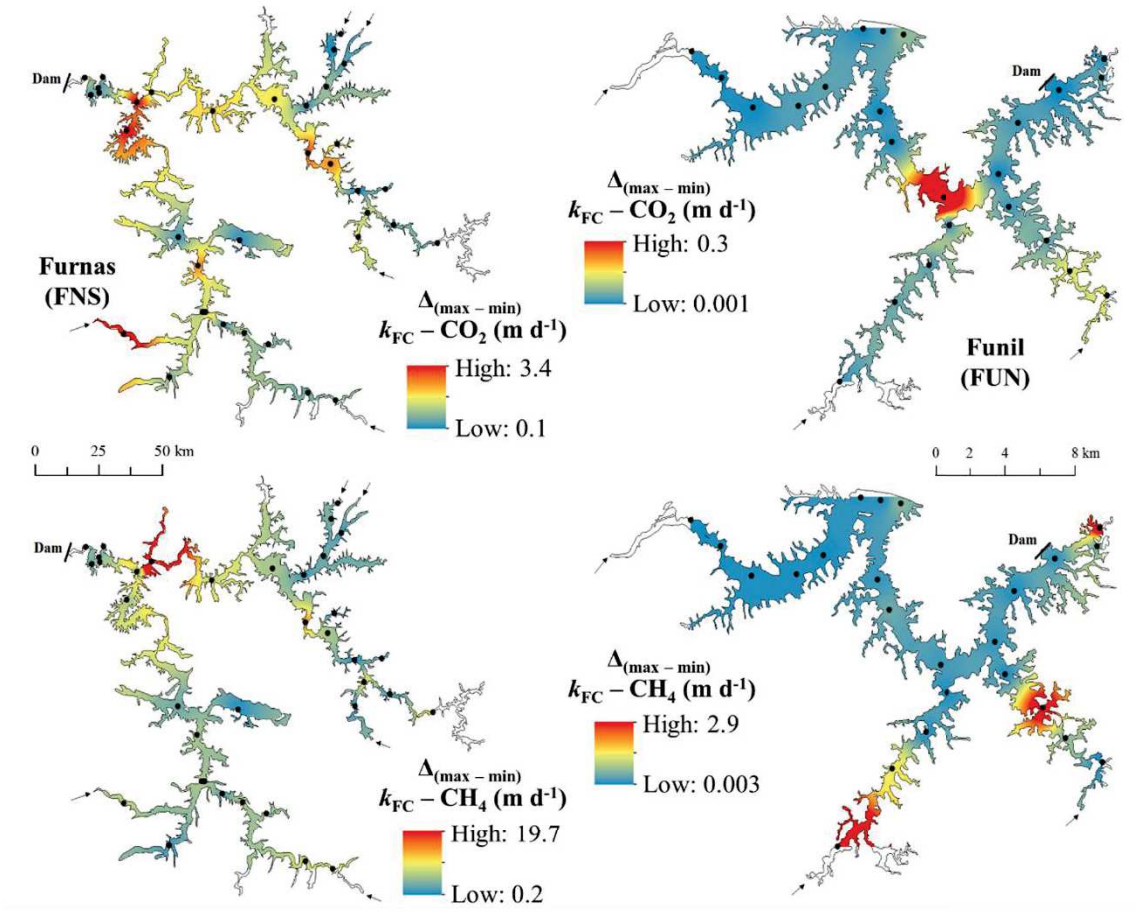

Figure S8: Variability of gas exchange velocity between seasons in Furnas (FNS) and Funil (FUN). IDW interpolation of the differences between $k_{FC} - CO_2$ (upper) and $k_{FC} - CH_4$ (bottom) calculated at each sampling site in FNS and FUN across hydrological seasons. The black arrows on the maps indicate major river inflows. Black dots represent the sampling sites of floating chambers and discrete samples.

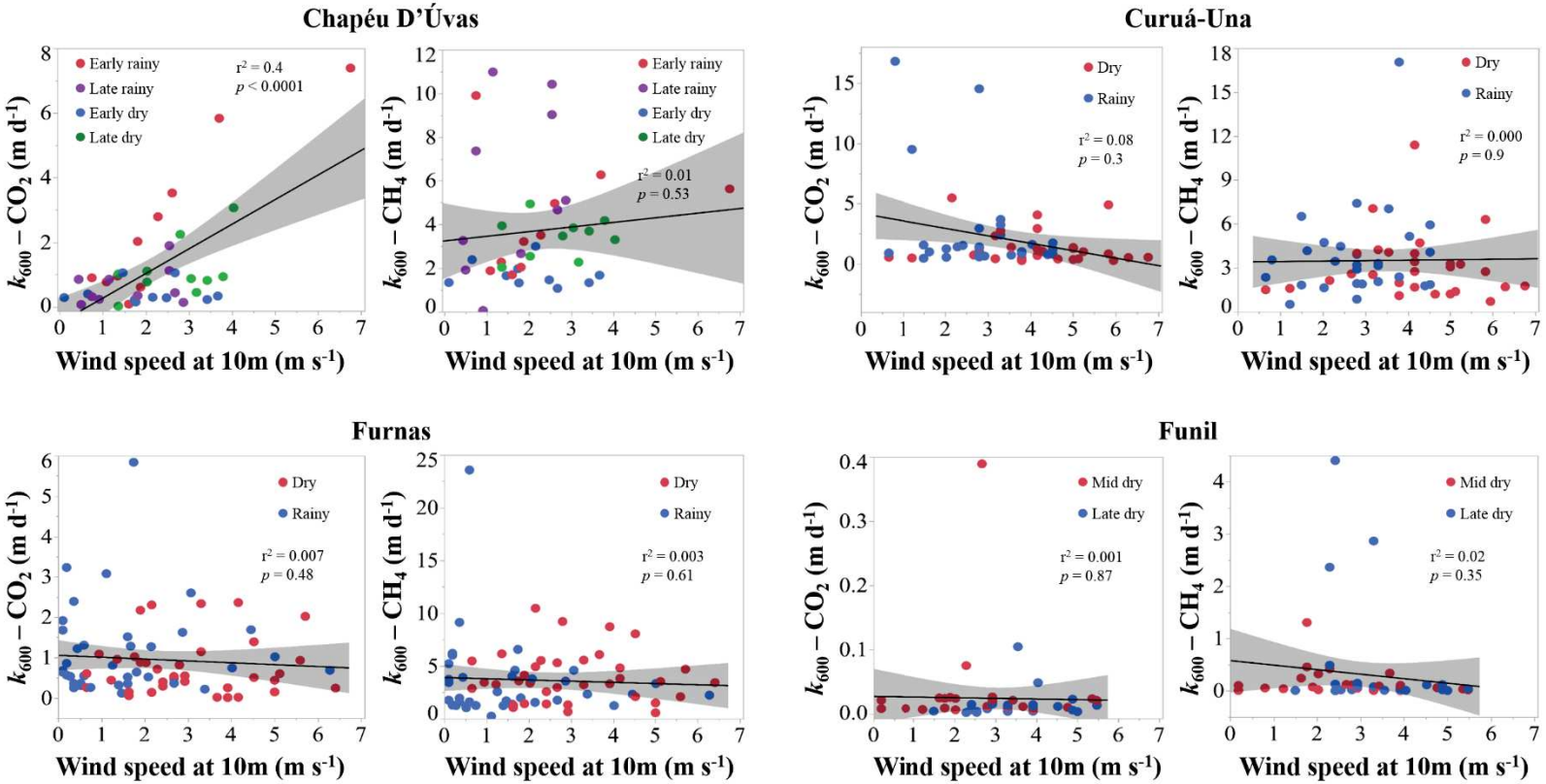

Figure S9: Relationships between wind speed (m s^{-1}) and k_{600} for CO_2 and CH_4 (m d^{-1}) in Chapéu D'Úvas (CDU), Curuá-Una (CUN), Furnas (FNS), and Funil (FUN) across different hydrological seasons. Every point represents the mean of 3 floating chamber measurements.

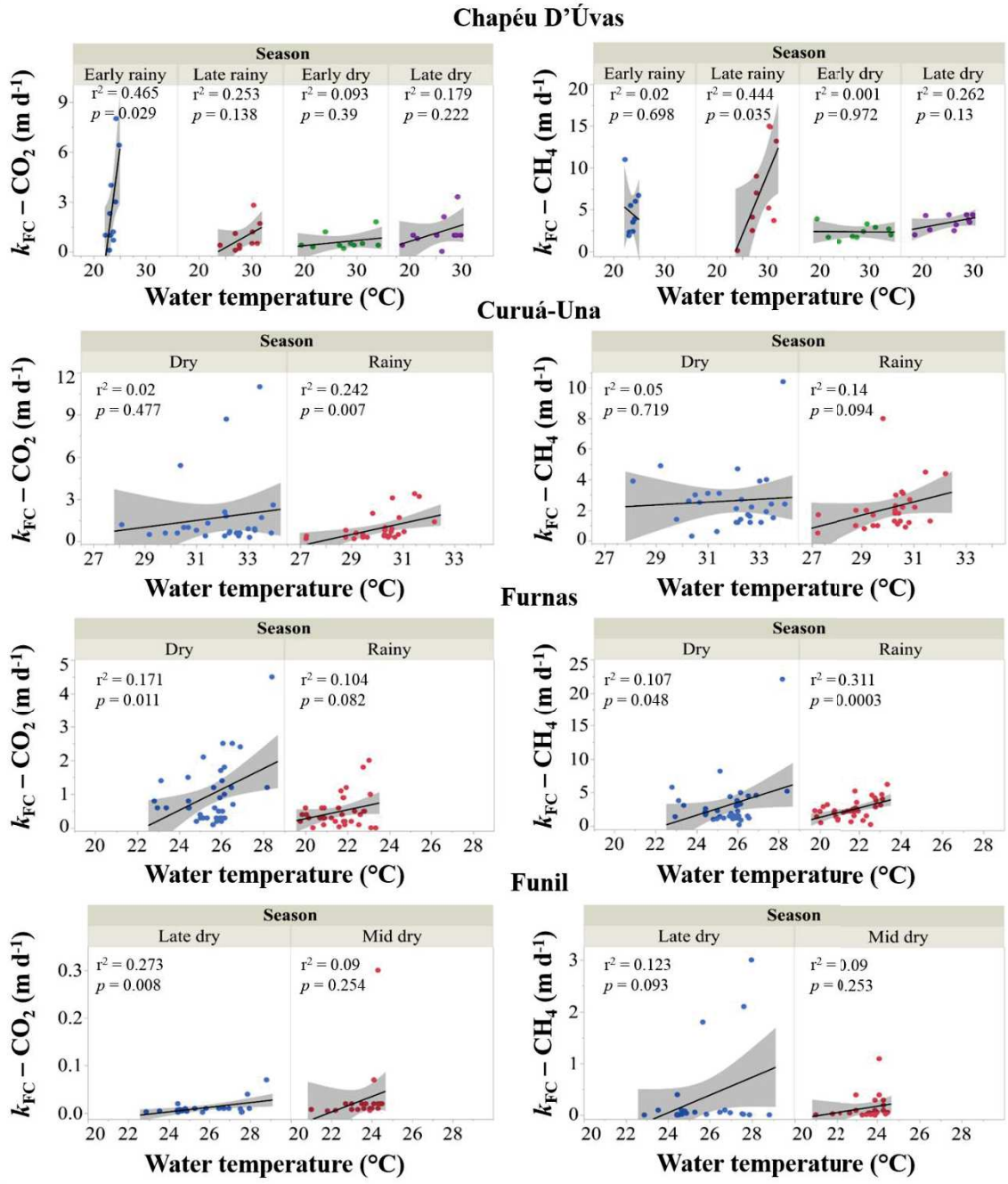

Figure S10: Relationships between water temperature (°C) and k_{FC} for CO_2 and CH_4 (m d^{-1}) in Chapéu D'Úvas (CDU), Curuá-Una (CUN), Furnas (FNS), and Funil (FUN) across different hydrological seasons. Every point represents the mean of 3 measurements.

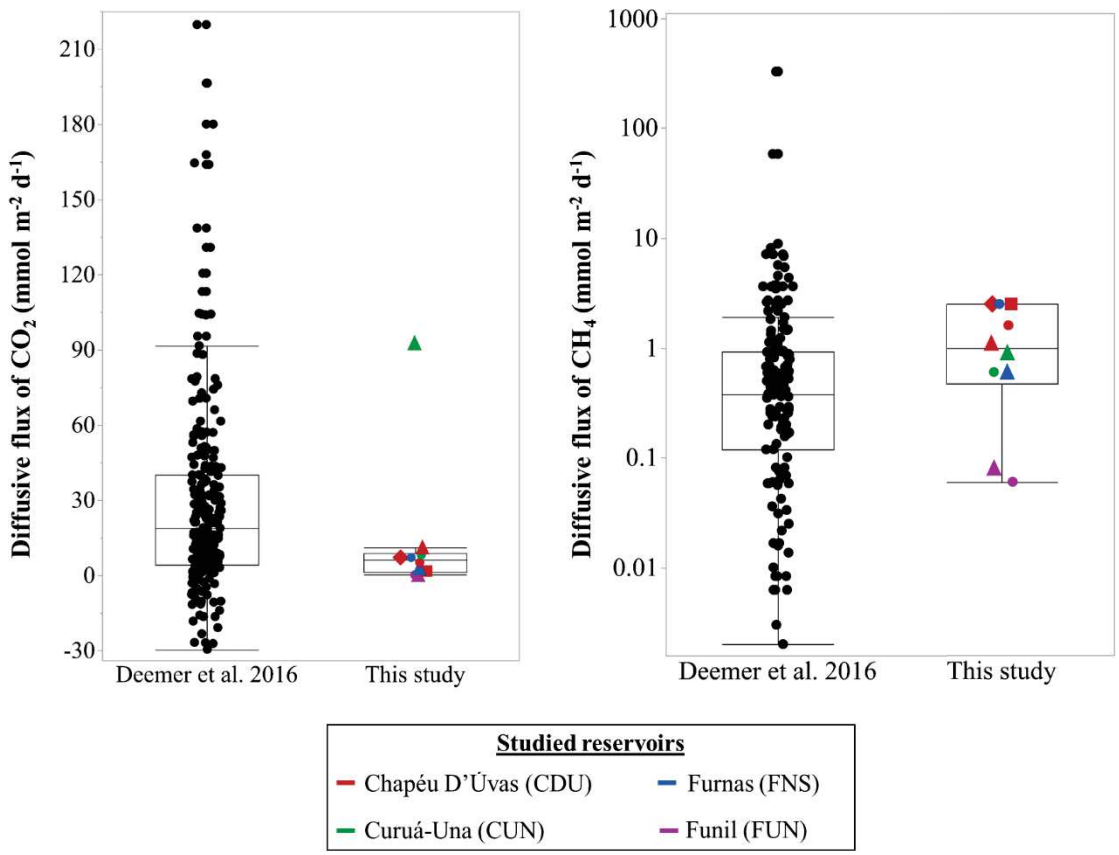

Figure S11: Comparison of the average diffusive CO_2 and CH_4 fluxes (mmol m^{-2} d^{-1}) in Chapéu D'Úvas (CDU: red), Curuá-Una (CUN: green), Furnas (FNS: blue), and Funil (FUN: purple) across hydrologically different seasons with the average diffusive CO_2 and CH_4 fluxes (mmol m^{-2} d^{-1}) from the water surface of 228 reservoirs by Deemer et al. (2016) (black circles). The y-axis of the diffusive flux of CH_4 is shown as logarithmic scale.

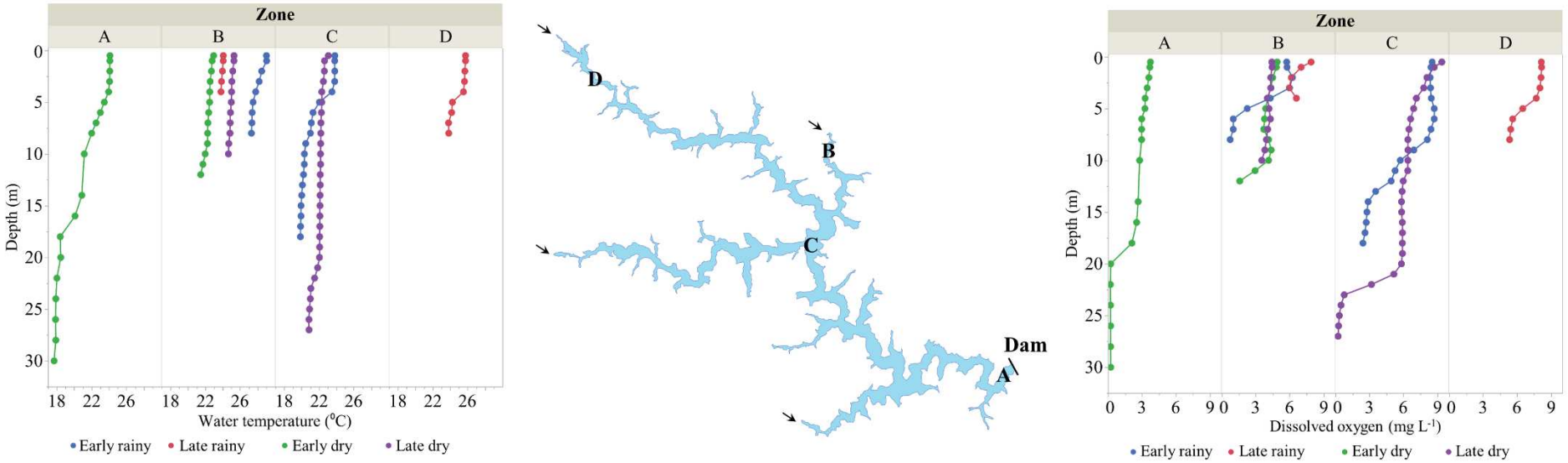

Figure S12: Water temperature (^{0}C) and dissolved oxygen (mg L^{-1}) profiles in different zones (A, B, C, and D) of Chapéu D'Úvas (CDU) reservoir across the hydrological seasons (early rainy: blue; late rainy: red; early dry: green; and late dry: purple). The black arrows indicate river inflow areas in the reservoir.

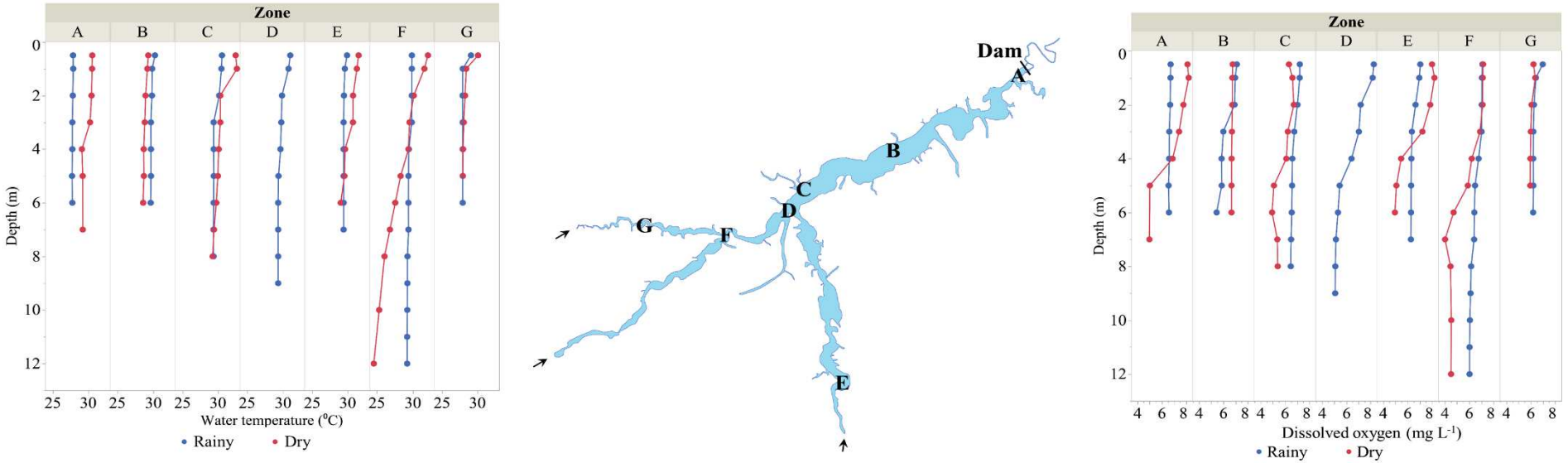

Figure S13: Water temperature (°C) and dissolved oxygen (mg L^{-1}) profiles in different zones (A, B, C, D, E, F, and G) of Curuá-Una (CUN) reservoir across the hydrological seasons (rainy: blue; dry: red). The black arrows indicate river inflow areas in the reservoir.

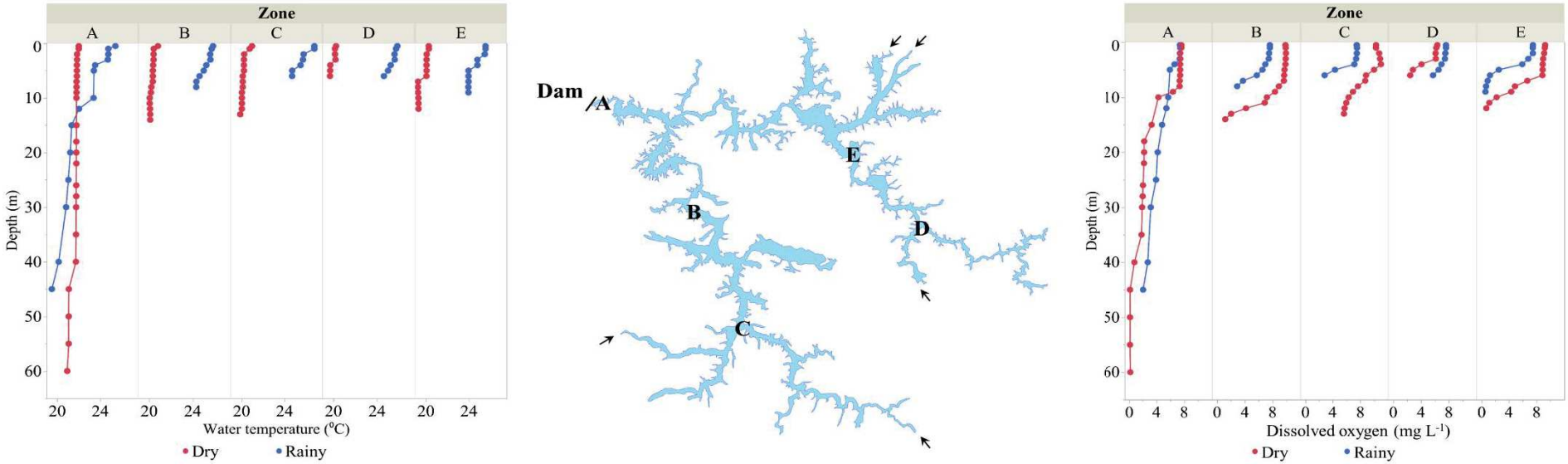

Figure S14: Water temperature (°C) and dissolved oxygen (mg L^{-1}) profiles in different zones (A, B, C, D, and E) of Furnas (FNS) reservoir across the hydrological seasons (rainy: blue; dry: red). The black arrows indicate river inflow areas in the reservoir.

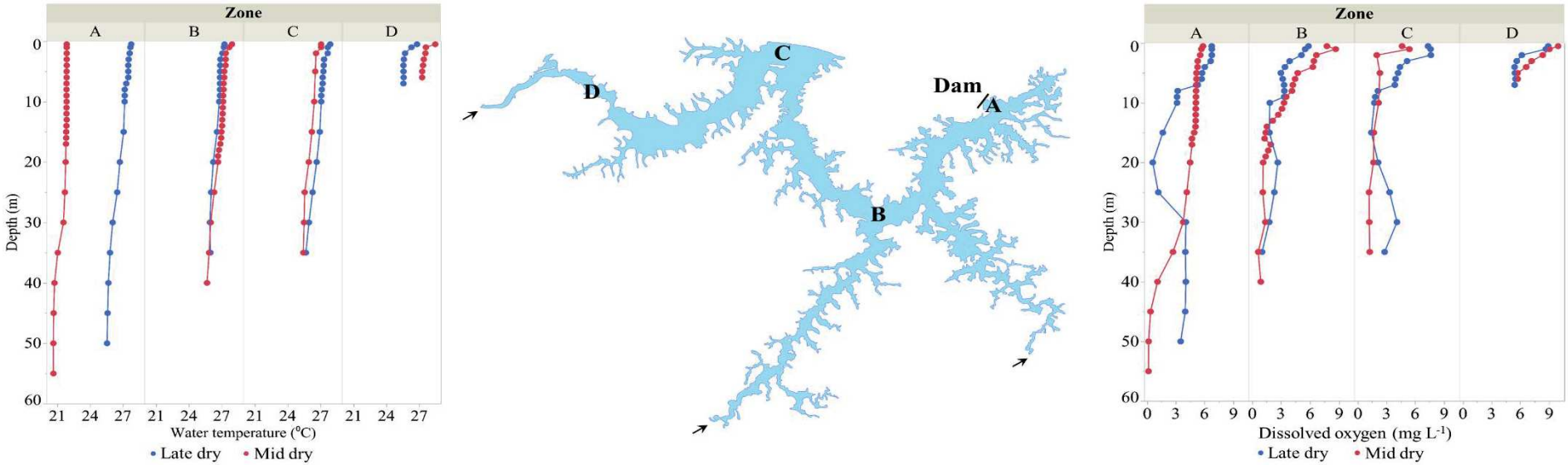

Figure S15: Water temperature (°C) and dissolved oxygen (mg L^{-1}) profiles in different zones (A, B, C, and D) of Funil (FUN) reservoir across the hydrological seasons (late dry: blue; mid dry: red). The black arrows indicate river inflow areas in the reservoir.

Methods

Table S1: Characteristics of the reservoirs Chapéu D'Úvas (CDU), Curuá-Una (CUN), Furnas (FNS) and Funil (FUN).

	CDU	**CUN**	**FNS**	**FUN**
Coordinates	S 21^0 33' W 43^0 35'	S 2^0 50' W 54^0 18'	S 20^0 39' W 46^0 18'	S 22^0 31' W 44^0 34'
Biome	Atlantic Forest	Amazon	Cerrado (Savannah)	Atlantic Forest
Year of operation	1994	1977	1963	1969
Reservoir use	Water supply	Hydroelectricity	Hydroelectricity	Hydroelectricity
Trophic state	Oligotrophic	Oligotrophic	Mesotrophic (northern arm) Eutrophic (southern arm)	Eutrophic
Surface water area (km^2)	12	72	1342	40
Watershed area (km^2)	316	15300	51773	16680
Residence time (years)	1.9	0.08	1.38	0.09
Elevation (m)	682	68	755	468
Mean total phosphorus ($\mu g\ L^{-1}$)	12	19	39	34
Mean total nitrogen ($\mu g\ L^{-1}$)	452	661	1204	1278
Annual mean air temperature (°C)	18	28	20	20.5
Annual precipitation (mm)	1600	2200	1126	1805

Table S2: Description of the sampling campaigns carried out in Chapéu D'Úvas (CDU), Curuá-Una (CUN), Furnas (FNS), and Funil (FUN).

Reservoir	Season	Stage of the water level	Year
CDU	Early rainy	Falling water	2015
	Late rainy	Rising water	2015
	Early dry	High stagnant water	2016
	Late dry	Falling water	2016
CUN	Rainy	Rising water	2016
	Dry	Falling water	2017
FNS	Dry	Low stagnant water	2015
	Rainy	Falling water	2016
FUN	Late dry	Falling water	2016
	Mid dry	Falling water	2017

Results and Discussion

Table S3: Average and range values ($\Delta_{(max - min)}$) of CO_2 and CH_4 gas exchange coefficient (k_{FC}; m d^{-1}) at different sampling sites in Chapéu D'Úvas (CDU) during the sampling campaigns (seasons: early rainy, late rainy, early dry, and late dry). Geographical coordinates are expressed as decimal degree, WGS 1984.

Reservoir				k_{FC} - CO_2 (m d^{-1})					k_{FC} - CH_4 (m d^{-1})				
	Site	Lat (D^0)	Lon (D^0)	Early rainy	Late rainy	Early dry	Late dry	$\Delta_{(max - min)}$	Early rainy	Late rainy	Early dry	Late dry	$\Delta_{(max - min)}$
CDU	1	-21.511	-43.630	8	0.4	1.2	0.4	7.6	6	9	1.2	2	7.8
	2	-21.528	-43.603	6.4	1.1	1.8	2.1	5.3	6.7	4.1	2.7	3.2	4
	3	-21.550	-43.572	4	0.5	0.4	1	3.6	5.5	3.7	2	4.4	3.5
	4	-21.532	-43.572	1	2.8	0.4	3.3	2.9	11	14.9	3.3	3.5	11.6
	5	-21.555	-43.617	0.7	1.7	0.4	0.03	1.67	3.5	13.2	1.8	2.5	11.4
	6	-21.571	-43.568	0.1	0.2	0.5	1	0.9	1.9	7	2.9	4.4	5.1
	7	-21.581	-43.557	2.3	0.5	0.5	0.8	1.8	2.3	5.2	2.4	2.6	2.9
	8	-21.598	-43.572	3	0.1	0.2	1	2.9	3.9	2.5	1.7	4.3	2.6
	9	-21.583	-43.528	1.2	0.4	0.3	1	0.9	2.4	0.1	1.7	4.4	4.3
	10	-21.594	-43.534	1	1.2	0.4	1	0.8	2.3	15	3.9	3.8	12.7

Table S4: Average and range values ($\Delta_{(max - min)}$) of CO_2 and CH_4 gas exchange coefficient (k_{FC}; m d^{-1}) at different sites in Curuá-Una (CUN) during the sampling campaigns (seasons: rainy and dry). Geographical coordinates are expressed as decimal degree, WGS 1984.

Reservoir				k_{FC} - CO_2 (m d^{-1})			k_{FC} - CH_4 (m d^{-1})		
	Site	Lat (D^0)	Lon (D^0)	Rainy	Dry	$\Delta_{(max - min)}$	Rainy	Dry	$\Delta_{(max - min)}$
CUN	1	-2.811	-54.297	0.4	0.8	0.4	1.7	3.1	1.4
	2	-2.815	-54.294	0.5	0.7	0.2	1.2	2.7	1.5
	3	-2.816	-54.301	1.7	1.8	0.1	2.7	4.7	2
	4	-2.836	-54.285	0.5	0.6	0.1	1.7	2.2	0.5
	5	-2.828	-54.299	0.5	0.3	0.2	2	1.2	0.8
	6	-2.853	-54.319	0.2	0.4	0.2	0.8	1.2	0.4
	7	-2.856	-54.338	0.4	0.6	0.2	1.3	1.6	0.3
	8	-2.853	-54.359	0.4	0.9	0.5	1.3	1.9	0.6
	9	-2.869	-54.351	0.7	1	0.3	3.2	2.5	0.7
	10	-2.867	-54.375	0.5	0.6	0.1	1.8	1.4	0.4
	11	-2.884	-54.388	0.6	1.2	0.6	2	3.9	1.9
	12	-2.888	-54.418	0.8	0.5	0.3	2.3	4.9	2.6
	13	-2.909	-54.422	1	1.3	0.3	3	3.1	0.1
	14	-2.913	-54.465	0.9	0.6	0.3	2.2	1.4	0.8
	15	-2.899	-54.440	0.7	0.6	0.1	2.2	1.7	0.5
	16	-2.932	-54.489	3.2	0.8	2.4	1.3	4	2.7
	17	-2.958	-54.482	0.3	1.7	1.4	1.8	1.5	0.3
	18	-2.994	-54.462	0.8	2.6	1.8	2	2.4	0.4
	19	-3.033	-54.459	0.3	11	10.7	1	2.4	1.4
	20	-3.084	-54.450	0.2	5.4	5.2	0.5	0.3	0.2
	21	-3.102	-54.456	3.4	8.7	5.3	4.5	1.2	3.3
	22	-2.947	-54.503	2	0.6	1.4	8	10.4	2.4
	23	-2.961	-54.544	0.3	0.4	0.1	1	0.6	0.4
	24	-2.957	-54.576	3.1	0.4	2.7	3.1	1.2	1.9
	25	-2.946	-54.627	0.3	2.1	1.8	0.9	2.1	1.2
	26	-2.976	-54.559	0.3	1	0.7	1	3	2
	27	-2.994	-54.576	0.4	0.6	0.2	1.1	2.6	1.5
	28	-3.016	-54.611	1.4	0.9	0.5	4.4	3.9	0.5

Table S5: Average and range values ($\Delta_{(max - min)}$) of CO_2 and CH_4 gas exchange coefficient (k_{FC}; m d^{-1}) at different sites in Furnas (FNS) during the sampling campaigns (seasons: rainy and dry). Geographical coordinates are expressed as decimal degree, WGS 1984.

Reservoir				k_{FC} - CO_2 (m d^{-1})			k_{FC} - CH_4 (m d^{-1})		
	Site	Lat (D^0)	Lon (D^0)	Rainy	Dry	$\Delta_{(max - min)}$	Rainy	Dry	$\Delta_{(max - min)}$
FNS	1	-20.653	-46.267	0.3	1.4	1.1	2	3.8	1.8
	2	-20.696	-46.252	0.2	0.6	0.4	2.3	1.4	0.9
	3	-20.690	-46.230	0.3	0.8	0.5	2.9	5.8	2.9
	4	-20.678	-46.233	0.6	0.5	0.1	2.2	1.2	1
	5	-20.651	-46.220	0.5	1	0.5	1.7	3.3	1.6
	6	-20.714	-46.131	0.3	2.5	2.2	2.2	0.2	2
	7	-20.689	-46.092	0.2	1.2	1	2.4	22.1	19.7
	8	-20.737	-45.932	1.8	0.5	1.3	4.4	1.5	2.9
	9	-20.706	-45.771	0.2	1.4	1.2	1	3.2	2.2
	10	-20.722	-45.687	0.04	0.3	0.26	0.8	1.5	0.7
	11	-20.617	-45.587	0.6	0.9	0.3	2.4	3	0.6
	12	-20.582	-45.614	0.4	0.3	0.1	2.3	0.9	1.4
	13	-20.543	-45.596	0.5	0.3	0.2	3	1.2	1.8
	14	-20.676	-45.634	0.9	0.3	0.6	2.6	1.4	1.2
	15	-20.841	-45.683	0.2	2.1	1.9	2.9	8.2	5.3
	16	-20.868	-45.624	0.2	1.8	1.6	2.7	5	2.3
	17	-20.818	-45.606	0.5	1.7	1.2	4	3.8	0.2
	18	-20.935	-45.551	0.4	0.3	0.1	1.7	1.2	0.5
	19	-20.931	-45.479	0.3	0.6	0.3	1	1.9	0.9
	20	-20.991	-45.527	0.3	1.2	0.9	1	4.4	3.4
	21	-21.051	-45.551	0.1	1.2	1.1	0.9	1.5	0.6
	22	-21.020	-45.457	0.6	0.2	0.4	1.4	2.2	0.8
	23	-21.066	-45.343	0.4	0.7	0.3	4.8	1.2	3.6
	24	-20.785	-46.158	0.3	2.5	2.2	2.3	4.5	2.2
	25	-21.051	-46.022	0.6	0.3	0.3	1	2.3	1.3
	26	-21.060	-45.862	0.4	0.2	0.2	1.4	1	0.4
	27	-21.123	-45.971	2	0.4	1.6	3.3	1.1	2.2
	28	-21.269	-45.903	0.4	0.1	0.3	0.5	1.5	1
	29	-21.239	-45.959	0.01	0.2	0.19	4.2	1.6	2.6
	30	-21.239	-45.954	0.01	0.3	0.29	3.2	1.1	2.1
	31	-21.239	-45.951	0.006	2.4	2.394	6.4	4.6	1.8
	32	-21.236	-46.164	1.1	4.5	3.4	2.7	5.2	2.5
	33	-21.402	-46.045	1.2	0.6	0.6	2.4	3.1	0.7
	34	-21.291	-45.850	0.1	0.8	0.7	0.4	2.6	2.2
	35	-21.319	-45.787	0.1	0.6	0.5	3.7	1.7	2
	36	-21.441	-45.682	1	0.6	0.4	4.9	2	2.9
	37	-21.460	-45.610	0.9	1.5	0.6	5.4	2.1	3.3

Table S6: Average and range values ($\Delta_{(max - min)}$) of CO_2 and CH_4 gas exchange coefficient (k_{FC}; m d^{-1}) at different sites in Funil (FUN) during the sampling campaigns (seasons: late dry and mid dry). Geographical coordinates are expressed as decimal degree, WGS 1984.

Reservoir				k_{FC} - CO_2 (m d^{-1})			k_{FC} - CH_4 (m d^{-1})		
	Site	Lat (D^0)	Lon (D^0)	Late dry	Mid dry	$\Delta_{(max - min)}$	Late dry	Mid dry	$\Delta_{(max - min)}$
FUN	1	-22.518	-44.691	0.004	0.008	0.004	0.02	0.01	0.01
	2	-22.526	-44.681	0.007	0.005	0.002	0.005	0.03	0.025
	3	-22.536	-44.670	0.004	0.006	0.002	0.01	0.04	0.03
	4	-22.535	-44.654	0.007	0.02	0.013	0.02	0.05	0.03
	5	-22.529	-44.645	0.004	0.02	0.016	0.04	0.02	0.02
	6	-22.510	-44.632	0.008	0.01	0.002	0.01	0.05	0.04
	7	-22.511	-44.625	0.02	0.01	0.01	0.02	0.06	0.04
	8	-22.512	-44.618	0.04	0.006	0.034	0.01	0.3	0.29
	9	-22.537	-44.626	0.01	0.007	0.003	0.02	0.1	0.08
	10	-22.547	-44.622	0.005	0.01	0.005	0.1	0.3	0.2
	11	-22.565	-44.604	0.003	0.3	0.297	0.007	0.1	0.093
	12	-22.574	-44.602	0.01	0.02	0.01	0.06	0.03	0.03
	13	-22.587	-44.609	0.005	0.02	0.015	0.1	0.06	0.04
	14	-22.599	-44.621	0.002	0.02	0.018	0.4	1.1	0.7
	15	-22.625	-44.640	0.01	0.02	0.01	3	0.1	2.9
	16	-22.557	-44.585	0.01	0.008	0.002	0.08	0.01	0.07
	17	-22.568	-44.581	0.01	0.02	0.01	0.06	0.02	0.04
	18	-22.579	-44.568	0.002	0.02	0.018	1.8	0.05	1.75
	19	-22.589	-44.560	0.01	0.07	0.06	0.1	0.4	0.3
	20	-22.597	-44.547	0.07	0.01	0.06	0.01	0.007	0.003
	21	-22.541	-44.578	0.01	0.02	0.01	0.05	0.09	0.04
	22	-22.530	-44.564	0.009	0.01	0.001	0.03	0.1	0.07
	23	-22.526	-44.549	0.002	0.02	0.018	0.02	0.2	0.18
	24	-22.520	-44.548	0.003	0.008	0.005	2.1	0.4	1.7

Table S7: Statistical outcomes of the generalized linear mixed model (GLMM) of the gas exchange coefficient (k) values for CO_2 and CH_4 between the spatial variability

campaigns (different hydrological seasons) within and between reservoirs: Chapéu D'Úvas (CDU), Curuá-Una (CUN), Furnas (FNS), and Funil (FUN).

k_{FC} - CO_2			
Comparison	**z value**	**Pr(>|z|)**	
Within reservoirs			
CDU Early rainy x CDU Early dry	3.8	0.0035	**
CDU Late dry x CDU Early dry	1.6	0.8348	
CDU Late dry x CDU Early rainy	-2.2	0.4664	
CDU Late rainy x CDU Early dry	0.001	0.9946	
CDU Late rainy x CDU Early rainy	-2.8	0.1193	
CDU Late rainy x CDU Late dry	0.0	0.9996	
CUN Rainy x CUN Dry	-2.6	0.206	
FNS Rainy x FNS Dry	-3.4	0.0188	*
FUN Mid dry x FUN Late dry	3.6	0.0123	*
Between reservoirs			
CUN Dry x CDU Early dry	31.3	0.0515	.
CUN Dry x CDU Early rainy	-14.5	0.9066	
CUN Dry x CDU Late dry	11.8	0.9733	
CUN Dry x CDU Late rainy	19.9	0.5904	
CUN Rainy x CDU Early dry	12.5	0.9615	
CUN Rainy x CDU Early rainy	-33.3	0.0276	*
CUN Rainy x CDU Late dry	-0.007	0.9994	
CUN Rainy x CDU Late rainy	0.001	1.000	
FNS Dry x CDU Early dry	15.3	0.8729	
FNS Dry x CDU Early rainy	-32.0	0.0414	*
FNS Dry x CDU Late dry	-0.005	1.000	
FNS Dry x CDU Late rainy	0.003	1.000	
FNS Dry x CUN Dry	-24.3	0.2928	
FNS Dry x CUN Rainy	0.003	1.000	
FNS Rainy x CDU Early dry	-0.007	0.9994	
FNS Rainy x CDU Early rainy	-54.4	<0.001	***
FNS Rainy x CDU Late dry	-27.3	0.1522	
FNS Rainy x CDU Late rainy	-18.9	0.6575	
FNS Rainy x CUN Dry	-56.2	<0.001	***
FNS Rainy x CUN Rainy	-28.5	0.1126	
FUN Late dry x CDU Early dry	-118.7	<0.001	***
FUN Late dry x CDU Early rainy	-163.5	<0.001	***
FUN Late dry x CDU Late dry	-137.8	<0.001	***
FUN Late dry x CDU Late rainy	-129.9	<0.001	***
FUN Late dry x CUN Dry	-202.1	<0.001	***
FUN Late dry x CUN Rainy	-177.2	<0.001	***
FUN Late dry x FNS Dry	-191.3	<0.001	***
FUN Late dry x FNS Rainy	-160.8	<0.001	***
FUN Mid dry x CDU Early dry	-91.4	<0.001	***
FUN Mid dry x CDU Early rainy	-136.2	<0.001	***
FUN Mid dry x CDU Late dry	-110.5	<0.001	***
FUN Mid dry x CDU Late rainy	-102.6	<0.001	***
FUN Mid dry x CUN Dry	-165.1	<0.001	***
FUN Mid dry x CUN Rainy	-140.2	<0.001	***
FUN Mid dry x FNS Dry	-152.0	<0.001	***
FUN Mid dry x FNS Rainy	-121.5	<0.001	***

k_{FC} - CH_4			
Comparison	**z value**	**Pr(>|z|)**	
Within reservoirs			
CDU Early rainy x CDU Early dry	1.6	0.82648	
CDU Late dry x CDU Early dry	0.001	0.99262	
CDU Late dry x CDU Early rainy	-0.001	0.99974	
CDU Late rainy x CDU Early dry	2.9	0.11257	
CDU Late rainy x CDU Early rainy	1.2	0.96558	
CDU Late rainy x CDU Late dry	1.9	0.67582	
CUN Rainy x CUN Dry	-0.001	0.99816	
FNS Rainy x FNS Dry	-0.001	0.99581	
FUN Mid dry x FUN Late dry	-3.1	0.06205	.
Between reservoirs			
CUN Dry x CDU Early dry	0.0003	1.000	
CUN Dry x CDU Early rainy	-1.7	0.80231	
CUN Dry x CDU Late dry	-0.001	0.99649	
CUN Dry x CDU Late rainy	-3.2	0.04774	*
CUN Rainy x CDU Early dry	-0.0003	1.000	
CUN Rainy x CDU Early rainy	-2.3	0.39871	
CUN Rainy x CDU Late dry	-1.5	0.89236	
CUN Rainy x CDU Late rainy	-3.8	0.00619	**
FNS Dry x CDU Early dry	0.001	0.99782	
FNS Dry x CDU Early rainy	-1.2	0.96986	
FNS Dry x CDU Late dry	-0.0004	1.000	
FNS Dry x CDU Late rainy	-2.7	0.14827	
FNS Dry x CUN Dry	0.001	0.99914	
FNS Dry x CUN Rainy	1.6	0.83066	
FNS Rainy x CDU Early dry	0.0002	1.000	
FNS Rainy x CDU Early rainy	-1.8	0.72450	
FNS Rainy x CDU Late dry	-0.001	0.99214	
FNS Rainy x CDU Late rainy	-3.3	0.02708	*
FNS Rainy x CUN Dry	-0.0001	1.000	
FNS Rainy x CUN Rainy	0.0008	0.99884	
FUN Late dry x CDU Early dry	-5.7	<0.001	***
FUN Late dry x CDU Early rainy	-7.7	<0.001	***
FUN Late dry x CDU Late dry	-6.9	<0.001	***
FUN Late dry x CDU Late rainy	-9.1	<0.001	***
FUN Late dry x CUN Dry	-8.1	<0.001	***
FUN Late dry x CUN Rainy	-7.4	<0.001	***
FUN Late dry x FNS Dry	-9.4	<0.001	***
FUN Late dry x FNS Rainy	-8.6	<0.001	***
FUN Mid dry x CDU Early dry	-8.1	<0.001	***
FUN Mid dry x CDU Early rainy	-10.0	<0.001	***
FUN Mid dry x CDU Late dry	-9.2	<0.001	***
FUN Mid dry x CDU Late rainy	-11.5	<0.001	***
FUN Mid dry x CUN Dry	-11.3	<0.001	***
FUN Mid dry x CUN Rainy	-10.5	<0.001	***
FUN Mid dry x FNS Dry	-12.7	<0.001	***
FUN Mid dry x FNS Rainy	-11.9	<0.001	***

Table S8: Statistical outcomes of the generalized linear mixed model (GLMM) of the diffusive CO_2 and CH_4 fluxes between the spatial variability campaigns (different hydrological seasons) within and between reservoirs: Chapéu D'Úvas (CDU), Curuá-Una (CUN), Furnas (FNS), and Funil (FUN).

Diffusive flux of CO_2			
Comparison	**z value**	**Pr(>|z|)**	
Within reservoirs			
CDU Early rainy x CDU Early dry	-3.9	0.00377	**
CDU Late dry x CDU Early dry	2.2	0.42374	
CDU Late dry x CDU Early rainy	6.0	<0.001	***
CDU Late rainy x CDU Early dry	-5.6	<0.001	***
CDU Late rainy x CDU Early rainy	-1.8	0.70134	
CDU Late rainy x CDU Late dry	-7.8	<0.001	***
CUN Rainy x CUN Dry	-164.4	<0.001	***
FNS Rainy x FNS Dry	-28.8	<0.001	***
FUN Mid dry x FUN Late dry	2.5	0.23831	
Between reservoirs			
CUN Dry x CDU Early dry	32.9	<0.001	***
CUN Dry x CDU Early rainy	37.9	<0.001	***
CUN Dry x CDU Late dry	30.1	<0.001	***
CUN Dry x CDU Late rainy	40.2	<0.001	***
CUN Rainy x CDU Early dry	-62.9	<0.001	***
CUN Rainy x CDU Early rainy	-57.9	<0.001	***
CUN Rainy x CDU Late dry	-65.7	<0.001	***
CUN Rainy x CDU Late rainy	-55.6	<0.001	***
FNS Dry x CDU Early dry	11.0	<0.001	***
FNS Dry x CDU Early rainy	16.4	<0.001	***
FNS Dry x CDU Late dry	7.9	<0.001	***
FNS Dry x CDU Late rainy	18.8	<0.001	***
FNS Dry x CUN Dry	-52.9	<0.001	***
FNS Dry x CUN Rainy	169.2	<0.001	***
FNS Rainy x CDU Early dry	5.4	<0.001	***
FNS Rainy x CDU Early rainy	10.8	<0.001	***
FNS Rainy x CDU Late dry	2.3	0.31318	
FNS Rainy x CDU Late rainy	13.2	<0.001	***
FNS Rainy x CUN Dry	-64.9	<0.001	***
FNS Rainy x CUN Rainy	157.3	<0.001	***
FUN Late dry x CDU Early dry	-96.6	<0.001	***
FUN Late dry x CDU Early rainy	-92.1	<0.001	***
FUN Late dry x CDU Late dry	-99.2	<0.001	***
FUN Late dry x CDU Late rainy	-90.0	<0.001	***
FUN Late dry x CUN Dry	-191.6	<0.001	***
FUN Late dry x CUN Rainy	-58.4	<0.001	***
FUN Late dry x FNS Dry	-190.7	<0.001	***
FUN Late dry x FNS Rainy	-182.1	<0.001	***
FUN Mid dry x CDU Early dry	-94.8	<0.001	***
FUN Mid dry x CDU Early rainy	-90.2	<0.001	***
FUN Mid dry x CDU Late dry	-97.3	<0.001	***
FUN Mid dry x CDU Late rainy	-88.1	<0.001	***
FUN Mid dry x CUN Dry	-188.8	<0.001	***
FUN Mid dry x CUN Rainy	-55.6	<0.001	***
FUN Mid dry x FNS Dry	-187.3	<0.001	***
FUN Mid dry x FNS Rainy	-178.7	<0.001	***

Diffusive flux of CH_4			
Comparison	**z value**	**Pr(>|z|)**	
Within reservoirs			
CDU Early rainy x CDU Early dry	-20.1	0.533	
CDU Late dry x CDU Early dry	-107.6	<0.001	***
CDU Late dry x CDU Early rainy	-87.5	<0.001	***
CDU Late rainy x CDU Early dry	23.8	0.288	
CDU Late rainy x CDU Early rainy	43.8	<0.001	***
CDU Late rainy x CDU Late dry	131.3	<0.001	***
CUN Rainy x CUN Dry	-113.3	<0.001	***
FNS Rainy x FNS Dry	-1,504.9	<0.001	***
FUN Mid dry x FUN Late dry	-50.5	<0.001	***
Between reservoirs			
CUN Dry x CDU Early dry	-203.9	<0.001	***
CUN Dry x CDU Early rainy	-178.1	<0.001	***
CUN Dry x CDU Late dry	-65.3	<0.001	***
CUN Dry x CDU Late rainy	-234.5	<0.001	***
CUN Rainy x CDU Early dry	-269.9	<0.001	***
CUN Rainy x CDU Early rainy	-244.1	<0.001	***
CUN Rainy x CDU Late dry	-131.3	<0.001	***
CUN Rainy x CDU Late rainy	-300.5	<0.001	***
FNS Dry x CDU Early dry	-23.9	0.279	
FNS Dry x CDU Early rainy	0.0	1.000	
FNS Dry x CDU Late dry	126.8	<0.001	***
FNS Dry x CDU Late rainy	-57.2	<0.001	***
FNS Dry x CUN Dry	422.0	<0.001	***
FNS Dry x CUN Rainy	575.1	<0.001	***
FNS Rainy x CDU Early dry	-317.5	<0.001	***
FNS Rainy x CDU Early rainy	-289.4	<0.001	***
FNS Rainy x CDU Late dry	-166.8	<0.001	***
FNS Rainy x CDU Late rainy	-350.8	<0.001	***
FNS Rainy x CUN Dry	-204.6	<0.001	***
FNS Rainy x CUN Rainy	-51.5	<0.001	***
FUN Late dry x CDU Early dry	-599.6	<0.001	***
FUN Late dry x CDU Early rainy	-575.8	<0.001	***
FUN Late dry x CDU Late dry	-471.8	<0.001	***
FUN Late dry x CDU Late rainy	-627.8	<0.001	***
FUN Late dry x CUN Dry	-621.3	<0.001	***
FUN Late dry x CUN Rainy	-529.4	<0.001	***
FUN Late dry x FNS Dry	-1,042.8	<0.001	***
FUN Late dry x FNS Rainy	-594.7	<0.001	***
FUN Mid dry x CDU Early dry	-638.3	<0.001	***
FUN Mid dry x CDU Early rainy	-614.6	<0.001	***
FUN Mid dry x CDU Late dry	-510.6	<0.001	***
FUN Mid dry x CDU Late rainy	-666.6	<0.001	***
FUN Mid dry x CUN Dry	-679.8	<0.001	***
FUN Mid dry x CUN Rainy	-588.0	<0.001	***
FUN Mid dry x FNS Dry	-1,112.6	<0.001	***
FUN Mid dry x FNS Rainy	-664.6	<0.001	***

Table S9: Total diffusive CO_2 and CH_4 emission ± standard error (kg d^{-1}, and Gg yr^{-1}) in Chapéu D'Úvas (CDU), Curuá-Una (CUN), Furnas (FNS) and Funil (FUN) during the sampling campaigns (different hydrological seasons). Max-Min ratios were computed by dividing the highest total daily diffusive emission by the lowest total daily diffusive emission for each gas in each reservoir.

Reservoir	Diffusive CO_2 emission (kg d^{-1})				Max-Min ratio	Diffusive CH_4 emission (kg d^{-1})				Max-Min ratio	Total diffusive CO_2 emission (Gg CO_2 y^{-1})	Total diffusive CH_4 emission (Gg CH_4 y^{-1})
	Rainy season		Dry season			Rainy season		Dry season				
CDU	392 ± 2.1 *(early)*	149 ± 0.9 *(late)*	656 ± 0.9 *(early)*	1000 ± 0.5 *(late)*	7	165 ± 0.8 *(early)*	240 ± 0.9 *(late)*	230 ± 0.5 *(early)*	104 ± 0.2 *(late)*	2.3	0.2 ± 0.0003	0.07 ± 0.00007
CUN	5200 ± 5.5		67600 ± 34.6		13	528 ± 0.3		736 ± 0.5		1.4	13 ± 0.01	0.2 ± 0.00009
FNS	24850 ± 10.7		86000 ± 12.3		3	6040 ± 1		26000 ± 3.9		4	20 ± 0.002	6 ± 0.0003
FUN			34 ± 0.1 *(late)*	61 ± 0.04 *(mid)*	1.8			23 ± 0.05 *(late)*	21 ± 0.07 *(mid)*	1.1	0.01 ± 0.008	0.008 ± 0.00009

Second chapter: *Carbon dioxide emission from drawdown areas of a Brazilian reservoir is linked to surrounding land cover*

Rafael M. Almeida[1]*, **José R. Paranaíba[1]***, Ícaro Barbosa[1], Sebastian Sobek[2], Sarian Kosten[3], Annika Linkhorst[2], Raquel Mendonça[1,2], Gabrielle Quadra[1], Fábio Roland[1], Nathan Barros[1]

1 Department of Biology, Federal University of Juiz de Fora, Juiz de Fora, MG, Brazil

2 Department of Ecology and Genetics, Uppsala University, Sweden

3 Department of Aquatic Ecology and Environmental Biology, Radboud University Nijmegen, Netherlands

**contributed equally to the manuscript*

Published at: *Aquatic Science*, 81, (4), 68-77, 2019.

DOI: 10.1007/s00027-019-0665-9

Date: December 7th, 2018

Abstract

Reservoir sediments exposed to air due to water level fluctuations are strong sources of atmospheric carbon dioxide (CO_2). The spatial variability of CO_2 fluxes from these drawdown areas are still poorly understood. In a reservoir in southeastern Brazil, we investigated whether CO_2 emissions from drawdown areas vary as a function of neighboring land cover types and assessed the magnitude of CO_2 fluxes from drawdown areas in relation to nearby water surface. Exposed sediments near forestland (average = 2733 mg C m^{-2} d^{-1}) emitted more CO_2 than exposed sediments near grassland (average = 1261 mg C m^{-2} d^{-1}), congruent with a difference in organic matter content between areas adjacent to forestland (average = 12.2%) and grassland (average = 10.9 %). Moisture also had a significant effect on CO_2 emission, with dry exposed sediments (average water content: 13.7%) emitting on average 2.5 times more CO_2 than wet exposed sediments (average water content: 23.5%). We carried out a systematic comparison with data from the literature, which indicates that CO_2 efflux from drawdown areas globally is about an order of magnitude higher than CO_2 efflux from adjacent water surfaces, and within the range of CO_2 efflux from terrestrial soils. Our findings suggest that emissions from exposed sediments may vary substantially in space, possibly related to organic matter supply from uphill vegetation, and that drawdown areas play a disproportionately important role in total reservoir CO_2 emissions with respect to the area they cover.

Keywords: exposed sediment, dry sediment, carbon dioxide, greenhouse gas, dam

Introduction

Although reservoirs provide key services to humans, the construction of numerous dams worldwide has been resulting in a vast range of ecological and hydrological alterations (Nilsson et al. 2005). By the damming of rivers and the resultant flooding of land, biogeochemical cycles in the original river and the flooded land areas are substantially altered (Friedl and Wüest 2002), which may result in increased greenhouse-gas emission (St. Louis et al. 2000). The most up-to-date review indicates that greenhouse-gas emission from reservoirs – predominantly as methane (CH_4) and carbon dioxide (CO_2) – is responsible for ~ 1.5% of the global anthropogenic CO_2-equivalent emissions (Deemer et al. 2016). The importance of understanding spatial and temporal variability in order to reliably assess total carbon emission from reservoirs is getting increasingly evident (Descloux et al. 2017; Paranaíba et al. 2018; Teodoru et al. 2012; Roland et al. 2010; Yang et al. 2013). Nevertheless, existing studies on reservoir emissions focus almost exclusively on emission from the water surface. Emissions from drawdown areas are largely neglected and these areas are considered blind spots in the global carbon cycle (Marcé et al. 2019).

Drawdown areas are referred to as the margins of reservoirs that are, due to seasonal hydrological cycles or dam operation, subject to water level fluctuation that causes periods of inundation and desiccation. The extent of these areas increases dramatically during periods of prolonged droughts. For instance, the extreme drought of 2014/2015 in Brazil has resulted in an additional exposure to air of ~1300 km^2 of reservoir sediments throughout Brazil, which substantially enhanced carbon emission rates (Kosten et al. 2018). An increasing number of studies – all of them very recent – indicate that exposed aquatic sediments are relevant net sources of atmospheric CO_2 (Catalán et al.

2014; Hyojin et al. 2016; Marcé et al. 2019; Obrador et al. 2018; Schiller et al. 2014). An important factor supporting enhanced CO_2 emission rates from exposed sediments is the increased microbial metabolism (e.g., enhanced enzyme activity of phenol oxidases and hydrolases) as sediment dries out (Hyojin et al. 2016; Weise et al. 2016). The importance of exposed sediments to reservoir carbon processing is clearly illustrated by a study in a Southeast Asian reservoir, which demonstrates that drawdown areas may contribute up to 75% of total annual CO_2 emissions (Deshmukh et al. 2018). Globally, dry exposed sediments are estimated to emit ~ 200 Tg of carbon as CO_2, which is equivalent to ~ 10% of global CO_2 emissions from inland waters (Marcé et al. 2019).

A more comprehensive understanding of carbon processing in drawdown areas is necessary for two principal reasons. First, there is growing evidence that exposed sediments are hotspots for carbon emission from freshwaters. Second, weather extremes can substantially affect CO_2 fluxes from freshwater systems (Almeida et al. 2017; Kosten et al. 2018), and the increased frequency of weather extremes associated with climate change is enhancing the desiccation of freshwater systems (Pekel et al. 2016) as well as the subsequent extent of drawdown areas (Kosten et al. 2018). Understanding the variability of CO_2 fluxes from drawdown areas over time and space is fundamental to support the definition of adequate sampling strategies and thus more realistic upscaling of CO_2 emissions from freshwater systems. While one study has reported limited spatial and annual variability in drawdown area CO_2 fluxes (Deshmukh et al. 2018), the scarcity of data makes it difficult to draw general conclusions about spatial or temporal variability of drawdown area CO_2 emission. Here we investigate the spatial variation in CO_2 fluxes from the drawdown areas of a reservoir in southeastern Brazil. More specifically, we studied whether emission varies as a function of neighboring land cover types (i.e., forestland and grassland), since drawdown areas are transitional zones between aquatic

and terrestrial ecosystems and, as such, are presumably influenced by both adjacent ecosystems. We further gauged the relative importance of drawdown zone emissions by assessing the magnitude of CO_2 emission from the drawdown areas in relation to water surface emissions on a seasonal and interannual time scale. Lastly, we compared the measured drawdown CO_2 emission with reported CO_2 fluxes from reservoir water surfaces and terrestrial soils worldwide, to understand whether exposed sediments align with terrestrial or aquatic ecosystems with respect to CO_2 emission.

Methods

Study area and quantification of drawdown areas

Chapéu D'Uvas (CDU) reservoir (21^0 33'S, 43^0 35'W) is an oligotrophic water supply reservoir constructed in 1994 in the Paraibuna River, Minas Gerais state, southeastern Brazil. The land cover of the reservoir's watershed is composed of grassland (~ 66%), natural forest (~ 30%), and Eucalyptus plantation (~ 4%) (Machado 2012). To estimate the total reservoir area, we contoured the reservoir shape on Google Earth based on satellite images from four periods with different water levels and generated a regression between water level and flooded area (flooded area = 0.4117*water level - 293.68; $r^2 = 0.91$, $p < 0.05$, $n = 4$). We then used daily water level data to calculate daily flooded area. Between November 2014 and August 2017, the flooded area ranged between 7.0 and 10.6 km^2. The difference between maximum and minimum flooded area was assumed to be the maximum drawdown area (i.e., 3.6 km^2), and the drawdown area was assumed to be zero at maximum flooded area. Daily drawdown area was then calculated by subtracting daily flooded area from the maximum flooded area.

CO_2 flux from water surface

We estimated CO_2 fluxes from open water surface during four sampling campaigns over hydrologically different seasons in 2015 and 2016. We used a combination of online equilibration system surveys and floating chamber measurements along the reservoir (see Paranaíba et al. 2018 for details on the approach). We performed continuous measurements (1-Hz frequency) of dissolved CO_2 concentrations in surface water using an open gas-flow equilibration system connected to an Ultra-portable Greenhouse Gas Analyzer (UGGA, Los Gatos Research, detection limit: 1.5 x 10^{-7} mol L^{-1}). We attached the inlet of the online equilibration system to the boat at 0.5 m depth, so that water was continuously pumped into the system (3 L min^{-1}) while the boat navigated through the reservoir at ~ 7 km h^{-1}. Each kilometer, the boat was stopped and the dissolved CO_2 measurements were interrupted for the measurements of the CO_2 gas exchange coefficient (described below).

We connected a transparent acrylic floating chamber (cylindrical, 17 L, 0.07 m^2) to the UGGA in a closed gas loop, and CO_2 concentration was monitored over 5-minute intervals. Measurements were done in triplicates at each sampling spot. At each spot, we also took discrete samples of surface water in triplicates for the determination of CO_2 surface water concentrations according to the headspace technique (Cole and Caraco, 1998). From these discrete samples, we further computed the CO_2 gas exchange coefficient following the equation below:

$$k_{CO2} = \frac{C_w - C_{eq}}{F_{CO2}} \quad (1)$$

where k_{CO2} (m d^{-1}) is the gas exchange coefficient for CO_2; C_w (mmol m^{-3}) is the concentration of CO_2 in water and C_{eq} (mmol m^{-3}) is the theoretical concentration of CO_2 in water if the water phase was in equilibrium with the atmosphere, both calculated from

the discrete samples; and F_{CO2} (mmol m^{-2} d^{-1}) is the CO_2 flux at the air-water interface, calculated from the floating chambers measurements.

We then combined the CO_2 concentrations from the online equilibration system with k_{CO2} to compute CO_2 emissions for the entire reservoir during each of the four campaigns. Specific details about the online equilibration system, floating chamber and discrete sample measurements, as well as flux calculation can be found in Paranaíba et al. 2018.

CO_2 flux from drawdown areas

We assessed the spatial variation of CO_2 fluxes from drawdown areas during the wet season in January 2018 (nine sites) and during the dry season in August 2018 (eight sites) using static chambers (cylindrical, 6.24 L, 0.07 m^2). To capture potential spatial variation related to neighboring land cover, we sampled sites in the drawdown area adjacent to the two main land cover types of the CDU watershed (forestland and grassland), which correspond to ~ 95% of the land cover. These land cover types were heterogeneously distributed along the reservoir (Figure 7). At each sampling site, we measured CO_2 flux in triplicates in three different areas: underwater shoreline (1-3 cm water depth), wet exposed sediments and dry exposed sediments (Figure 8), totaling nine chamber measurements per sampling site. We made the distinction between wet and dry sediment visually (Figure 8) and further confirmed that through moisture analysis in the laboratory – the average water contents of wet and dry exposed sediments were 24 ± 5 % (± SD) and 13 ± 4 % (± SD) of total weight, respectively. The triplicated chambers were deployed about 1 m apart from each other and connected to an Infrared Gas Analyzer (IRGA EGM-4 PP Systems) for five minutes to quantify changes in CO_2 concentration over time. The chambers were opaque to minimize temperature change.

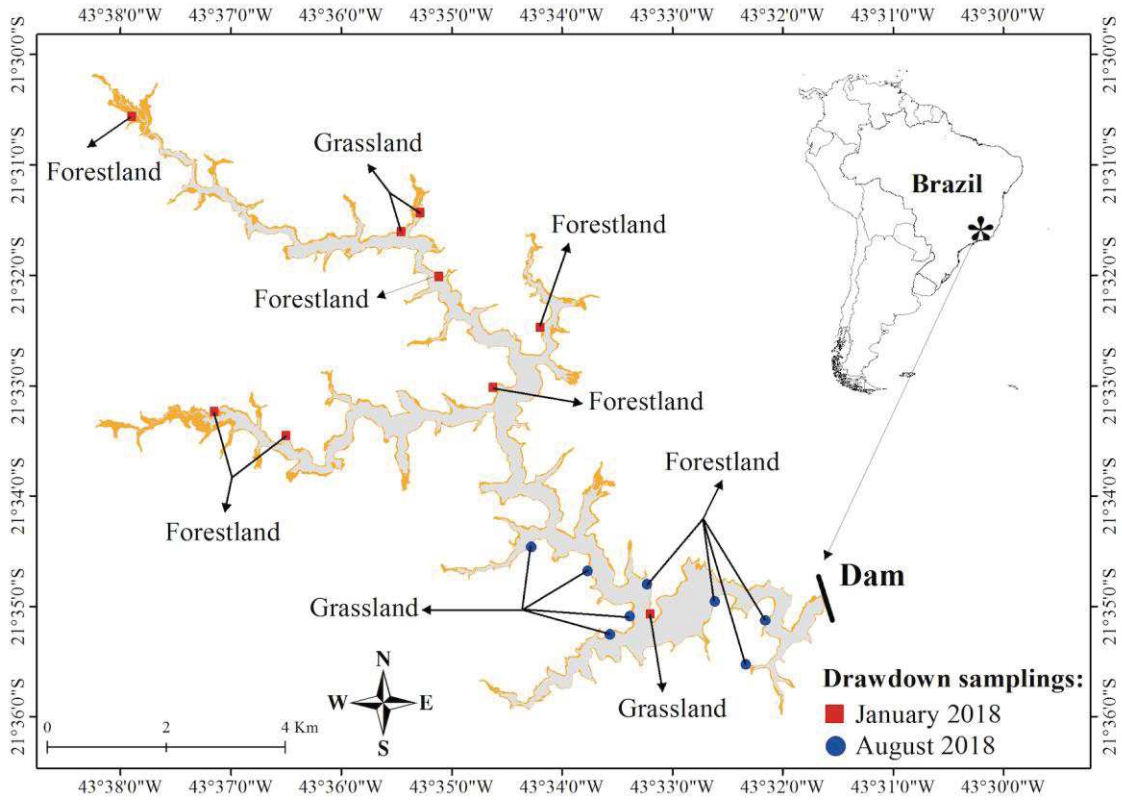

Figure 7: Map of Chapéu D'Uvas (CDU) reservoir, with drawdown areas highlighted in orange. The sampling sites for static chambers deployed to measure CO_2 fluxes from drawdown areas are shown in the map.

We used clay around the exterior of the chambers to avoid gas leakage (Lesmeister and Koschorreck 2017). Soil temperature and conductivity were determined using a conductivity meter (Akrom KR31). Surface soil samples of exposed sediments (wet and dry) were collected after each measurement and stored in coolers for laboratory analysis of moisture and organic matter content within two days. Moisture content was measured as the weight loss after drying 10 g of sediment sample at 105˚C for 2 h. The samples used for moisture analysis were further used to quantify the organic matter content, which was measured as loss on ignition (450˚C for 4 h).

We also performed measurements of CH_4 emission from drawdown areas at one grassland-neighbored site in May 2017, using static chambers connected to a UGGA. While CH_4 fluxes from exposed sediments can be important in some reservoir systems, these preliminary measurements indicated CH_4 uptake (4 mg CO_2eq m^{-2} d^{-1}, 100-year global warming potential of 34; data not shown). The magnitude of that uptake is, however, negligible compared to the magnitude of CO_2 emissions measured over the same time period (1452 mg CO_2 m^{-2} d^{-1}), and CH_4 uptake thus canceled less than 1% of CO_2 emissions. Our study therefore focuses exclusively on CO_2.

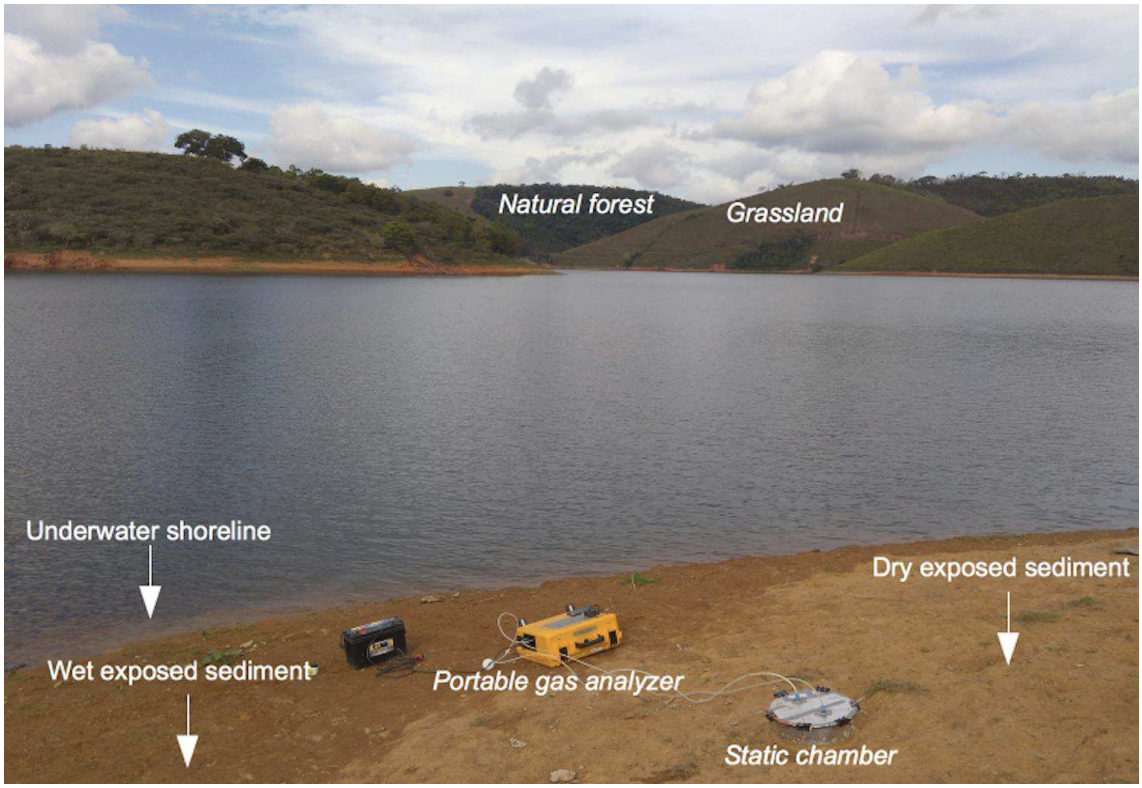

Figure 8: Photograph taken in May 2017 depicting a typical drawdown area of Chapéu D'Uvas (CDU) reservoir. We deployed static chambers connected to a portable gas analyzer to measure CO_2 fluxes at the underwater shoreline, wet exposed sediment, and dry exposed sediment.

Data analysis

We used analyses of variance to evaluate the effects of season, moisture and neighboring land cover on CO_2 flux, as well as the interaction between these two predictors. We log-transformed the CO_2 fluxes to meet the assumptions of normality and homoscedasticity and applied the *aov* function of R Statistical Software version 3.3.2 (R Development Core Team 2016).

We further compared CO_2 fluxes from exposed sediments of CDU reservoir with fluxes reported in the literature for exposed sediments of other freshwater systems, reservoir surfaces, and terrestrial soils. CO_2 fluxes from reservoir surfaces were taken from a recent compilation of CO_2 emissions from 228 reservoirs worldwide (Deemer et al. 2016). CO_2 fluxes from terrestrial soils were taken from a global database of soil respiration from all types of ecosystems worldwide (Bond-Lamberty and Thomson 2012).

Results and discussion

Extent of drawdown areas

The relative share of drawdown areas to the total area of CDU reservoir varies seasonally and interanually (Figure 9). The share was smallest right after the rainy season (<1% between March and May 2016) and largest right after the dry season (>30% in November and December 2014). In 2015, drawdown areas accounted on average for 24% of the total reservoir area, whereas in 2016 they accounted for 7%. According to the Brazilian National Institute of Meteorology (INMET; http://www.inmet.gov.br), the average annual rainfall near CDU (Juiz de Fora station) is 1597 mm. The INMET reports that 2014 and 2015 were characterized by below-normal total rainfall (906 and 1251 mm, respectively), whereas 2016 had above-normal total rainfall (1705 mm). Interannual variation in rainfall thus explains the high interannual variation in the share of drawdown

areas to the total reservoir area. On average, drawdown areas accounted for 17% of the total reservoir area between November 2014 and August 2017.

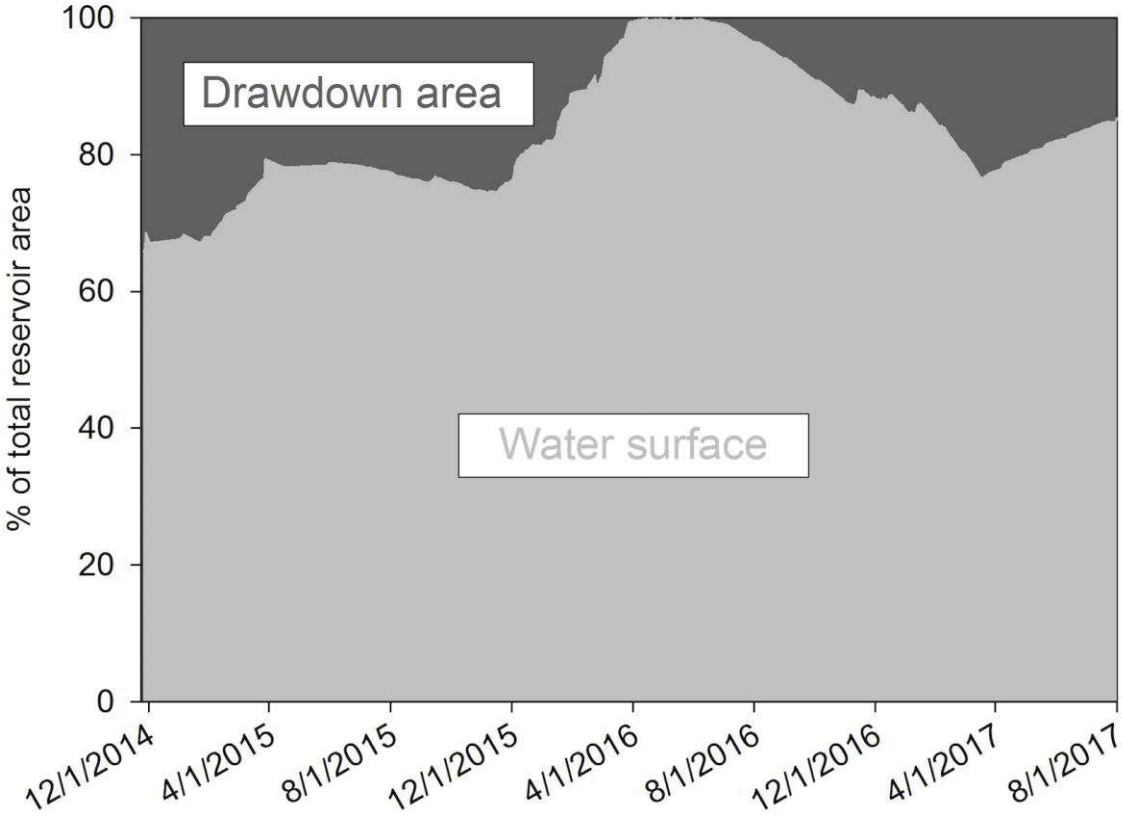

Figure 9: Relative contribution of drawdown area (dark grey) and water surface area (light grey) to the total reservoir area of Chapéu D'Uvas (CDU) reservoir over time.

CO_2 fluxes in drawdown areas

The average CO_2 emission from exposed sediments in drawdown areas of CDU reservoir was 1855 mg C m^{-2} d^{-1} (range: 204 – 6425 mg C m^{-2} d^{-1}, n = 18) during the wet season in January 2018 and 2432 mg C m^{-2} d^{-1} (range: 163 – 6857 mg C m^{-2} d^{-1}, n = 16) during the dry season in August 2018. The seasonal difference in CO_2 emission from exposed sediments was not significant ($F = 0.5$, $p = 0.48$, $df = 33$). Underwater shoreline areas near exposed sediments had average emissions of 353 mg C m^{-2} d^{-1} (range: 130 –

776 mg C m^{-2} d^{-1}, n = 9) in January 2018 and 726 mg C m^{-2} d^{-1} (range: 310 – 1330 mg C m^{-2} d^{-1}, n = 8) in August 2018. Notably, the rates of CO_2 efflux from the reservoir drawdown areas were on average 19 (January 2018) to 26 (August 2018) times higher than the average CO_2 efflux from the reservoir water surface (71 mg C m^{-2} d^{-1}; Figure 10a-b).

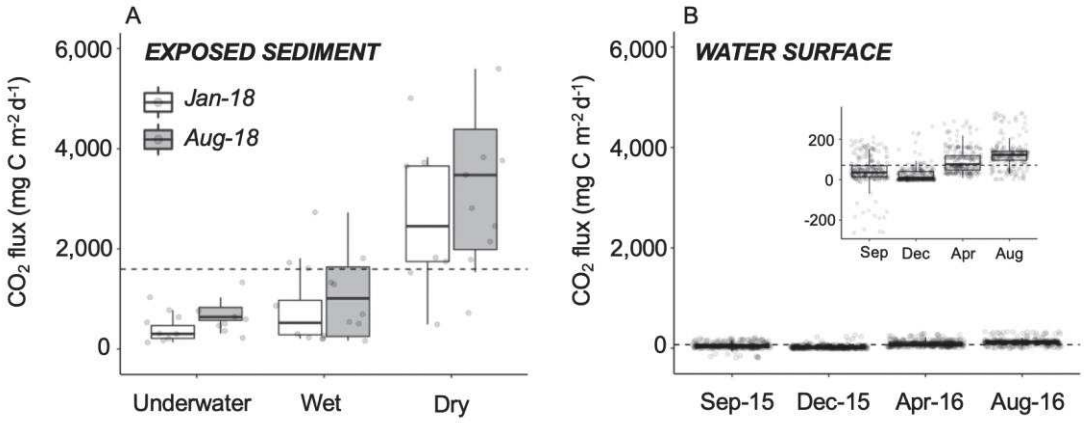

Figure 10: CO_2 fluxes from (A) exposed sediment (underwater shoreline, wet exposed sediments, and dry exposed sediments) in January and August 2018, and (B) the water surface in September 2015, December 2015, April 2016 and August 2016 in Chapéu D'Uvas reservoir. The inset figure in B shows the water surface results on a different scale for better visualization of the seasonal variability. The lines within the boxes indicate the median, the boxes delimit the 25th and 75th percentiles, and the whiskers delimit the 5th and 95th percentiles.

CO_2 emissions significantly differed between dry exposed sediments, wet exposed sediments, and neighboring underwater shoreline in both January 2018 ($F = 10.9$, $p < 0.05$, $df = 26$) and August 2018 ($F = 11.8$, $p < 0.05$, $df = 23$) (Figure 10a). A Tukey post-hoc test indicated higher emissions from dry exposed sediments than from wet exposed sediments (January: $t = 2.5$, $p < 0.05$; August: $t = 4.1$, $p < 0.05$) and underwater shoreline

(January: $t = 4.7$, $p < 0.05$; August: $t = 4.3$, $p < 0.05$) in both seasons. In contrast, there was no difference between emissions from wet exposed sediments and underwater shoreline in either January ($t = 2.1$, $p = 0.10$) or August ($t = 0.2$, $p = 0.98$). Our results are in agreement with other recent studies reporting increasing CO_2 efflux as exposed sediments dry out (Gilbert et al. 2017; Weise et al. 2016). We did not measure how long it takes for exposed sediments to transition from wet to dry, and this merits further investigation. The transition time is likely variable and may be influenced by many factors including solar irradiance, wind conditions, precipitation, temperature, and slope of the exposed area.

Cycles of wetting-desiccation accelerate carbon losses from freshwater systems (Reverey et al. 2016). Indeed, a growing number of studies in different types of aquatic ecosystems (reservoirs, intermittent streams, temporary ponds) suggest that exposed sediments emit substantially more CO_2 than adjacent water surfaces (Catalán et al. 2014; Deshmukh et al. 2018; Gilbert et al. 2017; Gómez-Gener et al. 2015; Hyojin et al. 2016; Looman et al. 2017; Obrador et al. 2018; Schiller et al. 2014). Higher CO_2 emission from exposed sediments compared to nearby water surfaces have been attributed to enhanced microbial metabolism: sediment desiccation stimulates bacterial growth and enzyme activity, which in turn enhances CO_2 production and subsequent efflux (Fenner and Freeman 2011; Hyojin et al. 2016; Weise et al. 2016). The solubility of oxygen in water is low and its diffusivity slow (Furrer and Wehrli 1996), such that in water-logged sediments oxygen supply to microbes is probably slow, which limits degradation rates (Zehnder and Svensson 1986). Once the void pore space in the sediments fills with air when sediment dries out, it is likely that microbial degradation rates are enhanced, increasing CO_2 production. In combination with the higher diffusion rates, this may then lead to higher CO_2 emission rates.

In addition to being affected by moisture, CO_2 emission from exposed sediments was significantly different among sites grouped according to the predominant land cover adjacent to the sampling locations (Figure 11). Exposed sediments near forestland exhibited significantly higher CO_2 emission rates than those near grassland in both January ($F = 7.8$, $p < 0.05$, $df = 17$) and August ($F = 5.6$, $p < 0.05$, $df = 15$). Unlike exposed sediments, CO_2 fluxes from underwater shoreline did not vary significantly among sites grouped according to the predominant adjacent land cover in either January ($F = 0.2$, $p = 0.68$, $df = 8$) or August ($F = 0.5$, $p = 0.49$, $df = 7$). Although thin (< 3 cm of depth), the layer of water above the sediment in underwater shoreline areas is still connected to pelagic water, such that CO_2 can be transported laterally, which may explain the more homogeneous spatial variability in these compartments compared to areas of exposed sediment.

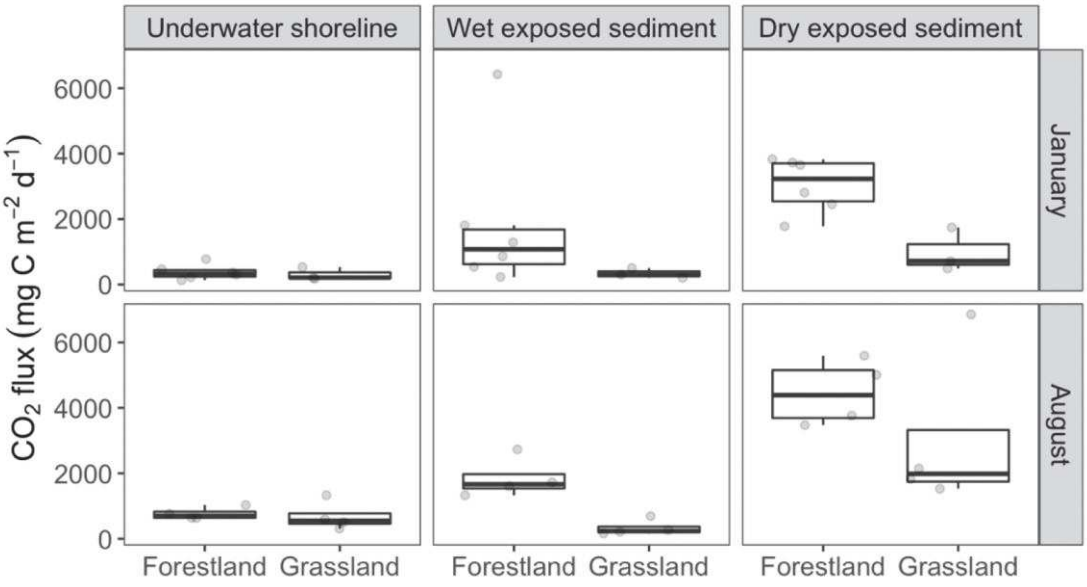

Figure 11: CO_2 fluxes from underwater shoreline, wet exposed sediment, and dry exposed sediment (left to right) in areas neighbored by forestland and grassland in Chapéu D'Uvas reservoir. The lines within the boxes indicate the median, the boxes delimit the 25th and 75th percentiles, and the whiskers delimit the 5th and 95th percentiles.

We found that exposed sediments adjacent to forestland had higher organic matter concentrations (average = 14.9% of dry weight) than those next to grassland (average = 11.3% of dry weight) in August (one-tailed *t*-test, $t = 1.9$, $p < 0.05$, $df = 14$). In January, however, we could not detect a significant difference between the organic matter content of exposed sediments in forestland- (average = 10.4%) and grassland-neighbored areas (average = 9.2%; one-tailed *t*-test, $t = 0.9$, $p = 0.19$, $df = 15$) (Figure 12). The substantial variability in organic matter content in exposed sediment within each group of adjacent land cover (Figure 12) indicates that uphill forests may export more organic matter to neighboring exposed sediments than grassland areas, which may in part explain the higher CO_2 emission rates observed in drawdown areas adjacent to forestland.

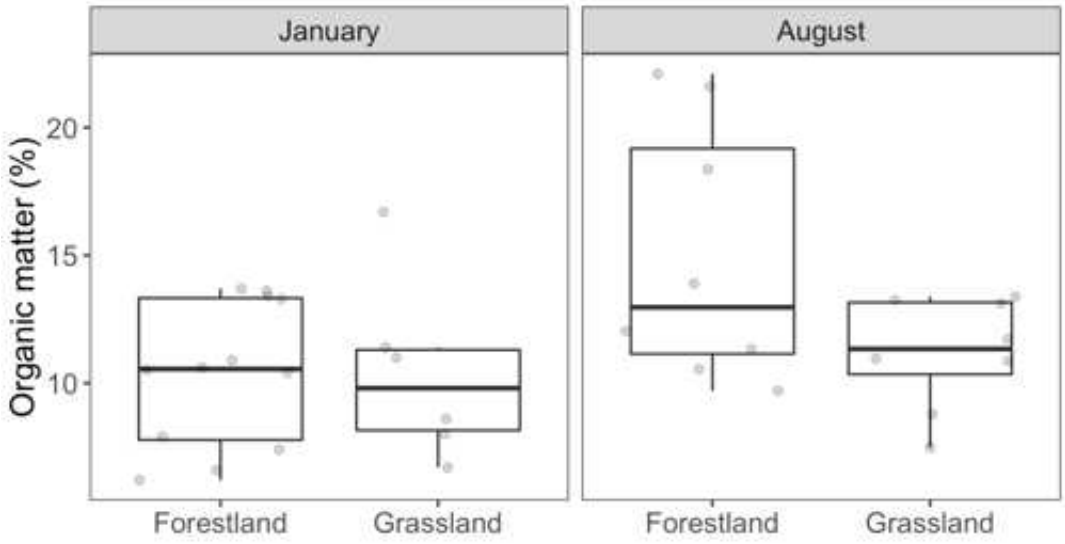

Figure 12: Concentrations of organic matter (in percentage of dry weight) in exposed sediments of Chapéu D'Uvas reservoir in January and August 2018. The lines within the boxes indicate the median, the boxes delimit the 25th and 75th percentiles, and the whiskers delimit the 5th and 95th percentiles.

Relative contribution of drawdown areas to total reservoir CO_2 emissions

To estimate the relative annual contribution of drawdown areas to total CO_2 emissions from CDU reservoir, we considered the average values of all water surface (September 2015, December 2015, April 2016 and August 2016) and drawdown (January and August 2018) measurements. These calculations were made considering the average CDU basin land cover (~ 66% grassland and 34% forestland). The weighted average CO_2 emission from the CDU drawdown area was 1736 mg C m^{-2} d^{-1}, and this gives a total CO_2 emission of 3038 kg C d^{-1} for 1.75 km^2 of drawdown area (i.e., the average extent of the drawdown area over time). The average CO_2 emission from the CDU water surface was 71 mg C m^{-2} d^{-1}, and this gives a total CO_2 emission of 628 kg C d^{-1} for 8.85 km^2 of water surface area (i.e., the average extent of the reservoir water surface area over time). The drawdown area thus accounted for <20% of the total reservoir area but contributed to >80% of total reservoir CO_2 emissions upstream the dam. Our results are in line with a recent study conducted in a reservoir in Southeast Asia, which found that drawdown areas accounted for 50-75% of total annual reservoir CO_2 emission (Deshmukh et al. 2018). Our findings indicate that drawdown areas are CO_2 emission hotspots in CDU reservoir, not only due to high emission rates in relation to reservoir water surface, but also because exposed sediments cover a large fraction of the total reservoir area over long periods of the year (Figure 9).

CO_2 emission from drawdown zones and other freshwater systems worldwide

In order to quantitatively compare our findings, we compiled data from reservoir water surfaces and exposed sediments of freshwater systems worldwide (Figure 13). The average flux from the drawdown zone of CDU reservoir (1736 mg C m^{-2} d^{-1}) is close to the average flux from exposed sediments of reservoirs, intermittent streams, and temporary ponds worldwide (2145 ± 1637 mg C m^{-2} d^{-1}, average ± standard deviation,

Table 3). The average CO_2 flux from global exposed sediments is roughly one order of magnitude higher than the average CO_2 flux from global reservoir surfaces (332 mg C m^{-2} d^{-1}) (Figure 13), which is a similar pattern as observed in CDU reservoir data alone (Figure 10). Although studies on CO_2 emissions from drawdown areas are scarce, existing data suggest that the range of CO_2 flux from drawdown zones resembles the range of CO_2 flux from terrestrial soils rather than from reservoir water surfaces (Figure 13).

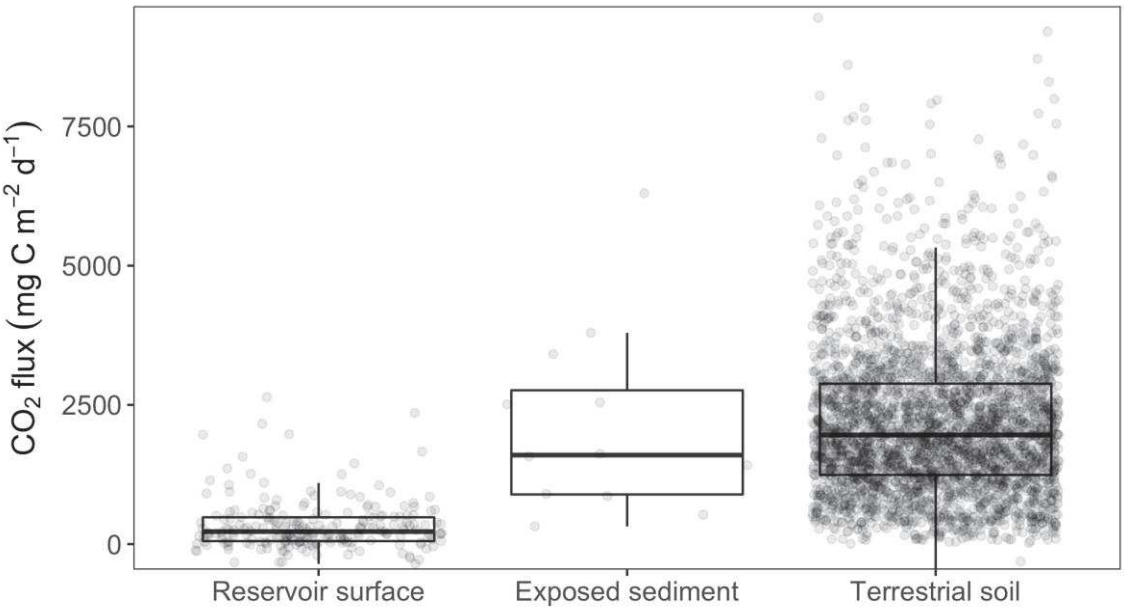

Figure 13: CO_2 fluxes from exposed sediment of freshwater systems, reservoir surface and terrestrial soils worldwide. Data on exposed sediment were compiled from published literature and are shown as median or mean fluxes of each study (Table 3), data on reservoir surface were taken from (Deemer et al. 2016), and data on terrestrial soil were taken from (Bond-Lamberty and Thomson 2012).

Table 3: Mean fluxes of CO_2 from exposed sediments of different types of freshwater systems worldwide reported in literature.

Site	Type	Country	CO_2 flux (mg C m^{-2} d^{-1})	Reference
Nan Theum 2 Reservoir	Reservoir drawdown	Lao PDR	3414	(Deshmukh et al. 2018)
Fluvià River	Dry streambed	Spain	2508	(Gómez-Gener et al. 2015; Schiller et al. 2014)
Lake Soyang	Reservoir drawdown	South Korea	6300	(Hyojin et al. 2016)
River Po	Exposed river sediment	Italy	317	(Bolpagni et al. 2017)
Temporary ponds on Menorca Island	Temporary pond	Spain	1576	(Catalán et al. 2014; Obrador et al. 2018)
Experimental temporary ponds	Temporary pond	England	3792	(Gilbert et al. 2017)
Rappbode Reservoir	Reservoir drawdown	Germany	1620	(Lesmeister and Koschorreck 2017)
Elbe River	Exposed river sediment	Germany	900	(Lesmeister and Koschorreck 2017)
Jamison Creek	Dry streambed	Australia	864	(Looman et al. 2017)
Urban temporary streams	Dry streambed	United States	528	(Gallo et al. 2014)
Chinese hydropower reservoirs	Reservoir drawdown	China	2110	(Li et al. 2015)
Chapéu D'Uvas Reservoir	Reservoir drawdown	Brazil	1736	This study

This has also been suggested by two separate studies in Mediterranean ecosystems (Gómez-Gener et al. 2015; Schiller et al. 2014). Importantly, however, terrestrial soil respiration is often counteracted by primary production from overlying vegetation, which typically results in positive net ecosystem production (i.e., net CO_2 sinks) in terrestrial ecosystems. In terrestrial sites with reported measurements of both soil respiration and net ecosystem production in the global soil respiration database (Bond-Lamberty and Thomson 2012), although the average soil CO_2 efflux is high (2148 mg C m^{-2} d^{-1}), the average net ecosystem production is positive (460 mg C m^{-2} d^{-1}). This indicates that despite elevated soil respiration, these terrestrial sites are overall net CO_2 sinks when the primary production of overlying vegetation is taken into account. Our findings suggest that exposed aquatic sediments respire organic matter at a similar rate as terrestrial soils, but unlike terrestrial sites they end up functioning as strong CO_2 sources since they frequently lack primary producers to compensate for CO_2 production during microbial respiration.

Implications and future directions

Most studies focusing on CO_2 emissions from exposed sediment are fairly recent (Table 3), and this area of research has been receiving increasing attention in the scientific literature. To our knowledge, our study is the first to demonstrate that CO_2 fluxes from drawdown areas vary significantly in space, which is possibly related to the adjacent land cover. In addition to demonstrating the importance of spatial dynamics for a comprehensive understanding of CO_2 fluxes from drawdown areas, our study presents a systematic comparison of reservoir water surface, freshwater drawdown, and soil fluxes of CO_2. Even though we could not find significant seasonal variability in drawdown CO_2

fluxes, our study is based on only two points in time, and does not preclude the existence of temporal variation of CO_2 fluxes from drawdown areas.

The pattern observed in CDU reservoir, with CO_2 emissions from drawdown areas exceeding those from the water surface, concurs with other freshwater systems around the globe (Figure 13). Globally, CO_2 emissions from exposed sediments in drawdown areas are about one order of magnitude higher than those from adjacent water surfaces. The current knowledge suggests that drawdown areas play a disproportionately important role in total CO_2 emissions with respect to the area they cover. The fact that drawdown zones of reservoirs are CO_2 emission hotspots has an important implication in light of a changing climate that may result in more frequent extended droughts throughout the world (Pachauri et al. 2014). Changing drawdown area extent may affect not only reservoir carbon emissions, but burial as well. Because submerged reservoir sediments typically act as carbon sinks and exposed sediments release a large fraction of organic carbon that would otherwise be buried for long timescales (Marcé et al. 2019), an increased drawdown area extent may reduce organic carbon burial efficiency on a reservoir scale. Finally, although we have not focused on methane emission, recent studies indicate that reservoir drawdown areas might be sites of intense methane release (Beaulieu et al. 2017; Harrison et al. 2017; Yang et al. 2012), which is also temporally heterogeneous (Kosten et al. 2018). Carbon processing in drawdown areas deserves more attention to support better constrained upscaling of carbon emission from freshwaters.

Acknowledgements. We are grateful to Iollanda I. P. Josué for her assistance during field work.

References

Almeida RM, Pacheco FS, Barros N, Rosi E, Roland F (2017) Extreme floods increase CO2 outgassing from a large Amazonian river. Limnol Oceanogr 62:989-999 doi:10.1002/lno.10480

Beaulieu JJ et al. (2017) Effects of an Experimental Water-level Drawdown on Methane Emissions from a Eutrophic Reservoir. Ecosystems 21(4):657-674 doi:10.1007/s10021-017-0176-2

Bolpagni R, Folegot S, Laini A, Bartoli M (2017) Role of ephemeral vegetation of emerging river bottoms in modulating CO2 exchanges across a temperate large lowland river stretch. Aquatic Sciences 79:149-158 doi:10.1007/s00027-016-0486-z

Bond-Lamberty BP, Thomson AM (2012) A Global Database of Soil Respiration Data, Version 3.0. Oak Ridge, Tennessee. doi:http://dx.doi.org/10.3334/ORNLDAAC/1235

Catalán N, von Schiller D, Marcé R, Koschorreck M, Gómez-Gener L, Obrador B (2014) Carbon dioxide efflux during the flooding phase of temporary ponds. Limnetica 33:349-360

Cole JJ, Caraco NF (1998) Atmospheric exchange of carbon dioxide in a low-wind oligotrophic lake measured by the addition of SF6. Limnl Oceanogr 43:647-656

Deemer BR et al. (2016) Greenhouse Gas Emissions from Reservoir Water Surfaces: A New Global Synthesis. BioScience 66:949-964 doi:10.1093/biosci/biw117

Descloux S, Chanudet V, Serça D, Guérin F (2017) Methane and nitrous oxide annual emissions from an old eutrophic temperate reservoir. Science of The Total Environment 598:959-972 doi:https://doi.org/10.1016/j.scitotenv.2017.04.066

Deshmukh C et al. (2018) Carbon dioxide emissions from the flat bottom and shallow Nam Theun 2 Reservoir: drawdown area as a neglected pathway to the atmosphere. Biogeosciences 15:1775-1794 doi:10.5194/bg-15-1775-2018

Fenner N, Freeman C (2011) Drought-induced carbon loss in peatlands. Nat Geosci 4:895 doi:10.1038/ngeo1323

Friedl G, Wüest A (2002) Disrupting biogeochemical cycles - Consequences of damming. Aquatic Sciences 64:55-65 doi:10.1007/s00027-002-8054-0

Furrer G, Wehrli B (1996) Microbial reactions, chemical speciation, and multicomponent diffusion in porewaters of a eutrophic lake. Geochimica et Cosmochimica Acta 60:2333-2346 doi:https://doi.org/10.1016/0016-7037(96)00086-5

Gallo EL, Lohse KA, Ferlin CM, Meixner T, Brooks PD (2014) Physical and biological controls on trace gas fluxes in semi-arid urban ephemeral waterways. Biogeochemistry 121:189-207 doi:10.1007/s10533-013-9927-0

Gilbert PJ, Cooke DA, Deary M, Taylor S, Jeffries MJ (2017) Quantifying rapid spatial and temporal variations of CO2 fluxes from small, lowland freshwater ponds. Hydrobiologia 793:83-93 doi:10.1007/s10750-016-2855-y

Gómez-Gener L et al. (2015) Hot spots for carbon emissions from Mediterranean fluvial networks during summer drought. Biogeochemistry 125:409-426 doi:10.1007/s10533-015-0139-7

Harrison JA, Deemer BR, Birchfield MK, O'Malley MT (2017) Reservoir Water-Level Drawdowns Accelerate and Amplify Methane Emission. Environmental Science & Technology 51:1267-1277 doi:10.1021/acs.est.6b03185

Hyojin J, Tae Kyung Y, Seung-Hoon L, Hojeong K, Jungho I, Ji-Hyung P (2016) Enhanced greenhouse gas emission from exposed sediments along a hydroelectric reservoir during an extreme drought event. Environ Res Lett 11:124003

Kosten S et al. (2018) Extreme drought boosts CO2 and CH4 emissions from reservoir drawdown areas. Inland Waters 8(3):329-340 doi:10.1080/20442041.2018.1483126

Lesmeister L, Koschorreck M (2017) A closed-chamber method to measure greenhouse gas fluxes from dry aquatic sediments. Atmos Meas Tech 10:2377-2382 doi:10.5194/amt-10-2377-2017

Li S, Zhang Q, Bush RT, Sullivan LA (2015) Methane and CO2 emissions from China's hydroelectric reservoirs: a new quantitative synthesis. Environmental Science and Pollution Research 22:5325-5339 doi:10.1007/s11356-015-4083-9

Looman A, Maher DT, Pendall E, Bass A, Santos IR (2017) The carbon dioxide evasion cycle of an intermittent first-order stream: contrasting water–air and soil–air exchange. Biogeochemistry 132:87-102 doi:10.1007/s10533-016-0289-2

Machado PJO (2012) Diagnóstico ambiental e ordenamento territorial – instrumentos para a gestão da Bacia de Contribuição da Represa de Chapéu D'Uvas/MG. PhD thesis, Universidade Federal Fluminense, Brazil

Marcé R et al. (2019) Emissions from dry inland waters are a blind spot in the global carbon cycle. Earth-Science Reviews 188:240-248 doi:https://doi.org/10.1016/j.earscirev.2018.11.012

Nilsson C, Reidy CA, Dynesius M, Revenga C (2005) Fragmentation and flow regulation of the world's large river systems. Science 308:405-408 doi:DOI 10.1126/science.1107887

Obrador B, von Schiller D, Marcé R, Gómez-Gener L, Koschorreck M, Borrego C, Catalán N (2018) Dry habitats sustain high CO2 emissions from temporary ponds across seasons. Scientific Reports 8:3015 doi:10.1038/s41598-018-20969-y

Pachauri RK et al. (2014) Climate change 2014: synthesis report. Contribution of Working Groups I, II and III to the fifth assessment report of the Intergovernmental Panel on Climate Change. 151 pp

Paranaíba JR et al. (2018) Spatially Resolved Measurements of CO2 and CH4 Concentration and Gas-Exchange Velocity Highly Influence Carbon-Emission Estimates of Reservoirs. Environmental Science & Technology 52:607-615 doi:10.1021/acs.est.7b05138

Pekel J-F, Cottam A, Gorelick N, Belward AS (2016) High-resolution mapping of global surface water and its long-term changes. Nature 540:418 doi:10.1038/nature20584

https://www.nature.com/articles/nature20584#supplementary-information

R Development Core Team (2016) R: A language and environment for statistical computing, 3.3.2 edn. R Foundation for Statistical Computing, Vienna, Austria

Reverey F, Grossart H-P, Premke K, Lischeid G (2016) Carbon and nutrient cycling in kettle hole sediments depending on hydrological dynamics: a review. Hydrobiologia 775:1-20 doi:10.1007/s10750-016-2715-9

Roland F et al. (2010) Variability of carbon dioxide flux from tropical (Cerrado) hydroelectric reservoirs. Aquatic Sciences 72:283-293 doi:DOI 10.1007/s00027-010-0140-0

Schiller Dv, Marcé R, Obrador B, Gómez-Gener L, Casas-Ruiz JP, Acuña V, Koschorreck M (2014) Carbon dioxide emissions from dry watercourses. Inland Waters 4:377-382 doi:10.5268/IW-4.4.746

St. Louis VL, Kelly CA, Duchemin É, Rudd JWM, Rosenberg DM (2000) Reservoir Surfaces as Sources of Greenhouse Gases to the Atmosphere: A Global Estimate. BioScience 50:766-775 doi:10.1641/0006-3568(2000)050[0766:RSASOG]2.0.CO;2

Teodoru CR et al. (2012) The net carbon footprint of a newly created boreal hydroelectric reservoir Global Biogeochemical Cycles 26 doi:doi:10.1029/2011GB004187

Weise L et al. (2016) Water level changes affect carbon turnover and microbial community composition in lake sediments. FEMS Microbiology Ecology 92:fiw035-fiw035 doi:10.1093/femsec/fiw035

Yang L et al. (2012) Surface methane emissions from different land use types during various water levels in three major drawdown areas of the Three Gorges Reservoir. Journal of Geophysical Research: Atmospheres 117 doi:10.1029/2011JD017362

Yang L, Lu F, Wang X, Duan X, Tong L, Ouyang Z, Li H (2013) Spatial and seasonal variability of CO2 flux at the air-water interface of the Three Gorges Reservoir. Journal of Environmental Sciences 25:2229-2238 doi:https://doi.org/10.1016/S1001-0742(12)60291-5

Zehnder AJB, Svensson BH (1986) Life without oxygen: what can and what cannot? Experientia 42:1197-1205 doi:10.1007/BF01946391

Third chapter: *Sediment drying-rewetting cycles enhance greenhouse gas emissions, nutrient and trace element release, and promote water cytogenotoxicity*

José R. Paranaíba[1], Gabrielle Quadra[1], Iollanda I. P. Josué[2], Rafael M. Almeida[3], Raquel Mendonça[1], Simone Jaqueline Cardoso[1], Júlio Silva[4,5], Sarian Kosten[6], José Marcello Campos[7], Joseane Almeida[4], Rafael Lethournon Araújo[7], Fábio Roland[1], Nathan Barros[1]

[1] Laboratório de Ecologia Aquática, Programa de Pós-Graduação em Ecologia, Universidade Federal de Juiz de Fora, Brazil

[2] Laboratório de Limnologia, Programa de Pós-Graduação em Ecologia, Universidade Federal do Rio de Janeiro, Brazil

[3] Department of Ecology and Evolutionary Biology, Cornell University, USA

[4] Grupo Baccan de Química Analítica, Departamento de Química, Universidade Federal de Juiz de Fora, Brazil

[5] Instituto Nacional de Ciência e Tecnologia (INCT) Acqua, Departamento de Engenharia Metalúrgica e de Minas, Escola de Engenharia, Universidade Federal de Minas Gerais, Brazil

[6] Department of Aquatic Ecology and Environmental Biology, Institute for Water and Wetland Research, Radboud University, Nijmegen, Netherlands

[7] Laboratório de Genética e Biotecnologia, Universidade Federal de Juiz de Fora, Brazil

Published at: *PLoS ONE*, 15, (4), 1-21, 2020.

DOI: 10.1371/journal.pone.0231082 **Date: April 2nd, 2020**

Abstract

Increased periods of prolonged droughts followed by severe precipitation events are expected throughout South America due to climate change. Freshwater sediments are especially sensitive to these changing climate conditions. The increased oscillation of water levels in aquatic ecosystems causes enhanced cycles of sediment drying and rewetting. Here we experimentally evaluate the effects of induced drought followed by a rewetting event on the release of carbon dioxide (CO_2), methane (CH_4), nutrients (nitrogen and phosphorus), and trace elements (iron, manganese, and zinc) from the sediment of a tropical reservoir in southeastern Brazil. Furthermore, we used bulb onions (*Allium cepa*) to assess the potential cytogenotoxicity of the water overlying sediments after rewetting. We found peaks in CO_2 and CH_4 emissions when sediments first transitioned from wet to dry, with fluxes declining as sediments dried out. CO_2 emissions peaked again upon rewetting, whereas CH_4 emissions remained unaltered. Our experiment also revealed average increases by up to a factor of ~5000 in the release rates of nutrients and trace elements in water overlying sediments after rewetting. These increased release rates of potentially toxic compounds likely explain the lower replication of *Allium cepa* cells (up to 22% reduction) exposed to water overlying sediments after rewetting. Our findings suggest that increased events of drought followed by rewetting may lead to a range of changes in freshwater ecosystems, including nutrient enrichment, increased toxicity following resuspension of contaminants, and higher emission of greenhouse gases to the atmosphere.

Introduction

Global temperature changes can alter the circulation patterns of water and air masses, which have direct effects on precipitation regimes worldwide (IPCC, 2013; Marengo et al., 2009). Accordingly, climate change projections suggest an increased occurrence of prolonged droughts followed by extreme precipitation events in different regions of South America (IPCC, 2013; Marengo et al., 2009). Indeed, Brazil has experiencing years of extreme precipitation interspersed by years with abnormal droughts, including the incidence of unusually dry summers in typically rainy regions of the country's Southeast (INMET, 2019).

Changes in the global climate patterns have been causing drastic modifications to various ecosystems on Earth (Dirzo et al., 2014). Freshwater ecosystems such as rivers, lakes, wetlands, and reservoirs are particularly vulnerable to environmental changes. In addition, these ecosystems have been deeply undermined by human activities, including land-use changes, landscape fragmentation, river damming, and wastewater loading (Maavara et al., 2015; Roland et al., 2012; Schwarzenbach et al., 2010). Damming, in particular, represents one of the most serious anthropogenic pressures on the world's rivers over the last decades (Maavara et al., 2014, 2015; Wang et al., 2018), and dam construction is expected to continue on the rise (Zarfl et al., 2015). One important consequence of damming is the increased entrapment of terrestrially-derived elements into the sediment (e.g. organic and inorganic carbon, nutrients, trace elements) and the subsequent reduction of their transport to downstream ecosystems, including the ocean (Van Cappellen & Maavara, 2016; Friedl & Wüest, 2002; Maavara et al., 2015; Teodoru & Wehrli, 2005). Another important consequence of damming is the intensification of microbial activity (e.g. decomposition, photosynthesis) within the constructed reservoir

due to the transformation of a lotic system into a lentic one, leading to direct and indirect effects of element processing in the reservoir's sediment and water column (Maavara et al., 2015; Stanley et al., 2016).

The sediment represents one of the most important pools for the accumulation, processing, and transfer of elements in aquatic systems (Calmano & Förstner, 1993). Elements may accumulate in the different geochemical layers of the sediment mainly through adsorption (Salomons & Forstner, 1984). Thus, this sediment "memory" can provide snapshots of the aquatic ecosystems over time, recording information of environmental impact episodes and accumulating chemical species either used or produced by anthropogenic activities (Junior et al., 2014; De La Guardia & Garrigues, 1998). Sediment-trapped elements are not inert and may return to the water column through different pathways, such as resuspension events caused by wind or wave actions, dredging, bioturbation, biological transformations (e.g. photosynthesis, transport through the food chain), changes in the physical chemical properties of the sediment-water interface (e.g. redox, pH), and diffusion (Calmano & Förstner, 1993; Eggleton & Thomas, 2004; Remaili et al., 2016).

The incidence of extreme droughts decreases reservoir water levels, exposing large areas of previously submerged aquatic sediment to direct contact with the atmosphere. Exposed aquatic sediments have been reported as significant sources of greenhouse gases (GHG) to the atmosphere, especially carbon dioxide (CO_2) and methane (CH_4) (Almeida et al., 2019; Jin et al., 2016; Kosten et al., 2018; Marcé et al., 2019). However, when precipitation levels return to normal and the reservoir water level rises, these exposed sediments become submerged again. This rewetting phenomenon may favor the release of the remaining elements in the sediment to the water column due to

the physical, chemical, and biological processes mentioned above. Although this is a natural process occurring on a seasonal scale, increased frequency of sediment drying and rewetting may exacerbate the release of elements buried in sediments either to the water column or directly to the atmosphere.

Enhanced release of elements and compounds from sediment to the water column may affect aquatic ecosystems. The release of nutrients such as nitrogen (N) and phosphorus (P) may support higher growth of bloom-forming phytoplankton, consequently increasing the internal production of organic matter and potentially leading to eutrophication (Josué et al., 2019; Tranvik et al., 2009). Furthermore, exposure to trace elements (e.g. iron, manganese, zinc) may be toxic to various aquatic organisms and enhances biomagnification in the food chain (Calmano & Förstner, 1993; Quadra, Lino, et al., 2019; Scott & Sloman, 2004). The implications of exposing sediments/soils to the atmosphere and their subsequent rewetting have been described in the literature, particularly with respect to changes in GHG fluxes and nutrient release. In contrast, much less is known about contaminant remobilization (trace elements). In addition, little is known about the effects of such phenomenon in sediments from freshwater reservoirs worldwide.

Here, we address the potential environmental impacts caused by a cycle of drought-rewetting in the sediment of a tropical reservoir. The environmental impacts considered here were: (1) contribution to greenhouse effect, through the release of the GHGs CO_2 and CH_4; (2) contribution to eutrophication, due to the release of nutrients (nitrogen and phosphorus); and (3) contribution to toxicity, caused by the release of trace elements (iron, Fe; manganese, Mn; and zinc, Zn). Furthermore, we used a cytogenotoxicity test (Allium test) to compare possible cytogenotoxic effects of the

overlying water from the induced-to-drought sediments (water samples from the rewetting period) with the overlying water from the sediments, which were kept permanently flooded. Our study was based on three hypotheses: (1) sediments under induced drying with subsequent rewetting show peaks of CO_2 and CH_4 emissions during both drying and rewetting periods, with total diffusive CO_2 and CH_4 fluxes being higher in the induced-to-drought sediments than in permanently flooded ones; (2) higher release rates and, therefore, higher total flux of nutrients and trace elements will be observed in the overlying water of the induced-to-drought sediments than in the permanently flooded ones; (3) cytogenotoxic effects will be observed in *Allium cepa* cells exposed to the overlying water from the rewetting period.

Material and methods

Sampling site characteristics

Chapéu D'Uvas reservoir (21º 33'S, 43º 35'W) is a 26-year-old reservoir constructed in Paraibuna River basin, 50 km downstream from the headwaters. It is located in the Atlantic forest biome (IBGE, 2012) and has 12 km^2 of maximum flooded area. Chapéu D'Uvas is mainly used for water supply purposes and is classified as oligotrophic (average of total nitrogen (TN) and total phosphorus (TP): 452 $\mu g\ L^{-1}$ and 12 $\mu g\ L^{-1}$, respectively) (Paranaíba et al., 2018). The region is characterized by dry winters and wet summers, with average annual temperature and precipitation ranging from 18 to 22 ºC and from 31 to 238 mm, respectively. The Federal University of Juiz de Fora holds a field station in the Chapéu D'Uvas reservoir (Núcleo de Integração Acadêmica para Sustentabilidade Sócioambiental, NIASSA); the field station is coordinated by two co-authors of this paper (F. Roland and N. Barros), who approved the field site access.

Experimental setup

Eight sediment cores were sampled at a permanently flooded zone of the reservoir (depth ~25 m) using a gravity corer equipped with a hammer device (UWITEC, Mondsee, Austria). After removal, the cores were closed with plastic lids and transported to the laboratory. In the laboratory, the upper 20 cm of sediment from each core was transferred to polyvinyl chloride (PVC) incubation cores (inner diameter = 6 cm; height = 70 cm) and the overlying water of the sediment was carefully replaced by 25 cm of distilled water in order to exclude the substances dissolved in reservoir water.

Later, we randomly assigned 4 cores to be induced to drought with a subsequent rewetting event, whereas 4 cores were kept with constant water level. The experiment was performed in the absence of light to avoid primary production and to reduce external interferences to the biogeochemical processes under investigation. The cores were then acclimated over a controlled air temperature of 35 ºC (± 3 ºC). This temperature was chosen to enhance evaporation (drought simulation). Although 35 ºC is above naturally occurring temperature ranges for submerged sediments of Chapéu D'Uvas reservoir (~20-27 ºC), exposed sediments in drawdown areas may reach temperatures around 35 ºC in summer months (data not shown). Distilled water was daily added until the original level in both induced-to-drought and permanently flooded cores during the first week, and afterwards only in the permanently flooded cores. Distilled water (24 ± 2 mL of distilled water d^{-1} - equivalent to 3 % of the total overlaying water) was added to the cores one hour prior to the measurements. Air temperature and pressure were monitored using a portable weather station (Skymaster Speedtech SM-28, accuracy: 3%). Water temperature was monitored using a digital thermometer in skewer format (INCOTERM – resolution ± 0.5 ºC).

Following the experimental setup of Kosten et al. (2018) (Kosten et al., 2018), we distinguished four different periods in our experiment that were described as: (i) "flooded period", which corresponds to the period when we added distilled water daily to the induced-to-drought cores during the first week of the experiment plus the second week when we stopped adding distilled water and the overlying water, corresponding to the period that the sediments were inundated, started to evaporate (days 0–14); (ii) "drying period", which started when the sediment from all induced-to-drought cores was directly exposed to the air, i.e. all overlying water had evaporated and the sediment moisture content started to decline (days 15–31); (iii) "dry period", when the moisture content was considered as zero, i.e. the weight of the induced-to-drought cores ceased to decline (days 32–60); and (iv) "rewetting period", when we started adding 100 mL of distilled water daily in the induced-to-drought cores until the end of the experiment (days 61–74). After starting the 100 mL additions in the rewetting period, water first filled the cracks created in the sediment in response to drying. It took two days until sediments became saturated and water began flooding over the surface of the sediment.

Estimates of the diffusive fluxes of CO_2 and CH_4

After 24 h of acclimatization, we started to perform measurements of diffusive fluxes of CO_2 and CH_4 using an infrared Ultraportable Greenhouse Gas Analyzer (UGGA, Los Gatos Research Inc., detection limit of 1.5×10^{-7} mmol L^{-1} for CO_2 and 2.76×10^{-10} mmol L^{-1} for CH_4). Before starting the incubations, the UGGA was calibrated using known concentration standards for both CO_2 and CH_4. We used a gas-tight expandable PVC stopper equipped with O-rings sealer on the top of the stopper to record linear increments of CO_2 and CH_4 over 4 minutes in the headspace of the cores. Measurements with non-linear increments were caused by the emission of gas bubbles

from the sediment and were therefore discarded. Then, further measurements were taken in order to capture only diffusive fluxes. Ebullitive fluxes were not included in our flux calculations due to human manipulation in the cores, which may favor the release of bubbles from the sediment to the water column and atmosphere, leading to interference in the flux results. Daily measurements were performed during the first and two last weeks of the experiment, whereas measurements were performed three times per week in the time in-between. All measurements were performed 1 h after adding distilled water in the permanently flooded cores throughout the experimental period, and in the induced-to-drought cores during the first week of the flooded period and during the rewetting period.

Total diffusive CO_2 and CH_4 emissions (as carbon (C) emissions) across the four experimental periods were estimated by calculating the area under the curve from the flux versus time plots. Moreover, total diffusive CH_4 emissions were converted into CO_2 equivalents ($CO_{2\text{-eq}}$) by multiplying by a factor of 34, according to the CH_4 Global Warming Potential (GWP) on a 100-year time horizon (IPCC, 2013).

Water sampling and replenishing

In order to understand how the release rate of compounds are affected during rewetting, we collected triplicate subsamples of 10 mL (i.e. 30 mL in total) of the overlying water at three different sampling times during the rewetting period (days 61, 67 and 74) for analysis of nutrient, trace elements, and cytogenotoxicity (described below). The subsamples were collected after the CO_2 and CH_4 flux measurements. At the end of each sampling day, 30 mL of distilled water was added to each core to compensate for the subsamples volume.

Nitrogen and phosphorus analyses

To estimate the TN and TP release from sediment to the overlying water, the samples were analyzed by spectrophotometry (Beckman Coulter, DU640; wavelengths of 230 nm for TN and 885 nm for TP) after alkaline persulfate digestion for nitrogen (Ferree & Shannon, 2001) and potassium persulfate digestion for phosphorus (Wetzel & Likens, 2013). Before analysis, glassware and volumetric materials were previously cleaned in an acid bath containing water and HNO_3 (9:1, v/v) for 24 h and, then, washed with distilled water. The distilled water was tested for possible contamination; both TN and TP contents were below the limits of detection (5 μg L^{-1} for TN and 3.1 μg L^{-1} for TP).

TN and TP masses (mg) in each core were calculated by multiplying measured concentrations (mg m^{-3}) by the amount of water in the core at the time of sampling (m^3); total masses were adjusted to compensate for the amount of water collected for analysis in each day. TN and TP masses were then divided by the core area (0.0113 m^2) to obtain masses per unit core area (mg m^{-2}). We then regressed nutrient mass per unit area (mg of N or P m^{-2}) against the sampling days (days 61, 67, and 74), with the slope of the relationship indicating TN and TP release rates over the sampling interval (mg of N or P m^{-2} d^{-1}).

Trace elements quantification

Trace elements quantification was performed using a Flame Atomization Atomic Absorption Spectrometer (FAAS), model (Thermo Scientific, Solaar M5 Series, Cambridge, United Kingdom). The wavelengths used were 248.3, 279.5, and 213.9 nm for Fe, Mn and Zn, respectively. The slit width was 0.2 nm for Fe, Mn, and Zn. The gas used was air/C_2H_2 at a flow rate of 1 L min^{-1} for Fe and Mn, and 1.2 L min^{-1} for Zn. Standard solutions were prepared from stock solutions (Quemis, Joinville, Brazil; 1000

mg L^{-1}) and maintained in 0.1% of HNO_3 (v/v). The concentrations used to construct the analytical curves ranged from 0.5 to 6 mg L^{-1} for Fe and Mn, and 0.25 to 3 mg L^{-1} for Zn. All glassware and volumetric materials were previously decontaminated in an acid bath containing water and HNO_3 (9:1, v/v) for 24 h and then washed with deionized water. The distilled water used was also previously tested for possible contamination by trace elements and no contamination was observed (samples below limits of detection). The Limits of Detection (LD) was 0.011 mg L^{-1} for Fe and Mn, and 0.006 mg L^{-1} for Zn. The sensitivity, in terms of characteristics concentration, was 0.096, 0.042, and 0.017 mg L^{-1} for Fe, Mn, and Zn, respectively. We calculated the release rate of trace elements following the same approach described for TN and TP.

Cytogenotoxicity test

The cytogenotoxicity test was performed using *Allium cepa* (onion) bulbs. First, the bulbs were placed in small cups with distilled water to stimulate root emergence. After 24 h, the bulbs were randomly exposed to permanently flooded and induced-to-drought water samples from the three different times (days 61, 67 and 74), in triplicates, and were kept in a Biological Oxygen Demand incubator (BOD) for 24 h. Afterward, the roots were washed and fixed in a cold solution of ethanol and acetic acid (3:1 v/v) for 24 h. Then, the roots were re-washed and slides were prepared using the squashing technique (for details, see Quadra et al. 2019 (Quadra, Roland, et al., 2019)). The slides were inspected at 400x magnification using an optical microscope to evaluate mitotic index and chromosomal aberrations: (i) aneugenic aberrations, which are usually related to chromosome losses, less adherence, and multipolarity; and (ii) clastogenic aberrations, which are related to DNA breaks (Leme & Marin-Morales, 2009; Quadra, Roland, et al., 2019).

Statistical procedures

We used an unpaired *t-test* to assess differences in the diffusive flux of CO_2 and CH_4 between induced-to-drought and permanently flooded cores within each experimental period (flooded, drying, dry and rewetting). The unpaired *t-test* was also used to assess the differences between induced-to-drought and permanently flooded cores in relation to the releases of nutrients that supposedly occurred after rewetting. The same statistical procedure was adopted to the cytogenotoxic analysis. We log-transformed diffusive CO_2 data in order to meet the assumption of normality and homoscedasticity. Cubic root function was applied for diffusive CH_4 data. Nutrient (TN and TP) and cytogenotoxicity data met normality assumptions and, therefore, no transformation was required. Trace element data did not meet the assumptions of normality and homoscedasticity, and the non-parametric Wilcoxon test was adopted to test the differences between groups. Cohen's *d* test was applied to determine the effect size of the CO_2 and CH_4, nutrients, trace elements, and cytogenotoxicity data. We assumed $p < 0.05$ as the threshold level of acceptance for all statistical tests. Statistical analyses were performed using JMP (version 14.0.0).

Results

Diffusive fluxes of CO_2 and CH_4 during a drying-rewetting cycle

We observed large variability in diffusive fluxes of CO_2 and CH_4 from induced-to-drought cores compared to the permanently flooded cores along the experimental periods (Figure 14, Table 4). The transition from the flooded to the drying period caused a peak in diffusive emissions for both gases (Figure 14), with values reaching up to 6677 mg C m^{-2} d^{-1} for CO_2 and 13696 mg C m^{-2} d^{-1} for CH_4 in the induced-to-drought cores.

As sediments dried out, diffusive emissions of both gases declined to values comparable to those observed in the initial flooded period (Figure 14). Rewetting dried-out sediments resulted in a new peak in CO_2 fluxes, but CH_4 fluxes remained unaffected (Figure 14). Notably, rewetting led to the highest rates of CO_2 emission throughout the experiment, with values reaching up to 9840 mg C m^{-2} d^{-1}.

Considering the entire length of the experiment, total diffusive CO_2 and CH_4 emissions (as C mass) from the induced-to-drought cores were, respectively, about 2.5 and 144 times higher than total diffusive CO_2 and CH_4 emissions observed in the permanently flooded cores (Table 4). In terms of $CO_{2\text{-eq}}$, induced-to-drought cores emitted about 24 times more than the permanently flooded cores (Table 4).

No statistical differences were observed in both CO_2 and CH_4 fluxes between groups during the flooded period (Table 4). However, the diffusive flux of CO_2 and CH_4 significantly differed between induced-to-drought and permanently flooded cores during the drying period, during the dry period for CH_4, and during the rewetting period for CO_2 (Table 4).

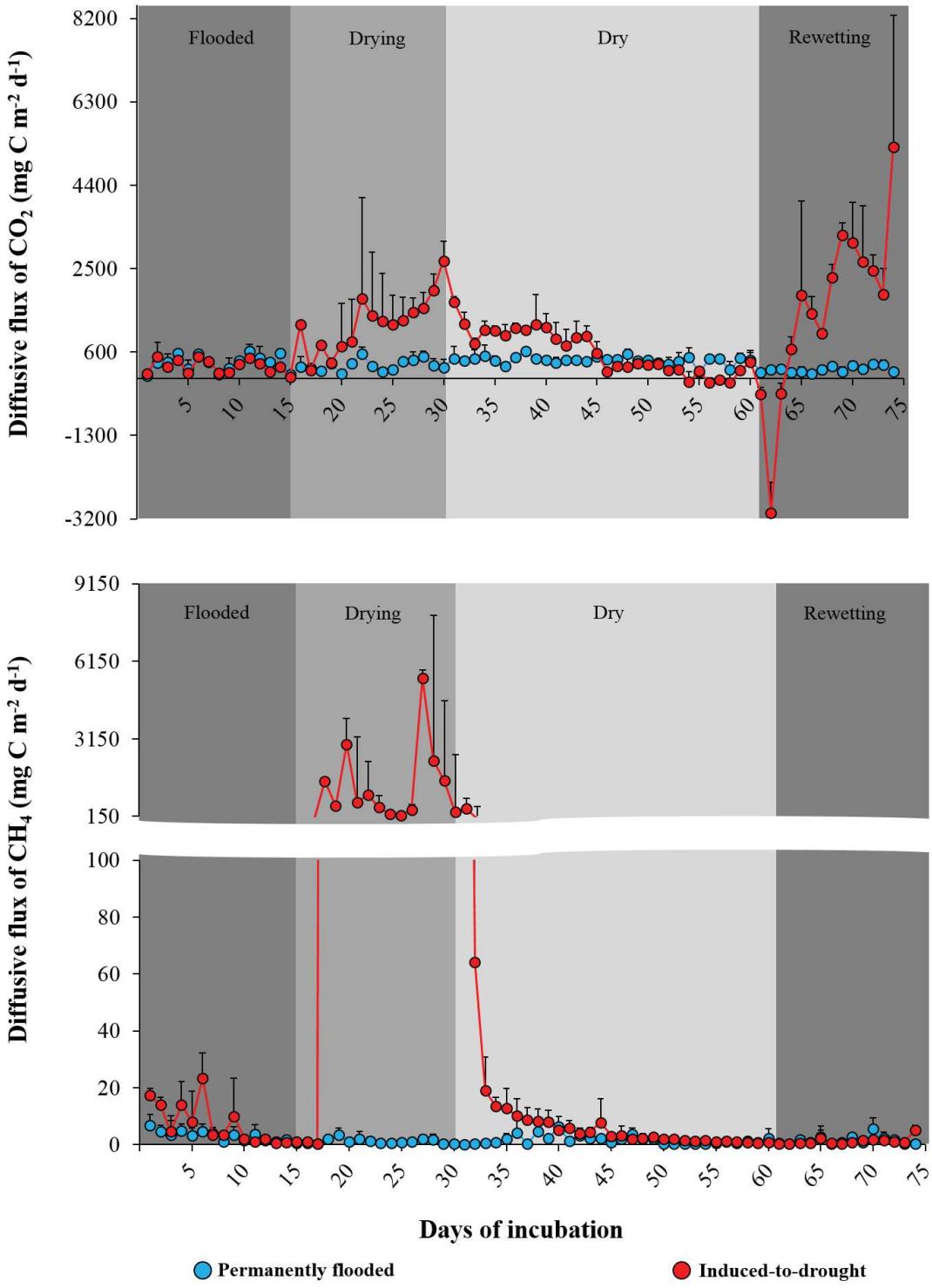

Figure 14: Diffusive flux of CO_2 (upper) and CH_4 (bottom) (average ± standard deviation; mg C m^{-2} d^{-1}) from permanently flooded (blue) and induced-to-drought cores (red) across the different experimental periods. For a better view of results, only the upper standard deviation is shown.

Table 4: Average ± standard deviation, median (bold), range (between parenthesis) of the diffusive CO_2 and CH_4 fluxes (mg C m^{-2} d^{-1}), as well as total diffusive carbon emissions (mg C m^{-2} and g $CO_{2\text{-eq}}$ m^{-2}) from the permanently flooded and induced-to-drought cores across the four experimental periods (flooded, drying, dry and rewetting). Statistical results from the unpaired t-test are shown as t-Ratio and p values (between parenthesis) for each experimental period. Results from Cohen's d Effect Size Test (ES) are shown right after t-test results.

	Diffusive CO_2 emissions						**Diffusive CH_4 emissions**						**Total emission as $CO_{2\text{-eq}}$ (g $CO_{2\text{-eq}}$ m^{-2}) [a]**	
	Flux (mg C m^{-2} d^{-1})				**Total emission (mg C m^{-2})**		**Flux (mg C m^{-2} d^{-1})**				**Total emission (mg C m^{-2})**			
	Permanently Flooded	**Induced-to-drought**	***t-Ratio (p)***	***ES***	**Permanently Flooded**	**Induced-to-drought**	**Permanently Flooded**	**Induced-to-drought**	***t-Ratio (p)***	***ES***	**Permanently Flooded**	**Induced-to-drought**	**Permanently Flooded**	**Induced-to-drought**
Flooded period	375 ± 170 **374** (55—619)	293 ± 141 **298** (108—496)	*1.35* *(0.18)*	*-42.8 — 209.4*	5271 ± 111	4050 ± 92	3.2 ± 1.6 **3.4** (0.9—6.8)	8.6 ± 7.8 **5.7** (0.5—23)	*1.95 (0.073)*	0.13 — *8.3*	42 ± 1.3	96 ± 5.4	6.7	7.4
Drying period	296 ± 131 **272** (87—562)	1225 ± 667 **1302** (30—2694)	*5.45 (0.0001)*	528.2 — 1276	5186 ± 98	21433 ± 559	1 ± 0.8 **0.8** (0.2—3.4)	1065 ± 1376 **512** (0.3—5510)	*3.09 (0.007)*	363.3 — 1765	18 ± 0.7	18139 ± 1055	5.8	638
Dry period	413 ± 95 **414** (134—627)	566 ± 450 **374** (-101—1244)	*1.75 (0.09)*	-21.9 — 326.9	11856 ± 68	15609 ± 441	1.7 ± 1.5 **1.3** (0.2—6.2)	7 ± 12 **3** (0.5—64)	*2.3 (0.03)*	0.6 — 9.6	48 ± 1	165 ± 8	13.5	21.2
Rewetting period	206 ± 67 **198** (106—329)	1600 ± 1926 **1924** (-3065—5291)	*2.6 (0.02)*	294.1 — 2492	2736 ± 51	19921 ± 1644	1.5 ± 1.4 **0.8** (0.2—5.6)	1.3 ± 1.2 **0.8** (0.3—5.1)	*0.5 (0.62)*	-0.08 — 1.3	20 ± 1	14 ± 0.7	3.4	20.4
Total period					25050 ± 111	61013 ± 924					128 ± 1.2	18415 ± 677	29.4	687

[a] CH_4 emissions were converted into $CO_{2\text{-eq}}$ emission using a GWP of 34 on a 100-year time horizon (IPCC 2013).

Nitrogen and phosphorus release during rewetting

The release rate of TN ranged from -1.4 to 1.1 mg m^{-2} d^{-1} (average ± SD: -0.2 ± 1, median: -0.8 mg m^{-2} d^{-1}) in the permanently flooded cores, and from 33.4 to 52.7 mg m^{-2} d^{-1} (average ± SD: 42.4 ± 7, median: 41.1 µg m^{-2} d^{-1}) in the induced-to-drought cores (Table 5). The release rate of TP ranged from -0.007 to 0.03 mg m^{-2} d^{-1} (average ± SD: 0.01 ± 0.01, median: 0.008 mg m^{-2} d^{-1}) in the permanently flooded cores, and from 0.6 to 1.4 mg m^{-2} d^{-1} (average ± SD: 1 ± 0.3, median: 0.7 mg m^{-2} d^{-1}) in the induced-to-drought cores (Table 5). TN and TP fluxes to the overlying water of the induced-to-drought cores were consistently higher than those observed in the permanently flooded cores (Figure 15 and Table 5), with values up to ~380 times higher for nitrogen (*t-Ratio = 10.63*, *p = 0.001*) and ~210 times higher for phosphorus (*t-Ratio = 5.26*, *p = 0.01*). Results from Cohen's *d* test revealed a confidence interval (lower 95% — higher 95%) ranging from 32.8 to 52.4 mg m^{-2} d^{-1} (*p = 0.001*) for TN, and from 0.5 to 1.4 mg m^{-2} d^{-1} (*p = 0.01*) for TP.

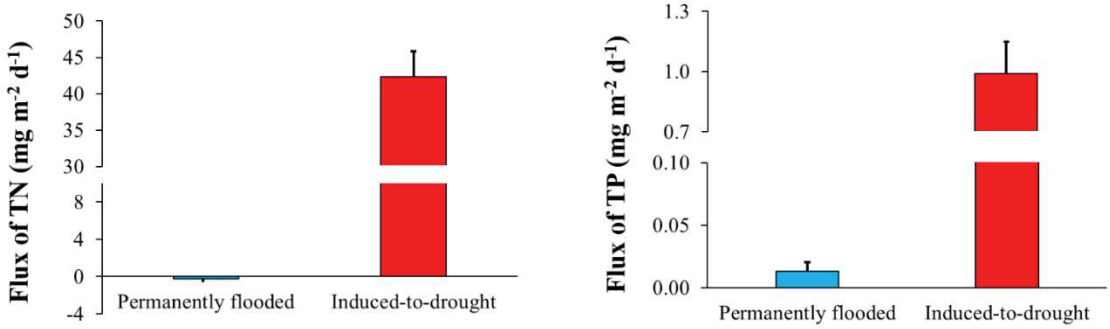

Figure 15: Average ± standard error of total nitrogen (TN) and total phosphorus (TP) release rates (mg m^{-2} d^{-1}) from permanently flooded (blue) and induced-to-drought cores (red)during the rewetting period. For a better view of results, only the upper standard error is shown.

Table 5: Nutrient release rates (TN and TP - mg m^{-2} d^{-1}) and r^2 from the regression of nutrient mass per unit area against sampling interval for each core of the permanently flooded and induced-to-drought groups during the rewetting period. Statistical results from the unpaired *t-test* are shown as *t* and *p* values.

Nutrient	Group	Core number	Flux (mg m^{-2} d^{-1})	r^2	Statistical significance
Total Nitrogen	Permanently flooded	C1	-0.8	0.789	
		C2	1.1	0.977	
		C3	-1.4	0.696	
		C4	0.2	0.313	*t = 10.63*
Total Nitrogen	Induced-to-drought	T1	42.3	0.979	*p = 0.001*
		T2	52.7	0.986	
		T3	41.1	0.995	
		T4	33.4	0.954	
Total Phosphorus	Permanently flooded	C1	-0.01	0.093	
		C2	0.03	0.344	
		C3	0.01	0.039	
		C4	0.02	0.038	*t = 5.26*
Total Phosphorus	Induced-to-drought	T1	1.4	0.999	*p = 0.01*
		T2	1.1	0.968	
		T3	0.7	0.971	
		T4	0.6	0.985	

Trace element release during rewetting

Statistically higher release rates and, consequently, higher total flux of Fe, Mn, and Zn were observed in the induced-to-drought cores compared to permanently flooded cores (Fe: $Z = 2.16$, $p = 0.03$; Mn: $Z = 2.21$, $p = 0.02$; Zn: $Z = 2.21$, $p = 0.02$) (Figure 16 and Table 6). Average release rates of dissolved Fe, Mn, and Zn observed in induced-to-drought cores were 40, 86, and 5220 times, respectively, higher than the average release rates observed in permanently flooded cores. Results from Cohen's *d* test revealed a confidence interval ranging from 35.4 to 114 mg m^{-2} d^{-1} ($p = 0.03$) for Fe, from -0.7 to 11.1 mg m^{-2} d^{-1} ($p = 0.02$) for Mn, and from -0.6 to 4.6 mg m^{-2} d^{-1} ($p = 0.02$) for Zn.

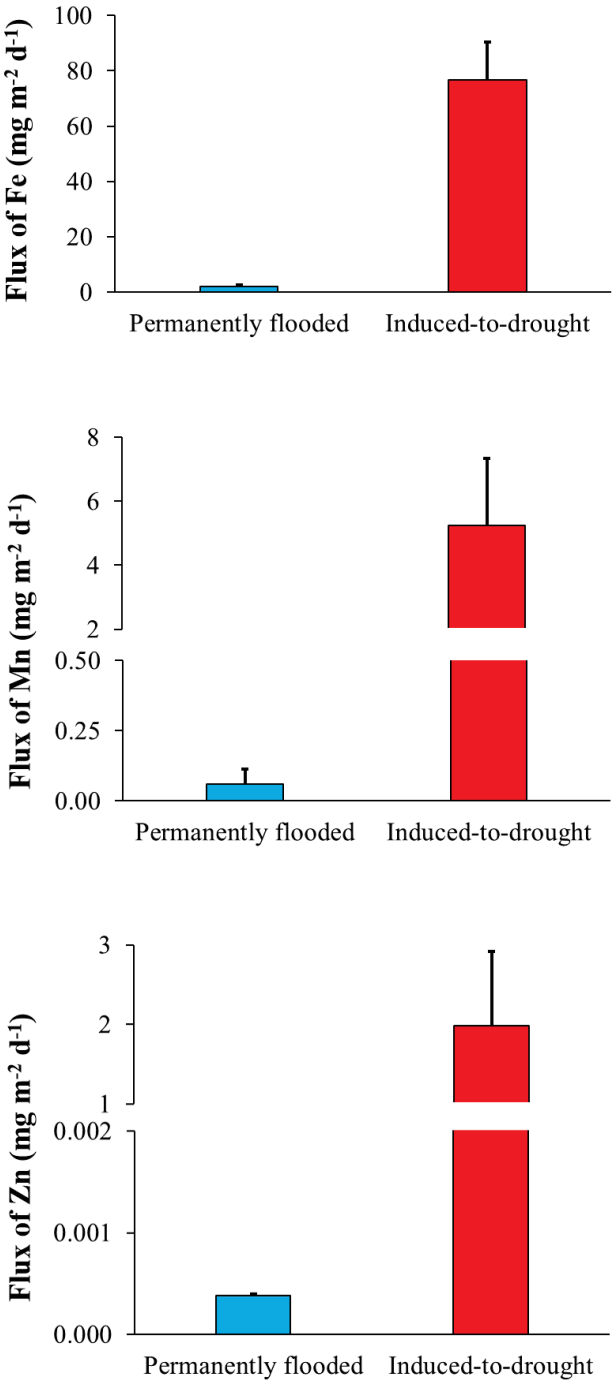

Figure 16: Average ± standard error of Iron (Fe), Manganese (Mn) and Zinc (Zn) release rates (mg m^{-2} d^{-1}) from permanently flooded (blue) and induced-to-drought cores (red) during the rewetting period. For a better view of results, only the upper standard error is shown.

Table 6: Trace element release rates (Fe, Mn, and Zn - mg m^{-2} d^{-1}) and r^2 from the regression of trace element mass per unit area against sampling interval for each core of the permanently flooded and induced-to-drought groups during the rewetting period. Statistical results from Wilcoxon test are shown as *Z* and *p* values.

Trace element	Group	Core number	Flux (mg m^{-2} d^{-1})	r^2	Statistical significance
Iron	Permanently flooded	C1	3.81	0.980	
		C2	1.54	0.906	
		C3	1.14	0.999	
		C4	1.26	0.873	*Z = 2.16*
Iron	Induced-to-drought	T1	111.03	0.986	*p = 0.03*
		T2	77.94	0.983	
		T3	83.94	0.943	
		T4	33.65	0.998	
Manganese	Permanently flooded	C1	0.24	0.788	
		C2	0.0007	0.711	
		C3	0.0007	0.711	
		C4	0.0007	0.711	*Z = 2.21*
Manganese	Induced-to-drought	T1	1.66	0.782	*p = 0.02*
		T2	11.44	0.994	
		T3	6.71	0.895	
		T4	1.16	0.917	
Zinc	Permanently flooded	C1	0.0004	0.711	
		C2	0.0003	0.019	
		C3	0.0004	0.711	
		C4	0.0004	0.711	*Z = 2.21*
Zinc	Induced-to-drought	T1	0.05	0.999	*p = 0.02*
		T2	4.56	0.791	
		T3	2.97	0.996	
		T4	0.34	0.839	

Cytogenotoxic responses between groups

Significant mitotic index reduction was observed in *Allium cepa* cells exposed to water samples from induced-to-drought cores when compared to cells exposed to permanently

flooded water samples (12 to 22% less cell replication; *t-Ratio = 5.26*, $p < 0.0001$) (Figure 17). Moreover, the aneugenic alterations were 28 to 114% higher in cells exposed to water samples from the induced-to-drought cores than the cells exposed to permanently flooded water samples (*t-Ratio = 5.79*, $p < 0.0001$) (Figure 17). No statistical difference was observed between groups in relation to clastogenic alterations (*t-Ratio = 0.95*, $p = 0.35$) (Figure 17). Results from Cohen's *d* test revealed a confidence interval ranging from 0.59 to 1.35 % ($p < 0.0001$) for mitotic index, from 0.41 to 0.87 % ($p < 0.0001$) for aneugenic alterations, and from 0.15 to 0.4 % ($p = 0.35$) for clastogenic alterations.

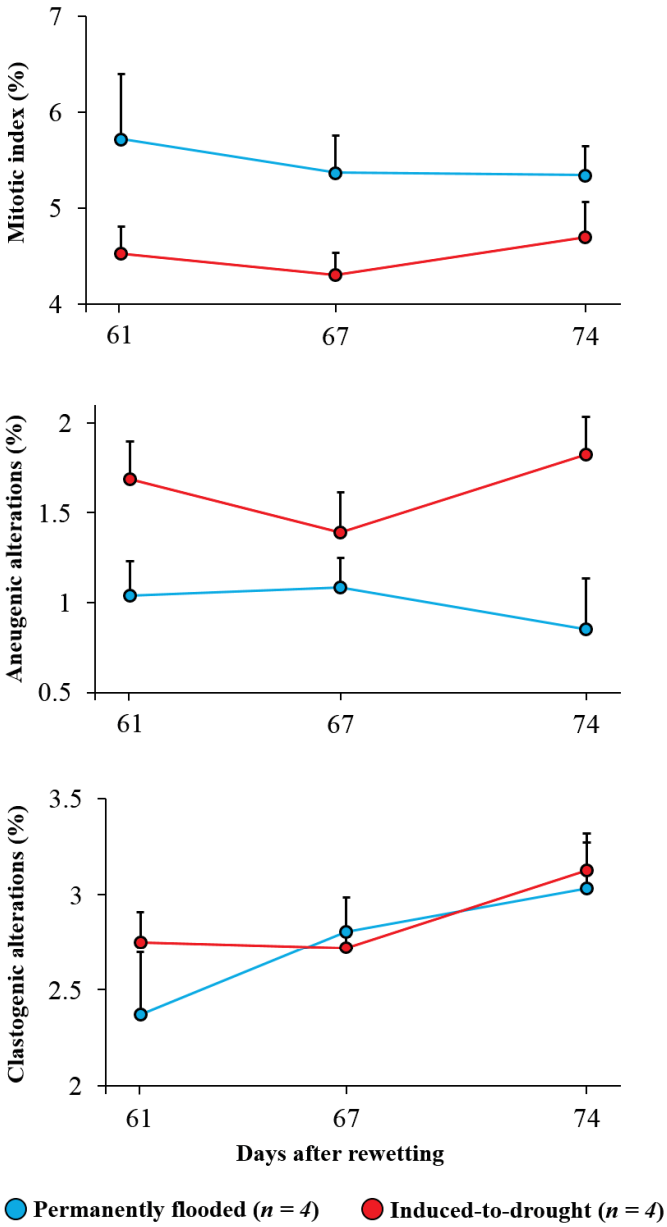

Figure 17: Average ± standard deviation of mitotic index, and aneugenic and clastogenic alterations from *Allium cepa* tests between groups (permanently flooded: blue, and induced-to-drought: red) on different sampling days during the rewetting period. For a better view of results, only the upper standard deviation is shown.

Discussion

Sediment drying with subsequent rewetting boosts GHG emission

We observed a significant increase of CO_2 and CH_4 emissions resulting from the drying and rewetting of freshwater sediments, similar to what has been found in previous studies (W Borken et al., 2003; Fromin et al., 2010; Jarvis et al., 2007; Kim et al., 2012; Kosten et al., 2018). The observed pattern is attributed to a phenomenon generally known as the "Birch effect", in reference to studies carried out by H.F. Birch in the 1950s and 1960s on the effects of droughts and rewetting events on the carbon and nitrogen cycle in agricultural and forest soils (Birch, 1958; Birch & Friend, 1956).

Accordingly, the biological processes that occur in aquatic sediments are directly associated with its water content (D.S. Baldwin & Mitchell, 2000; Rodrigo et al., 1997). According to our findings, the first peak of both CO_2 and CH_4 emissions occurs in sediments shortly after the sediment surface is exposed to the atmosphere (in our induced-to-drought cores these peaks corresponded to the first and second days after the overlying water was absent, Figure 14). Subsequently, during the entire drying period, the magnitude of CO_2 and CH_4 emissions from the induced-to-drought cores remained substantially higher than the emissions observed in the permanently flooded cores (4 and 1000 times higher for CO_2 and CH_4, respectively, after 15 days of drying) (Figure 14).

When sediments are exposed to direct contact with the atmosphere, we may expect a series of changes ultimately affecting the CO_2 and CH_4 dynamics, as follows: (i) the now exposed sediment has direct contact with atmospheric oxygen stimulating the decomposition of the usually high amount of labile organic matter in the surface sediment (Mendonça et al., 2014) and resulting in substantial carbon losses to the atmosphere (Kosten et al., 2018); (ii) as drought persists, sediment may crack causing the penetration of oxygen into deeper layers, which triggers more organic matter mineralization (Fromin et al., 2010); (iii) the cracks formed by the sediment desiccation may also favor the release

of gases, that were retained in lower parts of the sediment, to the atmosphere, especially CH_4, which tends to form gas bubbles (not accounted here) in the sediment due to its low solubility (Kosten et al., 2018; Rosenberry et al., 2006); (iv) the gas-exchange velocity between the sediment-air interface is much faster (> 10000 times faster) than between the water-air interface, which considerably increases the diffusive carbon emissions between sediment-air interface (Lide, 2004); (v) the boosted organic matter degradation by the increase in oxygen availability tends to decrease the pore water pH, potentially leading to gas dissolutions (i.e. CO_2) from the sediment into the atmosphere (Skinner et al., 2014).

When the water content of the sediments approached zero (i.e. when the weight of the induced-to-drought cores stabilized, ~30 days after the start of the incubations), we observed a substantial decrease in the sediment CO_2 and CH_4 emissions from the induced-to-drought cores (Figure 14). The paucity of water in previously submerged sediments likely promoted the desiccation of the sediment microbial communities (Werner Borken & Matzner, 2009; Jin et al., 2016; Rodrigo et al., 1997), directly affecting their capacity to decompose organic matter into CO_2 and CH_4. We observed a slightly significant difference in CH_4 emissions between the induced-to-drought and permanently flooded cores during the dry period (*t-Ratio = 2.3*, *p = 0.03*), caused by the high fluxes registered in the first days after the sediment was completely dry (Figure 14). It is possible that during this period there was still some microbial activity or that these fluxes correspond to the emission of the remnant gases produced during the drying phase.

Finally, the rewetting simulation resulted in a rapid, and short, influx of CO_2 from the atmosphere to the recent overlying water of the induced-to-drought cores during the first three days of the rewetting period (Figure 14). The observed CO_2 uptake may be caused by a possible lag-phase between rewetting and initiation of microbial production

of CO_2 leading to a flux of atmospheric CO_2 into the potentially CO_2-undersaturated distilled water. However, after 96 h of rewetting, the induced-to-drought cores became, again, strong CO_2 sources to the atmosphere, reaching the highest recorded values until the end of the experiment (Figure 14). On the other hand, we did not observe any CH_4 peaks occurring in the induced-to-drought cores during the rewetting period, with values similar to those observed in the permanently flooded cores (Figure 14). Some studies describe that 24 h of wet conditions are enough to stimulate heterotrophic microbial activities in the surface of sediments, promoting shifts in the microbial communities and increasing their biomass (Evans & Wallenstein, 2012; Fromin et al., 2010). Borken et al. (2003) and Kosten et al. (2018) showed that rewetting events on sediments induced to drought triggered instantaneous CO_2 emissions to the atmosphere, which remained increasing as the water content was also increasing. The same pattern was also observed in situ by Fromin et al. (2010), who reported peaks of CO_2 emissions after a rain event on dry sediments from a Mediterranean pond. Accordingly, the occurrence and magnitude of CO_2 and CH_4 emissions have been related to the frequency and intensity of dry and rewetting periods. For instance, different microbial responses (respiration) were observed in sediments that experienced distinct periods of dry conditions as well as the frequency of rewetting phases (Fierer & Schimel, 2002; Fromin et al., 2010; Kosten et al., 2018). Therefore, the duration of droughts in conjunction with different rewetting periods may be considered a stressful process for microbial communities, playing a crucial role in the microbial dynamics submitted to such unstable conditions, resulting in contrasts of GHG production/emission (Fromin et al., 2010; Gordon et al., 2008).

Even though ebullition was observed at certain times throughout the experimental time in both groups, our findings do not take into account the contribution of this CH_4 release pathway, which tends to increase in intensity when the water column lowers

(Harrison et al., 2017). Moreover, possible incomplete carbon mineralization not resulting in CO_2 or CH_4 production but in dissolved organic carbon production, is not captured by our analyses. In addition, we may have also missed a CO_2 sink by suppressing photosynthesis in our dark experimental conditions.

Rewetting-related release of nitrogen and phosphorus

The rewetting of desiccated sediments led to substantial releases of nitrogen and phosphorus from the sediment to the overlying water in the induced-to-drought cores, where the release rates were higher than those observed in the permanently flooded cores throughout the rewetting period (14 days; Figure 15). When previously exposed sediments are re-flooded, an initial flush of nitrogen and phosphorus usually occurs to the overlying water (the so-called Birch effect) (Birch, 1958, 1960; West et al., 1988), mainly due to the enhancement of aerobic organic matter mineralization that tends to accumulate inorganic nitrogen in dry sediments, and due to the release of nitrogen and phosphorus bound to organisms that died when the sediments were drying out (D.S. Baldwin & Mitchell, 2000; Fromin et al., 2010; Wilson & Baldwin, 2008).

Previous studies have shown the release of phosphorus during drying-rewetting events (Kinsman-Costello et al., 2014; Schönbrunner et al., 2012), and the longer the drought period was, the greater subsequent release of phosphorus (Schönbrunner et al., 2012). Moreover, events of drought in sediments increase the crystallinity of iron species, which leads to a loss of phosphorus binding capacity (Qiu & McComb, 1994; Schönbrunner et al., 2012). Our results also corroborate previous studies showing nitrogen release from sediments after drying and rewetting events, mostly in the form of N-ammonium (Darren S. Baldwin et al., 2008; Dabrowski et al., 2017; Wilson & Baldwin, 2008). N-ammonium can be toxic to aquatic fauna, such as fish and crustaceans

(Ip & Chew, 2010), which means that the effects of drying and rewetting of sediments may increase the incidence of ammonium toxicity. In addition, our study site is oligotrophic, but if we investigate a nutrient-enriched aquatic ecosystem, it is likely that the amount of nitrogen and phosphorus released may be even higher (Corstanje & Reddy, 2010). Beyond the quantity of nutrients in the sediments, other factors may influence these nutrient releases, such as the history of drying and rewetting events, the exposure time to air during the dry period, sediment properties and microbial community metabolism (D.S. Baldwin & Mitchell, 2000; Qiu & McComb, 1994; Schönbrunner et al., 2012; Steinman et al., 2014; Wilson & Baldwin, 2008).

After rewetting, microbial activity picks up, possibly in part due to the higher availability of nutrients as a result of drought induced cell lysis (D.S. Baldwin & Mitchell, 2000). This enhanced metabolic activity quickly results in anaerobic conditions triggering denitrification and the release of iron-bound phosphorus (D.S. Baldwin & Mitchell, 2000). Last but not least, rewetting exposed sediments may pose a risk (stress) for the sediment biota, which will potentially face cell lysis and, consequently, release more intracellular nitrogen and phosphorus to the overlying water (Fierer & Schimel, 2002; Qiu & McComb, 1994).

The observed strong increase in sediment nutrient release as a result of desiccation-rewetting may favor eutrophication in our study system. In addition, our results substantiate that climate change related to changes in precipitation patterns may affect nutrient cycling in aquatic ecosystems globally (D.S. Baldwin & Mitchell, 2000).

Rewetting-related release of trace elements

The contamination history of aquatic ecosystems may be a factor that influences the amount of trace elements released after the exposures of droughts and rewetting. The watershed of our study site, however, does not contain much urban or industrial development (land cover: ~66% of grassland, ~30% of natural forest, and ~4% of Eucalyptus plantation) (Machado, 2012) and, therefore, we did not expect high release rates of trace elements. On the other hand, high concentrations of Fe have already been reported in the sediments of Chapéu D'Uvas reservoir (Quadra, Lino, et al., 2019).

Our results showed that Fe, Mn and Zn release rates were, in general, higher in the induced-to-drought water samples than in the permanently flooded water samples (Figure 16). This means that an effect of drying and rewetting sediments was observed on the release of trace elements to the water column. The mobility of trace elements changes during drying and rewetting periods, possibly due to alterations in physical-chemical properties such as pH and redox potential (Calmano & Ahlf, 1990; Calmano & Förstner, 1993; Tack et al., 1996). When sediments are exposed to oxygen, a release of trace elements such as Fe and Zn is expected mainly due to changes in pH that consequently decrease the buffer capacity of the sediments (Calmano & Ahlf, 1990). Another possible explanation that corroborates the release of trace elements is their affinity for organic matter, which under oxidizing conditions may compromise the adsorption capacity of sediments, leading to the release of these elements to the water column after rewetting (Anju & Banerjee, 2010; Hass & Fine, 2010).

A strong release of Fe and Mn (Dabrowski et al., 2017; Lucassen et al., 2005), as well as Al and Zn (Lucassen et al., 2005), have been found after rewetting events in exposed sediments. The Fe cycle is coupled to the phosphorus cycle (Schönbrunner et al., 2012), and the sediments exposed to oxygen may alter the production of iron species,

causing changes in these biogeochemical cycles (Dieter et al., 2015). The release of contaminants in seasonal rivers was reported by Ademollo et al. (2011) (Ademollo et al., 2011), which showed that the bioavailable fraction of trace elements was more frequently found. This observation has ecological importance since the bioavailable fractions are more relevant in terms of environmental risks (Ademollo et al., 2011; Quadra, Lino, et al., 2019). Thus, according to our results and previous studies, the maintenance of flooded sediments is important for the management of polluted areas.

The release rates of trace elements reported here may not likely lead to concentrations in the overlying water capable to cause acute and chronic toxicity on aquatic organisms, such as Mn in *Ceriodaphnia dubia* and *Hyalella Azteca* (Lasier et al., 2000), Zn in *Litopenaeus vannamei* and *Rhithrogena hageni* (Brinkman & Johnston, 2008; Wu & Chen, 2004), as well as for Fe in *Asellus aquaticus* and *Leptophlebia marginata* (Gerhardt & Westermann, 1995; T. R. Martin & Holdich, 1986). However, as above-mentioned, the release of compounds depends also on the contamination history of the aquatic ecosystem, where a more polluted environment may release more trace elements into the water column, likely leading to adverse effects on aquatic organisms. Beyond toxic effects, the trace elements may cause other environmental impacts, such as eutrophication. For example, Fe plays an important role in primary production and is, therefore, a limiting nutrient in aquatic ecosystems (J. H. Martin et al., 1990). However, when in excess, it may lead to toxicity in aquatic organisms (T. R. Martin & Holdich, 1986).

Cytogenotoxic effects of compounds released upon rewetting

Allium test is a highly sensitive bioassay whose results correlates with those observed in other organisms; thus, it is widely used to investigate chemical contamination

and toxicity effects in aquatic ecosystems (Athanásio et al., 2014; Radić et al., 2010). The mitotic index indicates the number of cells in division during the cell cycle (Leme & Marin-Morales, 2009). Allium cells exposed to induced-to-drought water samples showed a lower number of cells replicating when compared to cells exposed to permanently flooded water samples (Figure 17). Aneugenic effects are related to toxic effects in the cells and they are expressed as chromosomal alterations such as chromosome losses, delays, adherence, multipolarity and C-metaphases (Leme & Marin-Morales, 2009). The aneugenic alterations were higher in the cells exposed to induced-to-drought water samples (Figure 17). Clastogenic effects are related to DNA breaks and they are expressed in chromosomal alterations such as bridges and breaks (Leme & Marin-Morales, 2009). We did not observe significant difference in clastogenic effects between cells exposed to induced-to-drought and permanently flooded water samples (Figure 17). Given that only aneugenic alterations were observed, rather than both alterations studied (aneugenic and clastogenic), the contaminants presented in the water overlying sediments are likely related to the induction of chromosomal alterations linked to mitotic spindle dysfunctions (Fiskesjo, 1985; Ray et al., 2013).

Our results indicate the possibility of adverse effects occurring after sediment exposure followed by rewetting events. The cell proliferation was affected as well as toxic effects were observed, expressed by mitotic index and aneugenic effects. Previous studies reported cytogenotoxic effects of trace elements (Al, Cd, Fe, Mn, and Zn) using the Allium test (Panda et al., 1996; Quadra, Roland, et al., 2019; Steinkellner et al., 1998). Moreover, N-ammonium was also related to cause genotoxicity in *Oreochromis niloticus* (Abumourad et al., 2012). Then, the cytogenotoxic results reported here may be attributed to synergistic effects of trace elements and nutrients (including other elements and

compounds not investigated here) released during rewetting in the induced-to-drought sediments.

Conclusions

This study showed different consequences of a cycle of induced drought followed by rewetting on the dynamics of GHG, nutrients, and trace elements in the sediment of a tropical reservoir. Our findings confirmed our three postulated hypotheses: (i) CO_2 and CH_4 emission peaks occurring at distinct experimental periods in induced-to-drought cores, with average fluxes up to 140 times higher than those observed in the permanently flooded cores; (ii) higher release rates of nutrients and trace elements in the overlying water of the induced-to-drought cores, reaching average values up to 206 times (TN) and 5220 times (Zn) higher than in the permanently flooded cores; and (iii) lower mitotic index values in *Allium cepa* cells exposed to water samples from the induced-to-drought cores during the rewetting period, leading to up to 22% less cell replication when compared to cells exposed to water samples from the permanently flooded cores. Understanding the effects of exposing aquatic sediments to the atmosphere and its subsequent flooding is a challenge, especially due to the wide variation in sediment quality. Therefore, it is critical to stimulate further efforts into this subject in order to comprehend the extent of these events in aquatic biogeochemical cycles, given that upcoming projections related to severe droughts appear to be an unavoidable fact.

Acknowledgments. We are grateful to Gladson Rezende Marques for his support in the nutrient analysis.

References

Abumourad, I. M. K., Hanna, M. I., & Girgis, S. M. (2012). Genotoxicity assessment of ammonia in cultured Oreochromis niloticus using RAPD assay. *Journal of Genetic Engineering and Biotechnology*, *10*(2), 209–212. https://doi.org/10.1016/j.jgeb.2012.10.002

Ademollo, N., Capri, S., Froebrich, J., Patrolecco, L., Polesello, S., Puddu, A., et al. (2011). Fate and monitoring of hazardous substances in temporary rivers. *TrAC - Trends in Analytical Chemistry*, *30*(8), 1222–1232. https://doi.org/10.1016/j.trac.2011.05.002

Almeida, R. M., Paranaíba, J. R., Barbosa, Í., Sobek, S., Kosten, S., Linkhorst, A., et al. (2019). Carbon dioxide emission from drawdown areas of a Brazilian reservoir is linked to surrounding land cover. *Aquatic Sciences*, *81*(4), 1–9. https://doi.org/10.1007/s00027-019-0665-9

Anju, M., & Banerjee, D. K. (2010). Comparison of two sequential extraction procedures for heavy metal partitioning in mine tailings. *Chemosphere*, *78*(11), 1393–1402. https://doi.org/10.1016/j.chemosphere.2009.12.064

Athanásio, C. G., Prá, D., & Rieger, A. (2014). Water quality of urban streams: The Allium cepa seeds/seedlings test as a tool for surface water monitoring. *Scientific World Journal*, *24*, 1–7. https://doi.org/10.1155/2014/391367

Baldwin, D.S., & Mitchell, A. M. (2000). The effects of drying and re-flooding on the sediment and soil nutrient dynamics of lowland river-floodplain systems: a synthesis. *Regulated Rivers: Research & Management*, *16*(5), 457–467.

https://doi.org/10.1002/1099-1646(200009/10)16:5<457::aid-rrr597>3.3.co;2-2

Baldwin, Darren S., Gigney, H., Wilson, J. S., Watson, G., & Boulding, A. N. (2008). Drivers of water quality in a large water storage reservoir during a period of extreme drawdown. *Water Research*, *42*(19), 4711–4724. https://doi.org/10.1016/j.watres.2008.08.020

Birch, H. F. (1958). The effect of soil drying on humus decomposition and nitrogen availability. *Plant and Soil*, *10*(1), 9–31. https://doi.org/10.1007/BF01343734

Birch, H. F. (1960). *Nitrification in soils after different periods of dryness*. *Plant and Soil* (Vol. 12). https://doi.org/10.1007/BF01377763

Birch, H. F., & Friend, M. T. (1956). The organic-matter and nitrogen status of East African soils. *Journal of Soil Science*, *7*(1), 156–168. https://doi.org/https://doi.org/10.1111/j.1365-2389.1956.tb00871.x

Borken, W, Davidson, E. A., Savage, K., Gaudinski, J., & Trumbore, S. E. (2003). Drying and Wetting.Pdf. *Soil Sciente Society of America*, *67*(1999), 1888–1896.

Borken, Werner, & Matzner, E. (2009). Reappraisal of drying and wetting effects on C and N mineralization and fluxes in soils. *Global Change Biology*, *15*(4), 808–824. https://doi.org/10.1111/j.1365-2486.2008.01681.x

Brinkman, S. F., & Johnston, W. D. (2008). Acute toxicity of aqueous copper, cadmium, and zinc to the mayfly Rhithrogena hageni. *Archives of Environmental Contamination and Toxicology*, *54*(3), 466–472. https://doi.org/10.1007/s00244-007-9043-z

Calmano, W., & Ahlf, W. (1990). Exchange of heavy metals between sediment components and water. *Metal Speciation in the Environment*, *23*, 503–522. https://doi.org/10.1007/978-3-642-74206-4

Calmano, W., & Förstner, U. (1993). Binding and mobilization of heavy metals in contaminated sediments affected by pH and redox potential. *Water Science and Technology*, *28*(8–9), 223–235. https://doi.org/10.2166/wst.1993.0622

Van Cappellen, P., & Maavara, T. (2016). Rivers in the Anthropocene: Global scale modifications of riverine nutrient fluxes by damming. *Ecohydrology and Hydrobiology*, *16*(2), 106–111. https://doi.org/10.1016/j.ecohyd.2016.04.001

Corstanje, R., & Reddy, K. R. (2010). Response of Biogeochemical Indicators to a Drawdown and Subsequent Reflood. *Journal of Environment Quality*, *33*(6), 2357. https://doi.org/10.2134/jeq2004.2357

Dabrowski, J., Baldwin, D. S., Dabrowski, J. M., Hill, L., & Shadung, J. (2017). Impact of temporary desiccation on the mobility of nutrients and metals from sediments of loskop reservoir, olifants river. *Water SA*, *43*(1), 7–16. https://doi.org/10.4314/wsa.v43i1.02

Dieter, D., Herzog, C., & Hupfer, M. (2015). Effects of drying on phosphorus uptake in re-flooded lake sediments. *Environmental Science and Pollution Research*, *22*(21), 17065–17081. https://doi.org/10.1007/s11356-015-4904-x

Dirzo, R., Young, H. S., Galetti, M., Ceballos, G., Isaac, N. J. B., & Collen, B. (2014). Defaunation in the Anthropocene. *Science*, *345*(6195), 401–406.

Eggleton, J., & Thomas, K. (2004). A review of factors affecting the release and

bioavailability of contaminants during sediment disturbance events. *Environment International*, *30*(7), 973–980. https://doi.org/10.1016/j.envint.2004.03.001

Evans, S., & Wallenstein, M. (2012). Soil microbial community response to drying and rewetting stress: Does historical precipitation regime matter? *Biogeochemistry*, *109*(1–3), 101–116. https://doi.org/10.1007/s10533-011-9638-3

Ferree, M. A., & Shannon, R. D. (2001). Evaluation of a second derivative UV/visible spectroscopy technique for nitrate and total nitrogen analysis of wastewater samples. *Water Research*, *35*(1), 327–332. https://doi.org/10.1016/S0043-1354(00)00222-0

Fierer, N., & Schimel, J. P. (2002). Effects of drying-rewetting frequency on soil carbon and nitrogen transformations. *Soil Biology and Biochemistry*, *34*(6), 777–787. https://doi.org/10.1016/S0038-0717(02)00007-X

Fiskesjo, G. (1985). The Allium test as a standard in environmental monitoring. *Hereditas*, *102*(1), 99–112. https://doi.org/10.1111/j.1601-5223.1985.tb00471.x

Friedl, G., & Wüest, A. (2002). Disrupting biogeochemical cycles – Consequences of damming. *Aquatic Sciences*, *64*, 55–65. https://doi.org/10.1016/0025-326x(91)90729-c

Fromin, N., Pinay, G., Montuelle, B., Landais, D., Ourcival, J. M., Joffre, R., & Lensi, R. (2010). Impact of seasonal sediment desiccation and rewetting on microbial processes involved in greenhouse gas emissions. *Ecohydrology*, *3*, 339–348. https://doi.org/10.1002/eco.115

Gerhardt, A., & Westermann, F. (1995). Effects of precipitations of iron hydroxides on Leptophlebia marginata (L.) (Insecta: Ephemeroptera) in the field. *Archiv Fur*

Hydrobiologie.

Gordon, H., Haygarth, P. M., & Bardgett, R. D. (2008). Drying and rewetting effects on soil microbial community composition and nutrient leaching. *Soil Biology and Biochemistry*, *40*(2), 302–311. https://doi.org/10.1016/j.soilbio.2007.08.008

Harrison, J. A., Deemer, B. R., Birchfield, M. K., & O'Malley, M. T. (2017). Reservoir Water-Level Drawdowns Accelerate and Amplify Methane Emission. *Environmental Science and Technology*, *51*(3), 1267–1277. https://doi.org/10.1021/acs.est.6b03185

Hass, A., & Fine, P. (2010). Sequential Selective Extraction Procedures for the Study of Heavy Metals in Soils, Sediments, and Waste Materials—a Critical Review. *Critical Reviews in Environmental Science and Technology*, *40*(5), 365–399. https://doi.org/10.1080/10643380802377992

IBGE, I. B. de G. e E. (2012). Coordenação de Agropecuária. Produção Pecuária Municipal. Retrieved May 2, 2019, from https://agenciadenoticias.ibge.gov.br/media/com_mediaibge/arquivos/6d3123bbf5f78aa3492c41003c7a38f6.pdf

INMET, I. N. de M. (2019). Instituo Nacional de Meteorologia. Available in: http://www.inmet.gov.br/portal/index.php?r=bdmep/bdmep. Retrieved May 2, 2019, from http://www.inmet.gov.br/portal/

Ip, Y. K., & Chew, S. F. (2010). Ammonia production, excretion, toxicity, and defense in fish: A review. *Frontiers in Physiology*, *1*, 1–20. https://doi.org/10.3389/fphys.2010.00134

IPCC. (2013). *Climate Change 2013: The Physical Science Basis. Contribution of Working Group I to the fifth Assessment Report of the Intergovernmental Panel on Climate Change*.

Jarvis, P., Rey, A., Petsikos, C., Wingate, L., Rayment, M., Pereira, J., et al. (2007). Drying and wetting of Mediterranean soils stimulates decomposition and carbon dioxide emission: The "Birch effect." *Tree Physiology*, *27*(7), 929–940. https://doi.org/10.1093/treephys/27.7.929

Jin, H., Yoon, T. K., Lee, S.-H., Kang, H., Im, J., & Park, J.-H. (2016). Enhanced greenhouse gas emission from exposed sediments along a hydroelectric reservoir during an extreme drought event. *Environmental Research Letters*, *11*, 1–10. https://doi.org/10.1088/1748-9326/11/12/124003

Josué, I. I. P., Cardoso, S. J., Miranda, M., Mucci, M., Ger, K. A., Roland, F., & Marinho, M. M. (2019). Cyanobacteria dominance drives zooplankton functional dispersion. *Hydrobiologia*, *831*(1), 149–161. https://doi.org/10.1007/s10750-018-3710-0

Junior, R. A. M., Mimura, A. M. S., Divino, A. C., Silva, R. F., Silva, J. C. J., & Ciminelli, V. S. T. (2014). Levels of Metallic Cations in the Surface Sediments in the Vicinity of the Três Marias Dam Lake (Brazil) Determined by ICP-MS and Microwave Sample Preparation. *Soil and Sediment Contamination*, *23*(3), 257–269. https://doi.org/10.1080/15320383.2014.820166

Kim, D. G., Vargas, R., Bond-Lamberty, B., & Turetsky, M. R. (2012). Effects of soil rewetting and thawing on soil gas fluxes: A review of current literature and suggestions for future research. *Biogeosciences*, *9*(7), 2459–2483. https://doi.org/10.5194/bg-9-2459-2012

Kinsman-Costello, L. E., O'Brien, J., & Hamilton, S. K. (2014). Re-flooding a Historically Drained Wetland Leads to Rapid Sediment Phosphorus Release. *Ecosystems*, *17*(4), 641–656. https://doi.org/10.1007/s10021-014-9748-6

Kosten, S., van den Berg, S., Mendonça, R., Paranaíba, J. R., Roland, F., Sobek, S., et al. (2018). Extreme drought boosts CO2 and CH4 emissions from reservoir drawdown areas. *Inland Waters*, *8*(3), 329–340. https://doi.org/10.1080/20442041.2018.1483126

De La Guardia, M., & Garrigues, S. (1998). Strategies for the rapid characterization of metals and organic pollutants in solid wastes and contaminated soils by using mass spectrometry. *TrAC - Trends in Analytical Chemistry*, *17*(5), 263–272. https://doi.org/10.1016/S0165-9936(97)00104-0

Lasier, P. J., Winger, P. V., & Bogenrieder, K. J. (2000). Toxicity of manganese to Ceriodaphnia dubia and Hyalella azteca. *Archives of Environmental Contamination and Toxicology*, *38*(3), 298–304. https://doi.org/10.1007/s002449910039

Leme, D. M., & Marin-Morales, M. A. (2009). Allium cepa test in environmental monitoring: A review on its application. *Mutation Research - Reviews in Mutation Research*, *682*(1), 71–81. https://doi.org/10.1016/j.mrrev.2009.06.002

Lide, D. R. et al. (2004). *CRC Handbook of Chemistry and Physics*. *CRC press* (Vol. 85). https://doi.org/10.1021/ja906434c

Lucassen, E. C. H. E. T., Smolders, A. J. P., & Roelofs, J. G. M. (2005). Effects of temporary desiccation on the mobility of phosphorus and metals in sulphur-rich fens: Differential responses of sediments and consequences for water table management.

Wetlands Ecology and Management, *13*(2), 135–148. https://doi.org/10.1007/s11273-004-0314-4

Maavara, T., Dürr, H. H., & Van Cappellen, P. (2014). Worldwide retention of nutrient silicon by river damming: From sparse data set to global estimate. *Global Biogeochemical Cycles*, *28*(8), 842–855. https://doi.org/10.1002/2014GB004875

Maavara, T., Parsons, C. T., Ridenour, C., Stojanovic, S., Dürr, H. H., Powley, H. R., & Van Cappellen, P. (2015). Global phosphorus retention by river damming. *Proceedings of the National Academy of Sciences*, *12*(51), 15603–15608. https://doi.org/10.1073/pnas.1511797112

Machado, P. (2012). *Diagnóstico ambiental e ordenamento territorial – instrumentos para a gestão da Bacia de Contribuição da Represa de Chapéu D'Uvas/MG*. Universidade Federal Fluminense, Brazil.

Marcé, R., Obrador, B., Gómez-Gener, L., Catalán, N., Koschorreck, M., Arce, M. I., et al. (2019). Emissions from dry inland waters are a blind spot in the global carbon cycle. *Earth-Science Reviews*, *188*, 240–248. https://doi.org/10.1016/j.earscirev.2018.11.012

Marengo, J. A., Jones, R., Alves, L. M., & Valverde, M. C. (2009). Future change of temperature and precipitation extremes in South America as derived from the PRECIS regional climate modeling system. *International Journal of Climatology*, *29*(3), 2241–2255. https://doi.org/10.1002/joc

Martin, J. H., Fitzwater, S. E., & Gordon, R. M. (1990). Iron deficiency limits phytoplankton growth in antarctic waters. *Global Biogeochemical Cycles*, *4*(1), 5–

12.

Martin, T. R., & Holdich, D. M. (1986). The acute lethal toxicity of heavy metals to peracarid crustaceans (with particular reference to fresh-water asellids and gammarids). *Water Research*, *20*(9), 1137–1147. https://doi.org/10.1016/0043-1354(86)90060-6

Mendonça, R., Kosten, S., Sobek, S., Cole, J. J., Bastos, A. C., Albuquerque, A. L., et al. (2014). Carbon Sequestration in a Large Hydroelectric Reservoir: An Integrative Seismic Approach. *Ecosystems*, *17*(3), 430–441. https://doi.org/10.1007/s10021-013-9735-3

Panda, K. K., Patra, J., & Panda, B. B. (1996). Induction of sister chromatid exchanges by heavy metal salts in root meristem cells of Allium cepa L. *Biologia Plantarum*, *38*(4), 555–561. https://doi.org/10.1007/BF02890606

Paranaíba, J. R., Barros, N., Mendonça, R., Linkhorst, A., Isidorova, A., Roland, F., et al. (2018). Spatially Resolved Measurements of CO2 and CH4 Concentration and Gas-Exchange Velocity Highly Influence Carbon-Emission Estimates of Reservoirs. *Environmental Science and Technology*, *52*(2), 607–615. https://doi.org/10.1021/acs.est.7b05138

Qiu, S., & McComb, A. J. (1994). Effects of oxygen concentration on phosphorus release from reflooded air-dried wetland sediments. *Marine and Freshwater Research*, *45*(7), 1319–1328. https://doi.org/10.1071/MF9941319

Quadra, G. R., Lino, A., Sobek, A., Malm, O., Barros, N., Guida, Y., et al. (2019). Environmental Risk of Metal Contamination in Sediments of Tropical Reservoirs.

Bulletin of Environmental Contamination and Toxicology, *103*(2), 292–301. https://doi.org/10.1007/s00128-019-02668-0

Quadra, G. R., Roland, F., Barros, N., Malm, O., Lino, A. S., Azevedo, G. M., et al. (2019). Far-reaching cytogenotoxic effects of mine waste from the Fundão dam disaster in Brazil. *Chemosphere*, *215*, 753–757. https://doi.org/10.1016/j.chemosphere.2018.10.104

Radić, S., Stipaničev, D., Vujčić, V., Rajčić, M. M., Širac, S., & Pevalek-Kozlina, B. (2010). The evaluation of surface and wastewater genotoxicity using the Allium cepa test. *Science of the Total Environment*, *408*(5), 1228–1233. https://doi.org/10.1016/j.scitotenv.2009.11.055

Ray, S., Kundu, L. M., Goswami, S., Roy, G. C., Chatterjee, S., Dutta, S., et al. (2013). Metaphase arrest and delay in cell cycle kinetics of root apical meristems and mouse bone marrow cells treated with leaf aqueous extract of Clerodendrum viscosum Vent. *Cell Proliferation*, *46*(1), 109–117. https://doi.org/10.1111/cpr.12011

Remaili, T. M., Simpson, S. L., Amato, E. D., Spadaro, D. A., Jarolimek, C. V., & Jolley, D. F. (2016). The impact of sediment bioturbation by secondary organisms on metal bioavailability, bioaccumulation and toxicity to target organisms in benthic bioassays: Implications for sediment quality assessment. *Environmental Pollution*, *208*, 590–599. https://doi.org/10.1016/j.envpol.2015.10.033

Rodrigo, A., Recous, S., Neel, C., & Mary, B. (1997). Modelling temperature and moisture effects on C-N transformations in soils: Comparison of nine models. *Ecological Modelling*, *102*(2–3), 325–339. https://doi.org/10.1016/S0304-3800(97)00067-7

Roland, F., Huszar, V., Farjalla, V., Enrich-Prast, A., Amado, A., & Ometto, J. (2012). Climate change in Brazil: perspective on the biogeochemistry of inland waters. *Brazilian Journal of Biology*, *72*(3 suppl), 709–722. https://doi.org/10.1590/s1519-69842012000400009

Rosenberry, D. O., Glaser, P. H., & Siegel, D. I. (2006). The hydrology of northern peatlands as affected by biogenic gas: current developments and research needs. *Hydrological Processes*, *26*, 3601–3610. https://doi.org/10.1002/hyp

Salomons, W., & Forstner, U. (1984). *Metals in the hydrocycle. Metals in the hydrocycle.* Springer-Verlag Berlin Heidelberg. https://doi.org/10.2307/2403266

Schönbrunner, I. M., Preiner, S., & Hein, T. (2012). Impact of drying and re-flooding of sediment on phosphorus dynamics of river-floodplain systems. *Science of the Total Environment*, *432*, 329–337. https://doi.org/10.1016/j.scitotenv.2012.06.025

Schwarzenbach, R. P., Egli, T., Hofstetter, T. B., von Gunten, U., & Wehrli, B. (2010). Global Water Pollution and Human Health. *Annual Review of Environment and Resources*, *35*(1), 109–136. https://doi.org/10.1146/annurev-environ-100809-125342

Scott, G. R., & Sloman, K. A. (2004). The effects of environmental pollutants on complex fish behaviour: Integrating behavioural and physiological indicators of toxicity. *Aquatic Toxicology*, *68*(4), 369–392. https://doi.org/10.1016/j.aquatox.2004.03.016

Skinner, D., Oliver, R., Aldridge, K., & Brookes, J. (2014). Extreme water level decline effects sediment distribution and composition in Lake Alexandrina, South Australia. *Limnology*, *15*(2), 117–126. https://doi.org/10.1007/s10201-013-0422-z

Stanley, E. H., Casson, N. J., Christel, S. T., Crawford, J. T., Loken, L. C., & Oliver, S. K. (2016). The ecology of methane in streams and rivers: patterns, controls, and global significance. *Ecological Monographs*, *86*(2), 146–171.

Steinkellner, H., Mun-Sik, K., Helma, C., Ecker, S., Ma, T.-H., Mun-Sik, K., et al. (1998). Genotoxic effects of heavy metals: Comparative investigation with plant bioassays. *Environmental and Molecular Mutagenesis*, *31*(2), 183–191. https://doi.org/10.1002/(SICI)1098-2280(1998)31:2<183::AID-EM11>3.0.CO;2-8

Steinman, A. D., Ogdahl, M. E., Weinert, M., & Uzarski, D. G. (2014). Influence of water-level fluctuation duration and magnitude on sediment-water nutrient exchange in coastal wetlands. *Aquatic Ecology*, *48*(2), 143–159. https://doi.org/10.1007/s10452-014-9472-5

Tack, F. M., Callewaert, O. W. J. J., & Verloo, M. G. (1996). Metal solubility as a function of pH in a contaminated, dredged sediment affected by oxidation. *Environmental Pollution*, *91*(2), 199–208. https://doi.org/10.1016/0269-7491(95)00049-6

Teodoru, C., & Wehrli, B. (2005). Retention of sediments and nutrients in the Iron Gate I Reservoir on the Danube River. *Biogeochemistry*, *76*(3), 539–565. https://doi.org/10.1007/s10533-005-0230-6

Tranvik, L. J., Downing, J. A., Cotner, J. B., Loiselle, S. A., Striegl, R. G., Ballatore, T. J., et al. (2009). Lakes and reservoirs as regulators of carbon cycling and climate. *Limnology and Oceanography*, *54*, 2298–2314. https://doi.org/10.4319/lo.2009.54.6_part_2.2298

Wang, F., Maberly, S. C., Wang, B., & Liang, X. (2018). Effects of dams on riverine biogeochemical cycling and ecology. *Inland Waters*, *8*(2), 130–140. https://doi.org/10.1080/20442041.2018.1469335

West, A. W., Sparling, G. P., Speir, T. W., & Wood, J. M. (1988). Comparison of microbial c, n-fiush and atp, and certain enzyme activities of different textured soils subject to gradual drying. *Australian Journal of Soil Research*, *26*(1), 217–229. https://doi.org/10.1071/SR9880217

Wetzel, R. G., & Likens, G. E. (2013). *Limnological analyses*. (S. Science+Business, Ed.) (Third edit). New York: Science+Business, Springer. https://doi.org/10.1007/978-1-4757-3250-4

Wilson, J. S., & Baldwin, D. S. (2008). Exploring the "Birch effect" in reservoir sediments: Influence of inundation history on aerobic nutrient release. *Chemistry and Ecology*, *24*(6), 379–386. https://doi.org/10.1080/02757540802497582

Wu, J. P., & Chen, H. C. (2004). Effects of cadmium and zinc on oxygen consumption, ammonium excretion, and osmoregulation of white shrimp (Litopenaeus vannamei). *Chemosphere*, *57*(11), 1591–1598. https://doi.org/10.1016/j.chemosphere.2004.07.033

Zarfl, C., Lumsdon, A. E., Berlekamp, J., Tydecks, L., & Tockner, K. (2015). A global boom in hydropower dam construction. *Aquatic Sciences*, *77*(1), 161–170. https://doi.org/10.1007/s00027-014-0377-0

Fourth chapter: *Cross-continental importance of CH_4 emissions from dry sediments*

José. R. Paranaíba[1], Nathan Barros[1], Ralf Aben[2,3], Gabrielle Quadra[1], Annika Linkhorst[4], Raquel Mendonça[1], Sebastian Sobek[4], André M. Amado[1,5], Ernandes S. Oliveira Junior[3,6], Claumir C. Muniz[6], Haijun Wang[7], Julia Howitt[8], Jason Condon[9], Colin M. Finlayson[10], Catherine Leigh[11], Eva-Ingrid Rõõm[12], Alo Laas[12], Matthias Koschorreck[13], Hans-Peter Grossart[14,15], Gabriela Onandia[16], Florian Reverey[16], Sarian Kosten[2,3]

[1] Laboratório de Ecologia Aquática, Programa de Pós-Graduação em Ecologia, Universidade Federal de Juiz de Fora, Minas Gerais, Brazil.

[2] Department of Aquatic Ecology, Netherlands Institute of Ecology, Wageningen, The Netherlands.

[3] Department of Aquatic Ecology and Environmental Biology, Institute for Water and Wetland Research, Radboud University Nijmegen, Nijmegen, The Netherlands.

[4] Department of Ecology and Genetics, Limnology, Uppsala University, Uppsala, Sweden.

[5] Departamento de Oceanografia e Limnologia, Universidade Federal do Rio Grande do Norte, Natal, Brazil.

[6] Center of Ethnoecology, Limnology and Biodiversity, Laboratory of Ichthyology of the Pantanal North, University of the State of Mato Grosso, Cáceres, Brazil.

[7] State Key Laboratory of Freshwater Ecology and Biotechnology, Institute of Hydrobiology, Chinese Academy of Sciences, Wuhan, China.

[8] Institute for Land, Water and Society, Charles Sturt University, Wagga Wagga, Australia.

[9] Graham Centre for Agricultural Innovation, School of Agricultural & Wine Sciences, Charles Sturt University, Wagga Wagga, Australia.

[10] Institute for Land, Water and Society, Charles Sturt University, Albury, Australia.

[11] Australian Rivers Institute, Griffith University, Nathan, Queensland, Australia.

[12] Institute of Agricultural and Environmental Sciences, Estonian University of Life Sciences, Tartu, Estonia.

[13] Department of Lake Research, Helmholtz Center for Environmental Research - UFZ, Magdeburg, Germany.

[14] Department Experimental Limnology, Leibniz Institute of Freshwater Ecology and Inland Fisheries, Neuglobsow, Germany.

[15] Institute of Biology and Biochemistry, Potsdam University, Potsdam, Germany.

[16] Leibniz Centre for Agricultural Landscape Research, Müncheberg, Germany.

Article to be submitted to Science of the Total Environment

Abstract

Scientists around the world have recently made substantial efforts to quantify greenhouse gas (GHG) emissions from dry inland waters. Nevertheless, estimating their share in global inland water GHG emission inventories is still a challenge because dry inland water ecosystems are still poorly represented in the available literature. According to the most recent study of global carbon (C) emissions from dry inland waters, about 0.12 ± 0.13 Pg C are estimated to reach the atmosphere annually considering only carbon dioxide (CO_2) emissions. Thus, this work focuses on marginal sediments, highly dynamic wet-dry zones of inland waters that occasionally fall dry. This is the first study providing i) the global magnitude of measured methane (CH_4) emissions from atmosphere-exposed sediments (i.e. dry inland waters) in different types of aquatic systems (i.e. lakes, ponds, reservoirs, and streams) and climate zones (i.e. equatorial, snow, and warm temperate), and ii) the environmental interactions that control sediment-exposed CH_4 emissions at global scale. CH_4 emissions from dry inland waters were consistently higher than those emissions observed in adjacent uphill soils, in all aquatic systems (except for streams) and climate zones. In line with global dry inland water CO_2 emissions, CH_4 emissions are also controlled by common drivers across different types of aquatic systems and climate zones. Coupling CO_2 and CH_4 emissions revealed a global average CO_2-equivalent emission rate of 9.6 ± 17.4 g m^{-2} d^{-1} from dry inland waters, with the within-system CH_4 contribution varying from 10% (reservoirs) to 21% (streams). Compared to CO_2 emissions, global dry inland water CH_4 emissions were low (2.7 ± 2.6 Tg C y^{-1}), which could be acknowledge as a negligible fraction of current estimates of C emissions from inland waters (0.1 ± 0.1%).

Introduction

The past decades of research have revealed the importance of inland water ecosystems (e.g. lakes, ponds, reservoirs, rivers) for the global C cycle (J. J. Cole et al., 2007; Tranvik et al., 2009). These aquatic systems are complex environments that process large amounts of allochthonous and autochthonous organic matter (Van Cappellen & Maavara, 2016; Clair & Ehrman, 1996; Friedl & Wüest, 2002). In the aquatic ecosystem, the organic matter undergoes numerous physical and biogeochemical processes, including its decomposition into gaseous C species (Mattson & Likens, 1992) such as CO_2 and CH_4 (Bastviken et al., 2011; DelSontro et al., 2018; Raymond et al., 2013), and its storage in sediments (Heathcote et al., 2015; Mendonça et al., 2017). According to inland water C budget studies, approximately 0.2-1.6 Pg C y^{-1} are estimated to be buried into freshwater sediments worldwide (W. E. Dean & Gorham, 1998; Heathcote et al., 2015; Stallard, 1998), whereas approximately 2 Pg C y^{-1} are emitted to the atmosphere as CO_2, and 0.13 Pg C y^{-1} as CH_4 (DelSontro et al., 2018; Raymond et al., 2013; Stanley et al., 2016).

CH_4 is one of the gases that most contribute to the global greenhouse effect. Considering a Global Warming Potential (GWP) over a 100-year time horizon, one single CH_4 molecule exerts an atmospheric heating power equivalent to 34 molecules of CO_2 (Clarke et al., 2014). Of the 0.13 Pg of C emitted annually as CH_4, ~0.11 Pg C y^{-1} evades to the atmosphere from lentic systems (e.g. lakes, ponds and reservoirs) (Bastviken et al., 2011; DelSontro et al., 2018; Holgerson & Raymond, 2016), and ~0.02 Pg C y^{-1} from lotic systems (streams and rivers) (Stanley et al., 2016).

The CH_4 production in the aquatic system occurs primarily in anoxic sediments via microbial degradation of organic matter (Bastviken et al., 2004), and the resulting

CH_4, which does not go through the oxidation process in the water column (Granéli et al., 1996; Heilman & Carlton, 2001), can reach the atmosphere through diffusion (between both water-atmosphere and exposed sediment-atmosphere interfaces) (Bastviken et al., 2004; Jonathan J. Cole & Caraco, 1998; Marcé et al., 2019), ebullition (emission by bubbles that travel through the water column) (Bastviken et al., 2004), plant-mediated transport (Abril et al., 2005), and by the passage of CH_4-rich hypolimnetic waters through the turbines of hydroelectric reservoirs (so-called degassing) (Abril et al., 2005; Kemenes et al., 2016).

Inland water ecosystems worldwide face either permanent or periodic droughts (Marcé et al., 2019). Periods of droughts can either be a result of natural aspects such as the intermittency and ephemerality of rivers (Larned et al., 2010), or they are a result of artificial aspects such as water level fluctuations in lakes and reservoirs due to human needs (Beaulieu et al., 2018). During periods of droughts, considerable extensions of marginal aquatic sediments are exposed to direct contact with the atmosphere. Pekel et al. (2016) estimated that ~800,000 km^2 (or 18%) of the global surface area that is covered by inland waters are subjected to seasonal atmospheric exposure. The exposure of previously submerged sediments to direct contact with the atmosphere redraws the biogeochemical processes that routinely affect these sediments when submerged. Recent studies have shown that exposed aquatic sediments may represent a substantial source of GHG to the atmosphere. However, dry inland waters are explicitly neglected in the current global C emission estimates (Keller et al., 2020; Marcé et al., 2019; von Schiller et al., 2014). Recently, the interest in GHG emissions from dry inland waters has been growing worldwide (Beaulieu et al., 2018; Gallo et al., 2014; Harrison et al., 2017; Jin et al., 2016; Marcé et al., 2019), especially for CO_2 (Almeida et al., 2019; Catalán et al., 2014; Deshmukh et al., 2018; Keller et al., 2020; Obrador et al., 2018; von Schiller et al.,

2014). Keller et al. 2020 pointed out that a share of 0.12 ± 0.13 Pg C $year^{-1}$ (or 6 ± 6%) would be added to recent global inland water C emission estimates if CO_2 emissions from continental exposed sediments were accounted for. It remains open, however, how much CH_4 emissions from continental exposed sediments can add to global C emission estimates. Moreover, the number of existing studies is neither sufficient to understand potential drivers regulating CH_4 emissions from these continental areas, nor for generating reliable upscaling CH_4 emission estimates at global scale.

The aim of this study is to quantify CH_4 fluxes from exposed sediments from different types of aquatic systems (i.e. dry inland waters) in different climate zones of the globe. Moreover, dry inland water CH_4 fluxes were compared to those fluxes observed in adjacent uphill soil zones. Physical and chemical sediment/soil properties were concurrently sampled in order to identify potential drivers controlling CH_4 emissions from exposed sediments in a global scenario. Average sediment-exposed CH_4 flux of each type of aquatic system was upscaled to their respective global surface areas to comprehend whether these emissions represent a significant share of the global inland waters C emission estimates.

Methods

Studied sites and sampling strategy

This study includes measurements in 89 unconnected aquatic systems (lakes, n = 45; ponds, n = 16; reservoirs, n = 19; and streams, n = 9), located in three of the five global climate zones (equatorial, n = 24; snow, n = 11; and warm temperate, n = 54) (Kottek et al., 2006) (Figure 18) conducted by 9 research groups from 7 countries. These

89 systems are a subset of the 196 aquatic systems included in a recent global study on CO_2 emission from exposed sediments by Keller et al. (2020).

At each sampling site two distinct zones were sampled: i) exposed sediment or dry inland water, which corresponds to area of the aquatic system that lacks overlying water; and ii) adjacent uphill soil, which corresponds to the adjacent terrestrial zone that is not naturally flooded. At each zone, measurements were performed in triplicates, and, if possible, at least 1 meter apart from each other to capture spatial within-zone variability.

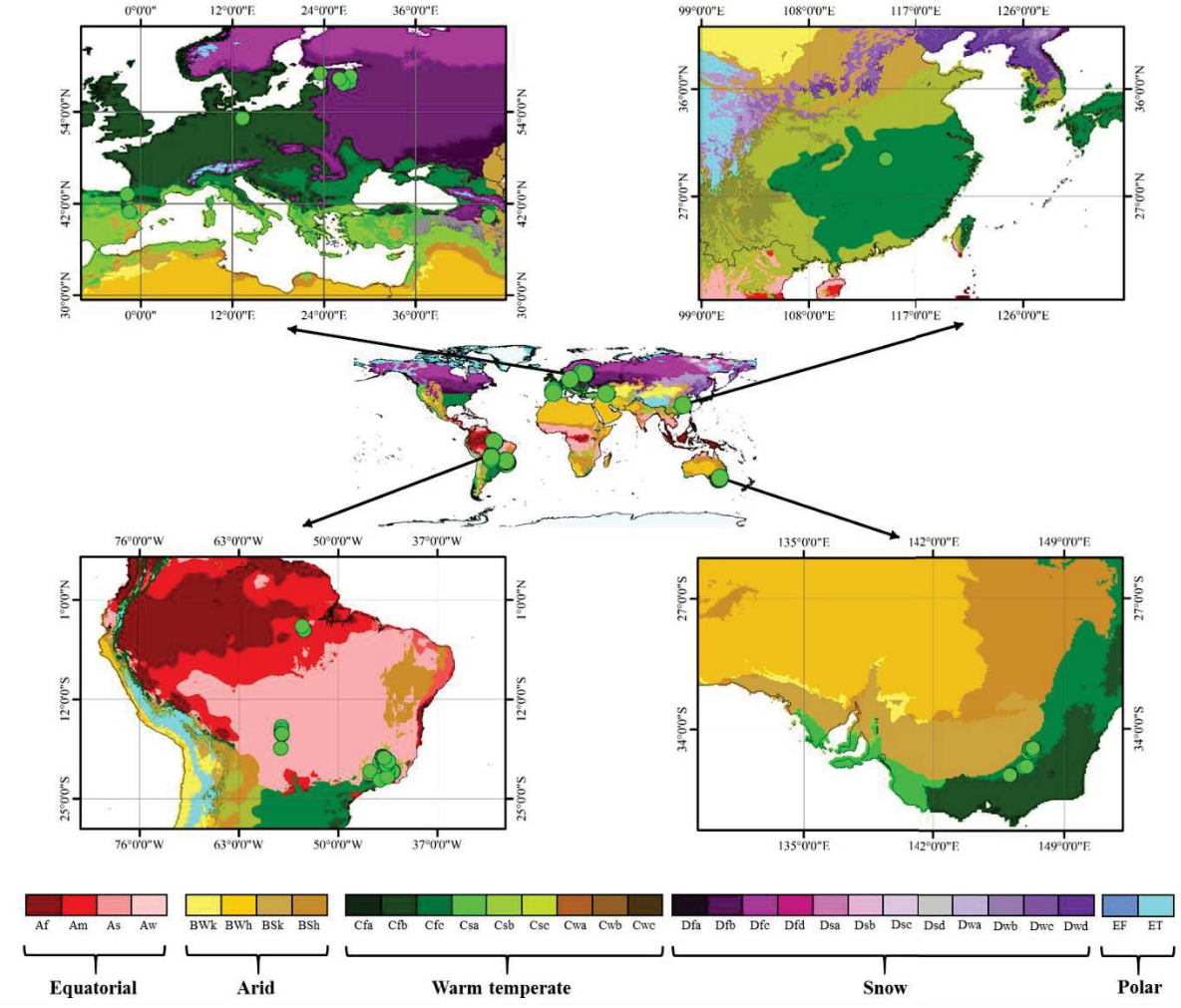

Figure 18: Global distribution of the sampling sites (green dots) across the different climate zones according to the Köppen-Geiger climate classification system (Kottek et al., 2006).

CH_4 flux measurements

In situ measurements of CH_4 flux (mg m^{-2} d^{-1}) were conducted using opaque chambers connected to a greenhouse gas analyzer in a closed gas loop. The chambers were gently placed over the sediment/soil surface and sealed-around with clay (Lesmeister & Koschorreck, 2017) to avoid disturbance and gas leakage during the measurements. Changes in CH_4 partial pressure (pCH_4) were monitored within the chambers over 3-5 minutes, and the fluxes were calculated following the equation below:

$$FCH_4 = (dpCH_4 / dt) * (V / RTA) \quad (1)$$

where $dpCH_4$ is the slope of change in pCH_4 (µatm) over time (dt), V is the volume of the chamber (m^3), A is the surface area covered by the chamber (m^2), T is the air temperature (K), and R is the gas constant = 0.082057 L atm mol^{-1} K^{-1}.

Opaque chambers were used in order to minimize temperature changes during measurements, which may affect the gas exchange between the sediment/soil-headspace interface. Chamber deployments were performed on top of bare sediment/soil, avoiding vegetated surfaces.

Sediment/soil characterization

After the flux measurements, surface sediment/soil samples were collected, placed in plastic bags and stored in thermal cooler boxes for subsequent laboratory analysis. Air and sediment/soil temperature (°C), as well as elevation (m.a.s.l., meters above the sea level) were measured *in situ*. In the laboratory, sediment/soil texture was determined following the Food and Agriculture Organization (FAO) of the United States manipulative text. Sediment/soil texture was distinguished as: clay, light clay, heavy

loam, loam, loamy sand, sand, and sandy loam. Additionally, in the laboratory, 10 g fresh sediment were mixed in 25 mL distilled water for the determination of conductivity (µS cm^{-1}) and pH by measuring the suspended solution (after 1 h standing) with conventional electrodes. Moisture content (% weight loss) was determined by drying 5 g of fresh sediment at 105 °C until constant weight. Afterwards, the samples were combusted at 500 °C until constant weight for the determination of the organic matter content (% weight loss) (W. Dean, 1974).

Data analysis and statistical procedures

For each sampling site we calculated the contribution of CH_4 emission to the total (i.e. CO_2 + CH_4) GHG emission in CO_2-eq. The CO_2 flux data was retrieved from Keller et al. (2020). Next we compared the contribution of CH_4 to the total emission between the 4 types of systems (lakes, ponds, reservoirs and streams). For all analyzes, triplicate measurements were averaged, and one average value per parameter at each sampling site was used.

Each sampling site was assigned to a climate zone according to the "The World Maps of Köppen-Geiger Climate Classification" (Kottek et al., 2006). Non-parametric tests (Wilcoxon and Kruskal-Wallis tests) were used to assess differences in CH_4 fluxes and other parameters between type of aquatic systems; between dry inland waters and upland soils and between climate zones (Wilcoxon test: dry inland waters versus uphill soils; Kruskal-Wallis test: dry inland waters between aquatic systems and between climate zones) using the software JMP 14.0.0. To test the relationships between environmental variables and dry inland water CH_4 fluxes, a generalized linear mixed model (GLMM) was performed using the glmer function in the "lmer4" package in R (v. 4.0.2) (R Core Team, 2018). Sediment texture, soil temperature, elevation, pH,

conductivity, moisture, organic matter content, latitude, annual mean precipitation, and annual mean air temperature were selected as fixed factors. Given that CH_4 production is mainly driven by the availability and quality of organic matter, sediment moisture and temperature (Aben et al., 2017; Grasset et al., 2018; Koschorreck, 2000; Sobek et al., 2012; Yvon-Durocher et al., 2014), the second-order interactions between organic matter and sediment temperature and organic matter and moisture were also included as a fixed factor. The variables research group, type of aquatic system, and climate zone were used as random factors to counterbalance the sample representativeness captured by each research group and account for their underlying characteristics. Sediment temperature, instead of air temperature, was chosen due to the high correlation between these two parameters ($r^2 = 0.9$, $p < 0.0001$). A factor of 13 was added to the CH_4 flux data (i.e. $x + 13$) in order to exclude negative values from the analysis. Logarithmic and cubic root transformations were adopted for conductivity and organic matter content ($x + 1$), and humidity and elevation, respectively, to meet the conditions of normality and homoscedasticity of variances. We used generalized models because preliminary analyzes showed that the distribution of the residuals of the linear mixed models followed a logarithmic distribution and, therefore, the gamma family (link=log) was applied in the GLMM. Before analysis, collinearity between predictor variables was assessed using the variance inflation factor (VIF) function in the "usdm" package in R (R Core Team, 2018). Variables with VIF values > 5 (i.e. indicative of collinearity) were excluded from the procedures (Akinwande et al., 2015). In this case, the excluded variables were annual precipitation and air temperature. Finally, we used the stepwise backward variable selection to select the best fitting model based on low AIC (Akaike information criterion) values. For all statistical procedures, a p value < 0.05 was adopted as the threshold level of acceptance.

Finally, to obtain an estimate of global CH_4 emission from dry inland waters we multiplied the average CH_4 flux rate of each type of aquatic system by their respective global surface areas and then summing them up. Also, CH_4 emission from dry inland waters was converted into CO_2-equivalent (CO_2-eq) emission by using the 100-year time horizon GWP factor of 34 (Clarke et al., 2014).

Results and Discussion

Contrasting CH_4 fluxes from dry inland waters and surrounding terrestrial area

CH_4 fluxes from both zones ranged from -8 to 352 mg m^{-2} d^{-1} (mean ± standard deviation: 20 ± 60 mg m^{-2} d^{-1}) (Figure 19). In 57% of uphill soil zones (51 locations) and 23% of dry inland water zones (21 locations) we found CH_4 uptake, but the strength of the CH_4 uptake was small in all cases. While CO_2 emissions from dry aquatic systems tend to be lower than those of uphill soils (Almeida et al., 2019; Catalán et al., 2014; Jin et al., 2016; Keller et al., 2020; von Schiller et al., 2014), the pattern for CH_4 flux is opposite. Dry inland water CH_4 fluxes were significantly higher than those observed in adjacent uphill soils (Figure 19) (dry inland water: 40 ± 80 mg m^{-2} d^{-1}; uphill soil: 1 ± 4 mg m^{-2} d^{-1}; Wilcoxon test: $p < 0.0001$). The difference in CH_4 emissions from the two zones may be attributed to differences in moisture content as well as the quality and quantity of organic matter (Dalal et al., 2008; Keller et al., 2020; Serça et al., 2016; Serrano-Silva et al., 2014). Moisture content in this study, indeed, was consistently higher in dry inland waters than in uphill soils across all systems globally (dry inland water: 33.1 ± 21.4%; uphill soil: 17 ± 9.4%; Wilcoxon test: $p < 0.0001$). Organic matter content, however, was surprisingly similar for the two zones (dry inland water: 7.9 ± 7%; uphill soil: 8.2 ± 7.5%; Wilcoxon test: $p = 0.73$). When exposed sediments are still wet, anoxia generally prevails below the upper few millimeters enabling CH_4 production. Also when

the sediment starts to dry out, CH_4 production can still take place in anoxic microhabitats (Dalal et al., 2008; Serrano-Silva et al., 2014). As exposed sediment of inland waters dries out, the contact with atmospheric oxygen in the sediment expands to deeper layers, due to fracture formation by decreasing moisture (Fromin et al., 2010; Kosten et al., 2018; Paranaíba et al., 2020). The expansion of oxic layers in the sediment leads to changes in bacterial communities (Borken & Matzner, 2009; Jin et al., 2016; Rodrigo et al., 1997), favoring aerobic metabolisms (e.g. CH_4 oxidation (Koschorreck, 2000)), and eventually leads to a reduction in CH_4 emission (Kosten et al., 2018; Paranaíba et al., 2020).

Dry inland waters CH_4 flux variability across aquatic systems and climate zones

Dry inland water CH_4 fluxes were highest in lakes (48 ± 91 mg m^{-2} d^{-1}, n = 45), followed by ponds (38 ± 63 mg m^{-2} d^{-1}, n = 16) and reservoirs (36 ± 78 mg m^{-2} d^{-1}, n = 19), and lowest in streams (7 ± 17 mg m^{-2} d^{-1}, n = 9) (Table 7, Figure 19), although these differences were not statistically significant (Kruskal-Wallis test: p = 0.25). The lower CH_4 emission from exposed sediments in streams matched their significantly lower values of moisture and organic matter content when compared to lakes, ponds and reservoirs (moisture, streams: 20 ± 27%; lakes: 31 ± 20; ponds: 52 ± 21%; reservoirs: 27 ± 10%; Kruskal-Wallis test and Dunn's post hoc test: p = 0.001; organic matter, streams: 1 ± 1%; lakes: 9 ± 8%; ponds: 8 ± 4%; reservoirs: 9 ± 6%; Kruskal-Wallis test and Dunn's post hoc test: p = 0.0005).

The above-mentioned variability in dry inland waters CH_4 flux is in accordance with previously documented values from local CH_4 emission studies, which cover the different types of aquatic systems studied here (middle part of Table 7). Moreover, from an aquatic system perspective, the CH_4 flux rates from both dry inland waters and surface waters were similar in magnitude for lakes (Deemer et al., 2016), ponds (Holgerson &

Raymond, 2016) and streams (Stanley et al., 2016). Only in reservoirs, mean dry inland water CH_4 flux rates were overall about one order of magnitude lower than mean CH_4 flux rates documented for reservoir water surfaces worldwide as documented by Deemer et al. (2016). This difference may be linked to the fact that in many reservoirs, water surface CH_4 emission is dominated by ebullition (i.e. emission of CH_4-rich bubbles), an emission pathway absent in sediments that are exposed to the atmosphere (Koschorreck, 2000; Marcé et al., 2019).

Between climate zones, significant differences in CH_4 fluxes from dry inland waters were observed. Highest CH_4 emission occurred in snow zones (96 ± 128 mg m^{-2} d^{-1}, n = 11), followed by equatorial zones (54 ± 77 mg m^{-2} d^{-1}, n = 24), and lowest CH_4 emissions occurred in warm temperate zones (22 ± 58 mg m^{-2} d^{-1}, n = 54) (Kruskal-Wallis test and Dunn's post hoc test: p = 0.005) (Figure 19c). Moisture content was, although not statistically significantly, highest in dry sediments located in warm temperate zones, followed by sites in snow and equatorial zones (warm temperate: 37 ± 22%; snow: 32 ± 27%; equatorial: 25 ± 14%; Kruskal-Wallis test: p = 0.1). Highest organic matter content was observed at sites located in equatorial zones (equatorial: 11 ± 9%; Kruskal-Wallis test, p = 0.01), followed by sites in warm temperate and snow zones (warm temperate: 7 ± 5%; snow: 4 ± 5%; Kruskal-Wallis test: p = 0.1).

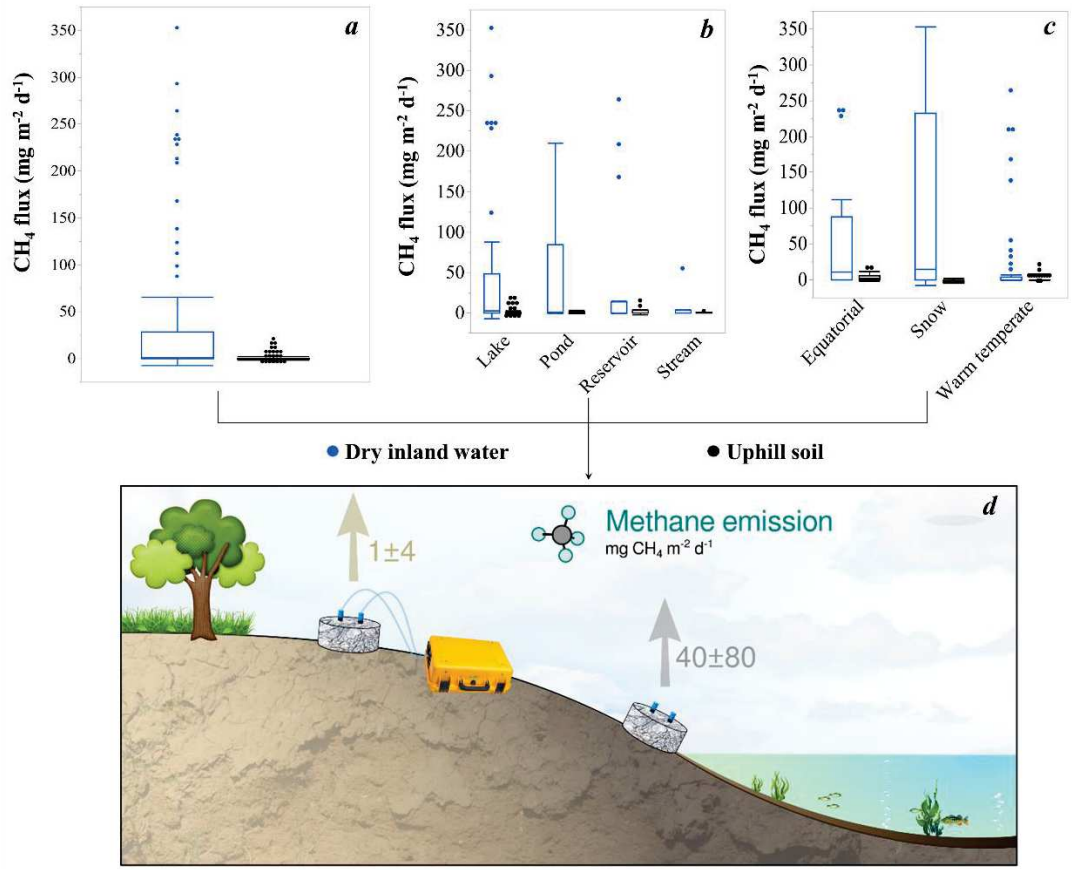

Figure 19: Average CH_4 flux rate (mg m^{-2} d^{-1}) from dry inland waters (blue boxes) and adjacent uphill soils (black boxes) (a); in different types of aquatic systems (b); and different climates zones (c). Conceptual figure d represents the sampling zones with their respective global mean ± standard deviation CH_4 flux rates (dry inland waters: grey arrow; adjacent uphill soils: beige arrow).

Table 7: Upper part: Mean ± standard deviation of CH_4 fluxes (mg m^{-2} d^{-1}) from dry inland waters and adjacent uphill soils among aquatic systems (lakes, ponds, reservoirs, and streams). **Middle part:** Mean CH_4 fluxes (mg m^{-2} d^{-1}) from different dry aquatic zones obtained from the literature. **Bottom part:** Global CH_4 emissions (mg m^{-2} d^{-1}) from surface waters of different aquatic systems obtained from the literature.

System type	CH_4 flux (mg m^{-2} d^{-1})	Reference
Lakes (n = 45)		
Dry inland water	48 ± 91	
Uphill soil	1 ± 5	
Ponds (n = 16)		
Dry inland water	38 ± 63	
Uphill soil	0.3 ± 1	
Reservoirs (n = 19)		
Dry inland water	36 ± 78	This study
Uphill soil	2 ± 4	
Streams (n = 9)		
Dry inland water	7 ± 17	
Uphill soil	0.2 ± 0.7	
All systems (n = 89)		
Dry inland water	40 ± 80	
Uphill soil	1 ± 4	
Lake (Brazil)	2.1 [a] (Amazonian floodplain)	Koschorreck (2000)
Kettle holes (Germany)	0.5 [a] (Dry bed)	Reverey et al. (2018)
Ponds (Spain)	1.6 [a] (Dry bed)	Obrador et al. (2018)
Reservoir (Brazil)	0.9 [a] (Drawdown zone)	Amorim et al. (2019)
Reservoir (China)	6.2 [a] (Drawdown zone)	Chen et al. (2011)
Reservoir (China)	9.6 [a] (Drawdown zone)	Yang et al. (2013)
Reservoir (China)	3.8 [a] (Drawdown zone)	Hao et al. (2019)
Reservoir (Laos)	27 [a] (Drawdown zone)	Serça et al. (2016)
Streams (United States)	0.4 [a] (Dry river bed)	Gallo et al. (2014)
Streams (Spain)	3.2 [a] (Dry river and impoundment beds)	Gómez-Gener et al. (2015)
Global CH_4 emission rates from surface waters (mg m^{-2} d^{-1})		
Lakes	40	Deemer et al. (2016)
Ponds	0.7 – 27 [b]	Holgerson and Raymond (2016)
Reservoirs	120	Deemer et al. (2016)
Streams	6 – 98 [b]	Stanley et al. (2016)

[a] Mean values
[b] Values based on different models

Drivers of CH_4 emissions

The fixed effect resulting from the GLMM modeling on dry inland water CH_4 emissions explained 20% of the total variance (marginal R squared, R^2m), and fixed and random effects together explained 55% of the total variance (conditional R squared, R^2c) (Table 8). The interaction between organic matter content and temperature was the strongest predictor of CH_4 fluxes from dry inland waters (analysis of variance, $p < 0.001$; Figure 20, Table 8), followed by organic matter content, moisture, conductivity (analysis of variance, $p < 0.01$; Figure 20, Table 8), and elevation (analysis of variance, $p < 0.05$; Figure 20, Table 8). Similar to what has been described for dry inland water CO_2 emissions by Keller et al. (2020), these findings suggest that these mechanisms may also prevail across different types of aquatic systems at a global perspective, but note that the significant drivers and their effects on CH_4 emissions from dry sediments were not exactly the same as those controlling CO_2 emissions. Although a few high emission events were observed at sites of low organic matter content and low temperature, the interaction between these two parameters positively affected dry inland waters CH_4 emission, with intermediate conditions of both organic matter content and temperature being sufficient to support high CH_4 evasion (Figure 21). Organic matter content in dry sediments alone was negatively correlated with CH_4 emission (Figure 20 and Table 8). This may be an indication that not the quantity but rather the quality of the available organic matter (i.e. labile material) (Dalal et al., 2008; Serça et al., 2016; Serrano-Silva et al., 2014; Strom et al., 2003) is the modulating factor of CH_4 production in the marginal sediments of the investigated aquatic systems. Previous studies have found that the more frequent a sediment is exposed to the atmosphere, the less labile its organic matter tends to be (Dalal et al., 2008; Serrano-Silva et al., 2014). The transition from flooded to drying stage triggers microbial processes responsible for organic matter breakdown (Fromin et al.,

2010; Jin et al., 2016) that in turn boosts CH_4 emission, mainly in the first hours and/or days after the transition (Jin et al., 2016; Koschorreck, 2000; Kosten et al., 2018; Paranaíba et al., 2020). A positive effect of moisture on dry inland water CH_4 emissions was observed (Figure 20 and Table 8), which may be associated to the fact that the moisture content regulates microbial activity in these water-stressed marginal zones (Baldwin & Mitchell, 2000; Manzoni et al., 2012; Sponseller, 2007). Further, moisture preserves anoxic microhabitats with characteristics that favor the presence and maintenance of methanogenic microbial communities (Dalal et al., 2008; Koschorreck, 2000; Serrano-Silva et al., 2014). Not many studies have discussed the relationship between conductivity and CH_4 production/emission, but some studies have shown a positive correlation between moisture and conductivity (Ekwue & Bartholomew, 2011; Molin & Faulin, 2013), as well as between microbial activity and conductivity (Atekwana et al., 2004). Therefore, the positive correlation between conductivity and CH_4 emission found here (Figure 20 and Table 8) may likely be related to moisture conditions withstanding microbial activity in these biogeochemically active aquatic zones. Finally, the positive correlation between elevation and CH_4 emissions may be associated with the influence of underlying regional-to-local underlying characteristics that are not directly included in the analysis, such as the effect of the surrounding land cover, as well as organic matter composition, microbial community structure of dry sediments, and the timing and history of their atmospheric exposure.

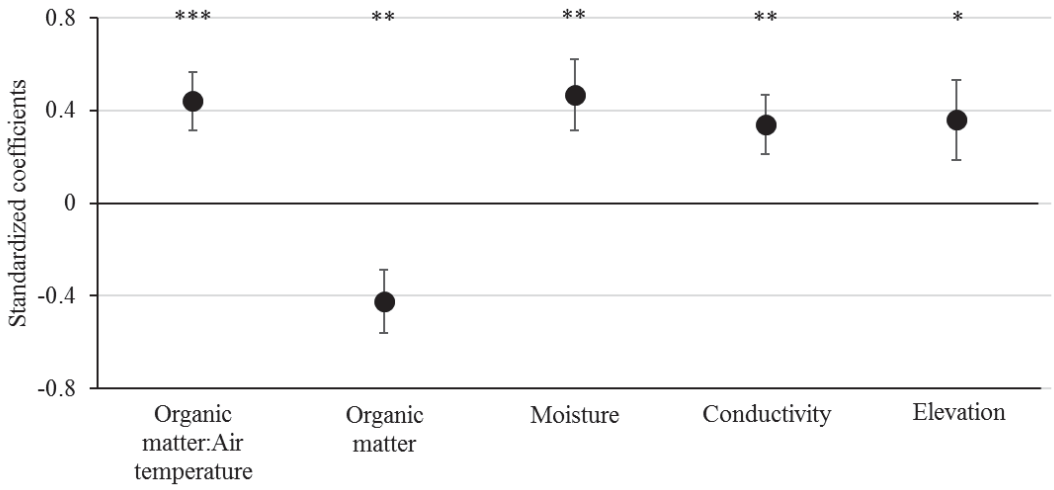

Figure 20: Resulting standardized coefficients (β) and error bars (95% confidence interval) from the generalized linear mixed model (GLMM) describing CH_4 emission from dry inland waters. Variables are shown in decreasing order of significance (analysis of variance, *** $p < 0.001$, ** $p < 0.01$, and * $p < 0.05$). Moisture and elevation data were transformed by cubic root, organic matter content and conductivity were log_{10}-transformed, and all variables were z-transformed before analysis. The colon indicates interaction between the respective variables.

Table 8: Results from the generalized linear mixed model (GLMM). Standardized coefficients (β), 95% confidence intervals (CI), marginal R squared (R^2m), and conditional R squared (R^2c) are reported. Moisture and elevation data were transformed by cubic root, organic matter content, and conductivity were log_{10}-transformed, and all variables were z-transformed before analysis. The colon indicates interaction between the respective variables.

Input variable	**CH_4 flux**	
	β	**CI**
(Intercept)	3.49	18.2 – 58.8
Interaction (Organic matter:Air temperature)	0.44	1.22 – 1.99
Organic matter	-0.42	-0.50 – 0.85
Moisture	0.46	1.18 –2.16
Conductivity	0.34	1.10 –1.81
Elevation	0.36	1.02 –2.01
R^2m		0.20
R^2c		0.55

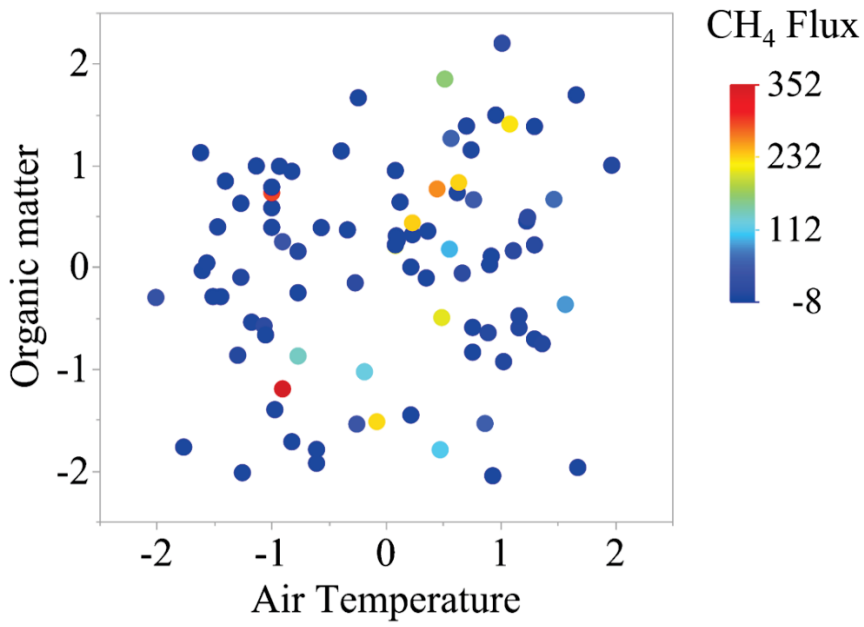

Figure 21: Response of dry inland water CH_4 fluxes to the interaction between organic matter and air temperature (both z-transformed) arising from the generalized linear mixed model (GLMM). Organic matter content (%) was log_{10}-transformed before analysis, and both organic matter and air temperature data (°C) are shown in a z-transformed scale. A factor equal to 13 was added to each CH_4–score in order to exclude negative values from the analysis.

Contribution of CH_4 to the global inland water CO_2-equivalent emissions

Summing dry inland water CO_2 fluxes from Keller et al. (2020) with the CH_4 fluxes presented here (as CO_2-eq) resulted in a global mean emission rate of 9.6 ± 17.4 g CO_2-eq m^{-2} d^{-1} (Figure 22), of which ~14% are attributed to CH_4. Among aquatic systems, reservoirs (12.4 ± 29 g CO_2-eq m^{-2} d^{-1}) and ponds (12.3 ± 11 g CO_2-eq m^{-2} d^{-1}) showed similar global average CO_2-eq emission rates, followed by lakes (9.2 ± 13 g CO_2-eq m^{-2} d^{-1}) and streams (1.1 ± 0.8 g CO_2-eq m^{-2} d^{-1}) (Figure 22). The CH_4 contribution varied from 10% (reservoirs) to 21% (streams) in the total CO_2-eq emissions from dry inland waters (Figure 22).

Upscaling the mean dry inland water CH_4 flux rates from lakes, reservoirs, ponds, and streams according to their respective global surface areas revealed that 3.6 ± 3.5 Tg CH_4 evade to the atmosphere annually (Table 9). That represents approximately 3 ± 3% of the global CH_4 emission estimates that are attributed to water surfaces of lentic and lotic inland waters ecosystems (0.13 Pg y^{-1}) (DelSontro et al., 2018; Stanley et al., 2016). Considering the above CH_4 estimates in the form of CO_2-equivalent emission suggests a global estimate of ~0.11 ± 0.11 Pg CO_2-eq y^{-1} (Table 9), or 0.034 ± 0.032 Pg C-CO_2-eq y^{-1} (where 1 g CH_4 is equivalent to 34 g CO_2-eq) (Clarke et al., 2014). Such estimates are equivalent to ~28 ± 24% of the global CO_2 emission recently reported for dry inland waters (mean ± SD: 0.12 ± 0.13 Pg C y^{-1}) (Keller et al., 2020) (Table 9). Converting global CH_4 emission from exposed sediments to C emission showed that ~2.7 ± 2.6 Tg C y^{-1} (or 0.1 ± 0.1%) would be added to the current global C emission estimates from inland waters (2.1 Pg C y^{-1}) (DelSontro et al., 2018; Raymond et al., 2013; Stanley et al., 2016) (Table 9).

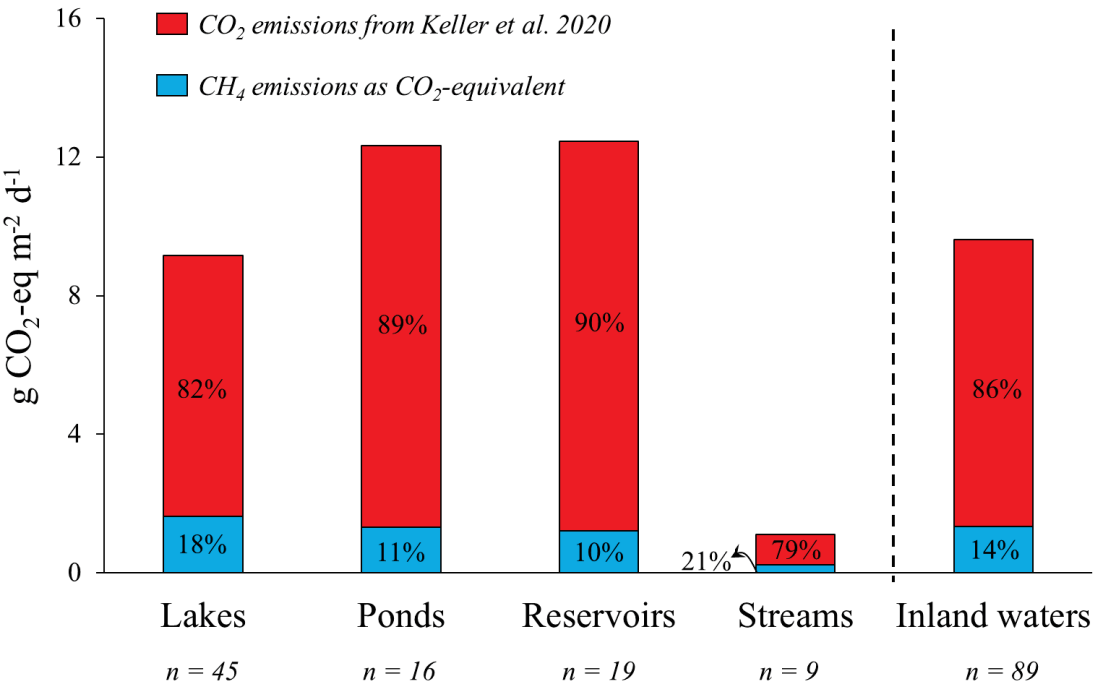

Figure 22: Global average CO_2-equivalent emission rates (CO_2 – red; CH_4 – blue; g CO_2-eq m^{-2} d^{-1}) by dry sediments from different types of aquatic systems (lakes, ponds, reservoirs, and streams). CO_2 emissions were obtained from Keller et al. (2020). CH_4 emissions were converted into CO_2-equivalents by multiplying the mass-based CH_4 flux by 34, according to the 100-year GWP (Clarke et al., 2014). Percentage values represent the contribution of each gas to the global average emission rate in each type of aquatic system.

Table 9: Global average flux rates (± standard deviation; mg m^{-2} d^{-1}) and global estimates of dry inland waters CH_4 emission (Tg y^{-1}, Tg C y^{-1}, Pg CO_2-eq y^{-1}, and Pg C-CO_2-eq y^{-1}) by different types of aquatic systems.

System type	Area of exposed aquatic sediments during one year [a] (km²)	CH_4 emission rate (mg m^{-2} d^{-1})	Global CH_4 emission (Tg y^{-1})	Global CH_4 emission in CO_2 equivalents (Pg CO_2-eq y^{-1})	Global CH_4 emission as C emission (Tg C y^{-1})	Global CH_4 emission in C-CO_2 equivalents (Pg C-CO_2-eq y^{-1})
Lakes and reservoirs	187,542 (Marcé et al., 2019)	44 ± 87	3.1 ± 6	0.1 ± 0.2	2.3 ± 4.5	0.03 ± 0.05
Ponds	18,390 (Marcé et al., 2019)	38 ± 63	0.26 ± 0.4	0.009 ± 0.01	0.2 ± 0.3	0.002 ± 0.004
Streams and rivers	84,461 (Raymond et al., 2013)	7 ± 17	0.21± 0.5	0.007 ± 0.01	0.16 ± 0.4	0.002 ± 0.005
Total	290,393		3.6 ± 3.5	0.11 ± 0.11	2.7 ± 2.6	0.034 ± 0.032

[a] Seasonal and permanent exposure

Implications and future perspectives

This study provides the first global assessment of CH_4 emissions from dry inland waters based on in situ measurements. Dry inland water CH_4 emissions, just as shown previously for CO_2, are also controlled by fundamental drivers prevailing across aquatic systems and climate zones. We found that 14% of the global CO_2-eq emissions from dry inland water can be attributed to CH_4. This is in line with previous studies suggesting that CH_4 emissions from dry sediments of inland waters are relatively low compared to CO_2 emissions (Fromin et al., 2010; Gómez-gener et al., 2015; Koschorreck, 2000; Marcé et al., 2019; Obrador et al., 2018). The present estimates are considered conservative and need to be taken with caution. First, global surface areas attributed to exposed sediments of inland waters are currently considered underestimated (Marcé et al., 2019; Pekel et al., 2016). Second, this study covered a comparatively low spatial within-system resolution. Third, the number of aquatic systems and climate zones that were contemplated here was non-uniformly represented (arid and polar regions were not represented at all, and warm temperate zones were unevenly represented). Fourth, this study does not account for temporal effects on the measurements (e.g. diel cycles, timing and history of exposure). However, a large share of the CH_4 produced in dry inland water sediments has been reported to be oxidized before evasion to the atmosphere (Koschorreck, 2000), making these emissions especially relevant in the first hours or days after overlying water loss (Jin et al., 2016; Koschorreck, 2000; Kosten et al., 2018; Paranaíba et al., 2020). In order to further improve the current knowledge about the dynamics and the role of these highly-active environments (dry inland waters) in the global C cycle, future work needs to address the above-mentioned research gaps. Ultimately, although exposed sediments occupy a varying fraction of the aquatic systems, due to cycles of rising and falling water levels, the predicted increase in the occurrence and intensity of extreme drought events

in different regions of the globe may further exacerbate the global CH_4 and CO_2 emissions from dry inland waters, since that such projections point to increasing atmospheric exposure of large extensions of marginal sediments from aquatic systems worldwide (Pekel et al., 2016; Steward et al., 2012).

Acknowledgments. Thanks to Diego Raymundo do Nascimento for his insightful comments on the data analysis. Thanks to those who provided assistance in fieldworks. In memory of Julia Howitt, who will be missed and always remembered by her colleagues, friends, and family.

References

Aben, R. C. H., Barros, N., Van Donk, E., Frenken, T., Hilt, S., Kazanjian, G., et al. (2017). Cross continental increase in methane ebullition under climate change. Nature Communications, 8(1), 1–8. https://doi.org/10.1038/s41467-017-01535-y

Abril, G., Guérin, F., Richard, S., Delmas, R., Galy-Lacaux, C., Gosse, P., et al. (2005). Carbon dioxide and methane emissions and the carbon budget of a 10-year old tropical reservoir (Petit Saut, French Guiana). Global Biogeochemical Cycles, 19(4), 1–16. https://doi.org/10.1029/2005GB002457

Akinwande, M. O., Dikko, H. G., & Samson, A. (2015). Variance Inflation Factor: As a Condition for the Inclusion of Suppressor Variable(s) in Regression Analysis. Open Journal of Statistics, 05(07), 754–767. https://doi.org/10.4236/ojs.2015.57075

Almeida, R. M., Paranaíba, J. R., Barbosa, Í., Sobek, S., Kosten, S., Linkhorst, A., et al. (2019). Carbon dioxide emission from drawdown areas of a Brazilian reservoir is linked to surrounding land cover. Aquatic Sciences, 81(4), 1–9. https://doi.org/10.1007/s00027-019-0665-9

Atekwana, E. A., Atekwana, E. A., Werkema, D. D., Allen, J. P., Smart, L. A., Duris, J. W., et al. (2004). Evidence for microbial enhanced electrical conductivity in hydrocarbon-contaminated sediments. Geophysical Research Letters, 31, 1–4. https://doi.org/10.1029/2004GL021359

Baldwin, D. S., & Mitchell, A. M. (2000). The effects of drying and re-flooding on the sediment and soil nutrient dynamics of lowland river-floodplain systems: a synthesis. Regulated Rivers: Research & Management, 16(5), 457–467.

https://doi.org/10.1002/1099-1646(200009/10)16:5<457::aid-rrr597>3.3.co;2-2

Bastviken, D., Cole, J., Pace, M., & Tranvik, L. (2004). Methane emissions from lakes: Dependence of lake characteristics, two regional assessments, and a global estimate. Global Biogeochemical Cycles, 18(4), 1–12. https://doi.org/10.1029/2004GB002238

Bastviken, D., Tranvik, L. J., Downing, J. A., Crill, P. M., & Enrich-Prast, A. (2011). Freshwater methane emissions offset the continental carbon sink. Science, 331(6013), 1–2. https://doi.org/10.1126/science.1196808

Beaulieu, J. J., Balz, D. A., Birchfield, M. K., Harrison, J. A., Nietch, C. T., Platz, M. C., et al. (2018). Effects of an Experimental Water-level Drawdown on Methane Emissions from a Eutrophic Reservoir. Ecosystems, 21(4), 657–674. https://doi.org/10.1007/s10021-017-0176-2

Borken, W., & Matzner, E. (2009). Reappraisal of drying and wetting effects on C and N mineralization and fluxes in soils. Global Change Biology, 15(4), 808–824. https://doi.org/10.1111/j.1365-2486.2008.01681.x

Van Cappellen, P., & Maavara, T. (2016). Rivers in the Anthropocene: Global scale modifications of riverine nutrient fluxes by damming. Ecohydrology and Hydrobiology, 16(2), 106–111. https://doi.org/10.1016/j.ecohyd.2016.04.001

Catalán, N., Schiller, D. Von, Marcé, R., Koschorreck, M., Gomez-gener, L., & Obrador, B. (2014). Carbon dioxide efflux during the flooding phase of temporary ponds. Limnetica, 33, 349–360.

Clair, T. A., & Ehrman, J. M. (1996). Variations in Discharge and Dissolved Organic

Carbon and Nitrogen Export from Terrestrial Basins with Changes in Climate : A Neural Network Approach. Limnology and Oceanography, 41(5), 921–927.

Clarke, L. E., Jiang, K., Akimoto, K., Babiker, M., J., B. G., Fisher-Vanden, K., et al. (2014). Chapter 6 Assessing Transformation Pathways. In: Climate Change 2014: Mitigation of Climate Change. Contribution of Working Group III to the Fifth Assessment Report of the Intergovernmental Panel on Climate Change. United Kingdom.

Cole, J. J., Prairie, Y. T., Caraco, N. F., McDowell, W. H., Tranvik, L. J., Striegl, R. G., et al. (2007). Plumbing the global carbon cycle: Integrating inland waters into the terrestrial carbon budget. Ecosystems, 10(1), 171–184. https://doi.org/10.1007/s10021-006-9013-8

Cole, Jonathan J., & Caraco, N. F. (1998). Atmospheric exchange of carbon dioxide in a low-wind oligotrophic lake measured by the addition of SF6. Limnology and Oceanography, 43(4), 647–656. https://doi.org/10.4319/lo.1998.43.4.0647

Dalal, R. C., Allen, D. E., & Livesley, S. J. (2008). Magnitude and biophysical regulators of methane emission and consumption in the Australian agricultural , forest , and submerged landscapes : a review. Plant and SoilSoil, 309, 43–76. https://doi.org/10.1007/s11104-007-9446-7

Dean, W. (1974). Determination of carbonate and organic matter in calcareous sediments and sedimentary rocks by loss on ignition; comparison with other methods. Journal of Sedimentary Research, 44(1), 242–248. https://doi.org/10.1306/74D729D2-2B21-11D7-8648000102C1865D

Dean, W. E., & Gorham, E. (1998). Magnitude and significance of carbon burial in lakes, reservoirs, and peatlands. Geology, 26(6), 535–538. https://doi.org/10.1130/0091-7613(1998)026<0535:MASOCB>2.3.CO;2

Deemer, B. R., Harrison, J. A., Li, S., Beaulieu, J. J., DelSontro, T., Barros, N., et al. (2016). Greenhouse Gas Emissions from Reservoir Water Surfaces: A New Global Synthesis. BioScience, 66(11), 949–964. https://doi.org/https://doi.org/10.1093/biosci/biw117

DelSontro, T., Beaulieu, J. J., & Downing, J. A. (2018). Greenhouse gas emissions from lakes and impoundments: Upscaling in the face of global change. Limnology and Oceanography Letters, 3(3), 64–75. https://doi.org/10.1002/lol2.10073

Deshmukh, C., Guérin, F., Vongkhamsao, A., Pighini, S., Oudone, P., Sopraseuth, S., et al. (2018). Carbon dioxide emissions from the flat bottom and shallow Nam Theun 2 Reservoir: Drawdown area as a neglected pathway to the atmosphere. Biogeosciences, 15(6), 1775–1794. https://doi.org/10.5194/bg-15-1775-2018

Ekwue, E. I., & Bartholomew, J. (2011). Electrical conductivity of some soils in Trinidad as affected by density , water and peat content. Biosystems Engineering, 108(2), 95–103. https://doi.org/10.1016/j.biosystemseng.2010.11.002

FAO - Food and Agriculture Organization of the United States. (n.d.). Definition of soil texture. Retrieved from http://www.fao.org/fishery/static/FAO_Training/FAO_Training/General/x6706e/x6706e06.htm#top

Friedl, G., & Wüest, A. (2002). Disrupting biogeochemical cycles – Consequences of

damming. Aquatic Sciences, 64, 55–65. https://doi.org/10.1016/0025-326x(91)90729-c

Fromin, N., Pinay, G., Montuelle, B., Landais, D., Ourcival, J. M., Joffre, R., & Lensi, R. (2010). Impact of seasonal sediment desiccation and rewetting on microbial processes involved in greenhouse gas emissions. Ecohydrology, 3, 339–348. https://doi.org/10.1002/eco.115

Gallo, E. L., Lohse, K. A., Ferlin, C. M., Meixner, T., & Brooks, P. D. (2014). Physical and biological controls on trace gas fluxes in semi-arid urban ephemeral waterways. Biogeochemistry, 121(1), 189–207. https://doi.org/10.1007/s10533-013-9927-0

Gómez-gener, L., Obrador, B., Schiller, D. Von, Marcé, R., Casas-ruiz, P., Proia, L., et al. (2015). Hot spots for carbon emissions from Mediterranean fluvial networks during summer drought. Biogeochemistry, 125(3), 409–426. https://doi.org/10.1007/s10533-015-0139-7

Granéli, W., Lindell, M., & Tranvik, L. (1996). Photo-oxidative production of dissolved inorganic carbon in lakes of different humic content. Limnology and Oceanography, 41(4), 698–706. https://doi.org/10.4319/lo.1996.41.4.0698

Grasset, C., Mendonça, R., Villamor Saucedo, G., Bastviken, D., Roland, F., & Sobek, S. (2018). Large but variable methane production in anoxic freshwater sediment upon addition of allochthonous and autochthonous organic matter. Limnology and Oceanography, 63(4), 1488–1501. https://doi.org/10.1002/lno.10786

Harrison, J. A., Deemer, B. R., Birchfield, M. K., & O'Malley, M. T. (2017). Reservoir Water-Level Drawdowns Accelerate and Amplify Methane Emission.

Environmental Science and Technology, 51(3), 1267–1277. https://doi.org/10.1021/acs.est.6b03185

Heathcote, A. J., Anderson, N. J., Prairie, Y. T., Engstrom, D. R., & Del Giorgio, P. A. (2015). Large increases in carbon burial in northern lakes during the Anthropocene. Nature Communications, 6, 1–6. https://doi.org/10.1038/ncomms10016

Heilman, M. A., & Carlton, R. G. (2001). Methane oxidation associated with submersed vascular macrophytes and its impact on plant diffusive methane flux. Biogeochemistry, 52(2), 207–224. https://doi.org/10.1023/A:1006427712846

Holgerson, M. A., & Raymond, P. A. (2016). Large contribution to inland water CO2 and CH4 emissions from very small ponds. Nature Geoscience, 9(3), 222–226. https://doi.org/10.1038/ngeo2654

Jin, H., Yoon, T. K., Lee, S.-H., Kang, H., Im, J., & Park, J.-H. (2016). Enhanced greenhouse gas emission from exposed sediments along a hydroelectric reservoir during an extreme drought event. Environmental Research Letters, 11, 1–10. https://doi.org/10.1088/1748-9326/11/12/124003

Keller, P. S., Catalán, N., Schiller, D. von, Grossart, H.-P., Koschorreck, M., Obrador, B., et al. (2020). Global CO2 emissions from dry inland waters share common drivers across ecosystems. Nature Communications, 11(2126), 1–8. https://doi.org/10.1038/s41467-020-15929-y

Kemenes, A., Forsberg, B. R., & Melack, J. M. (2016). Downstream emissions of CH4 and CO2 from hydroelectric reservoirs (Tucurui, Samuel, and Curua-Una) in the Amazon basin. Inland Waters, 6(3), 295–302. https://doi.org/10.5268/IW-6.3.980

Koschorreck, M. (2000). Methane turnover in exposed sediments of an Amazon floodplain lake. Biogeochemistry, 50(2), 195–206. https://doi.org/10.1023/A:1006326018597

Kosten, S., van den Berg, S., Mendonça, R., Paranaíba, J. R., Roland, F., Sobek, S., et al. (2018). Extreme drought boosts CO2 and CH4 emissions from reservoir drawdown areas. Inland Waters, 8(3), 329–340. https://doi.org/10.1080/20442041.2018.1483126

Kottek, M., Grieser, J., Beck, C., Rudolf, B., & Rubel, F. (2006). World Map of the Köppen-Geiger climate classification updated. Meteorologische Zeitschrift, 15(3), 259–263. https://doi.org/10.5194/hess-11-1633-2007

Larned, S. T., Datry, T., Arscott, D. B., & Tockner, K. (2010). Emerging concepts in temporary-river ecology. Freshwater Biology, 55, 717–738. https://doi.org/10.1111/j.1365-2427.2009.02322.x

Lesmeister, L., & Koschorreck, M. (2017). A closed-chamber method to measure greenhouse gas fluxes from dry aquatic sediments. Atmospheric Measurement Techniques, 10(6), 2377–2382. https://doi.org/10.5194/amt-10-2377-2017

Manzoni, S., Schimel, J. P., & Porporato, A. (2012). Responses of soil microbial communities to water stress : results from a meta-analysis. Ecology, 93(4), 930–938. https://doi.org/10.1890/11-0026.1

Marcé, R., Obrador, B., Gómez-Gener, L., Catalán, N., Koschorreck, M., Arce, M. I., et al. (2019). Emissions from dry inland waters are a blind spot in the global carbon cycle. Earth-Science Reviews, 188, 240–248.

https://doi.org/10.1016/j.earscirev.2018.11.012

Mattson, M. D., & Likens, G. E. (1992). Redox reactions of organic matter decomposition in a soft water lake. Biogeochemistry, 19(3), 149–172. https://doi.org/10.1007/BF00000876

Mendonça, R., Müller, R. A., Clow, D., Verpoorter, C., Raymond, P., Tranvik, L. J., & Sobek, S. (2017). Organic carbon burial in global lakes and reservoirs. Nature Communications, 8(1), 1–6. https://doi.org/10.1038/s41467-017-01789-6

Molin, J. P., & Faulin, G. D. C. (2013). Spatial and temporal variability of soil electrical conductivity related to soil moisture. Scientia Agricola, 70(1), 1–5. https://doi.org/https://doi.org/10.1590/S0103-90162013000100001

Obrador, B., Von Schiller, D., Marcé, R., Gómez-Gener, L., Koschorreck, M., Borrego, C., & Catalán, N. (2018). Dry habitats sustain high CO2 emissions from temporary ponds across seasons. Scientific Reports, 8(1), 1–12. https://doi.org/10.1038/s41598-018-20969-y

Paranaíba, J. R., Quadra, G., Josué, I. I. P., Almeida, R. M., Mendonça, R., Cardoso, S. J., et al. (2020). Sediment drying-rewetting cycles enhance greenhouse gas emissions, nutrient and trace element release, and promote water cytogenotoxicity. PLoS ONE, 15(4), 1–21. https://doi.org/10.1371/journal.pone.0231082

Pekel, J., Cottam, A., Gorelick, N., & Belward, A. S. (2016). High-resolution mapping of global surface water and its long-term changes. Nature, 540, 418–422. https://doi.org/10.1038/nature20584

R Core Team. (2018). R: A language and environment for statistical computing. Vienna,

Austria: R Foundation for Statistical Computing. Retrieved from https://www.r-project.org/

Raymond, P. A., Hartmann, J., Lauerwald, R., Sobek, S., McDonald, C., Hoover, M., et al. (2013). Global carbon dioxide emissions from inland waters. Nature, 503(7476), 355–359. https://doi.org/10.1038/nature12760

Rodrigo, A., Recous, S., Neel, C., & Mary, B. (1997). Modelling temperature and moisture effects on C-N transformations in soils: Comparison of nine models. Ecological Modelling, 102(2–3), 325–339. https://doi.org/10.1016/S0304-3800(97)00067-7

von Schiller, D., Marcé, R., Obrador, B., Gómez-Gener, L., Casas-Ruiz, J. P., Acuña, V., & Koschorreck, M. (2014). Carbon dioxide emissions from dry watercourses. Inland Waters, 4(4), 377–382. https://doi.org/10.5268/IW-4.4.746

Serça, D., Deshmukh, C., Pighini, S., Oudone, P., Vongkhamsao, A., Guédant, P., et al. (2016). Nam Theun 2 Reservoir four years after commissioning: significance of drawdown methane emissions and other pathways. Hydroécologie Appliquée, 19, 119–146. https://doi.org/10.1051/hydro/2016001

Serrano-Silva, N., Sarria-Guzmán, Y., Dendooven, L., & Luna-Guido, M. (2014). Methanogenesis and Methanotrophy in Soil : A Review. Pedosphere, 24(3), 291–307. https://doi.org/10.1016/S1002-0160(14)60016-3

Sobek, S., Delsontro, T., Wongfun, N., & Wehrli, B. (2012). Extreme organic carbon burial fuels intense methane bubbling in a temperate reservoir. Geophysical Research Letters, 39(1), 2–5. https://doi.org/10.1029/2011GL050144

Sponseller, R. A. (2007). Precipitation pulses and soil CO2 flux in a Sonoran Desert ecosystem. Global Change Biology, 13, 426–436. https://doi.org/10.1111/j.1365-2486.2006.01307.x

Stallard, R. F. (1998). Terrestrial sedimentation and the carbon cycle: Coupling weathering and erosion to carbon burial. Global Biogeochemical Cycles, 12(2), 231–257. https://doi.org/10.1029/98GB00741

Stanley, E. H., Casson, N. J., Christel, S. T., Crawford, J. T., Loken, L. C., & Oliver, S. K. (2016). The ecology of methane in streams and rivers: patterns, controls, and global significance. Ecological Monographs, 86(2), 146–171.

Steward, A. L., Schiller, D. Von, Tockner, K., Marshall, J. C., Bunn, S. E., Steward, A. L., et al. (2012). When the river runs dry : human and ecological values of dry riverbeds. Frontiers in Ecology and the Environment, 10(4), 202–209. https://doi.org/10.1890/110136

Strom, L., Ekberg, A., Mastepanov, M., & Christensen, T. R. (2003). The effect of vascular plants on carbon turnover and methane emissions from a tundra wetland. Global Change Biology, 9, 1185–1192. https://doi.org/https://doi.org/10.1046/j.1365-2486.2003.00655.x

Tranvik, L. J., Downing, J. A., Cotner, J. B., Loiselle, S. A., Striegl, R. G., Ballatore, T. J., et al. (2009). Lakes and reservoirs as regulators of carbon cycling and climate. Limnology and Oceanography, 54, 2298–2314. https://doi.org/10.4319/lo.2009.54.6_part_2.2298

Yvon-Durocher, G., Allen, A. P., Bastviken, D., Conrad, R., Gudasz, C., St-Pierre, A., et

al. (2014). Methane fluxes show consistent temperature dependence across microbial to ecosystem scales. Nature, 507(7493), 488–491. https://doi.org/10.1038/nature13164

General conclusions

In general, the chapters above have shown the role of aquatic systems in receiving, processing, and transferring organic and inorganic compounds between distinct compartments (e.g. atmospheric and terrestrial compartments) of the biosphere under different circumstances. It was shown that the aquatic environments studied here were active sources of CO_2 and CH_4 emissions to the atmosphere. In addition, the intensity and magnitude of these emissions varied greatly in space (resulting from the heterogeneity of the flooded soils and the internal primary production) and in time (resulting from the variation of inflow waters and OM and nutrient inputs). It was also shown that these emissions are highly influenced by the surrounding terrestrial areas, in which they end up boosting microbial activity by providing organic material for decomposition in the marginal areas of the aquatic environment. The magnitude and the patterns in emissions observed in these marginal aquatic zones suggest a disproportionately important role in total carbon emissions with respect to the area they cover and, therefore, deserves careful attention. Considering the current climate change scenario, changes in precipitation regimes are expected across the globe, which will eventually lead to significant fluctuations in the water level of aquatic ecosystems. Consequently, in addition to impacting the carbon burial process, these changes will further influence the exposure of marginal aquatic sediments to direct contact with the atmosphere, which will result in changes in the current inland waters carbon processing budgets (i.e. burial and emission budgets).

General references

Almeida, R.M., Paranaíba, J.R., Barbosa, Í., Sobek, S., Kosten, S., Linkhorst, A., Mendonça, R., Quadra, G., Roland, F., Barros, N., 2019. Carbon dioxide emission from drawdown areas of a Brazilian reservoir is linked to surrounding land cover. Aquat. Sci. 81, 1–9. https://doi.org/10.1007/s00027-019-0665-9

Barros, N., Cole, J.J., Tranvik, L.J., Prairie, Y.T., Bastviken, D., Huszar, V.L.M., Del Giorgio, P., Roland, F., 2011. Carbon emission from hydroelectric reservoirs linked to reservoir age and latitude. Nat. Geosci. 4, 593–596. https://doi.org/10.1038/ngeo1211

Bastviken, D., Tranvik, L.J., Downing, J.A., Crill, P.M., Enrich-Prast, A., 2011. Freshwater methane emissions offset the continental carbon sink. Science (80-.). 331, 1–2. https://doi.org/10.1126/science.1196808

Birch, H.F., 1958. The effect of soil drying on humus decomposition and nitrogen availability. Plant Soil 10, 9–31. https://doi.org/10.1007/BF01343734

Calmano, W., Förstner, U., 1993. Binding and mobilization of heavy metals in contaminated sediments affected by pH and redox potential. Water Sci. Technol. 28, 223–235. https://doi.org/10.2166/wst.1993.0622

De La Guardia, M., Garrigues, S., 1998. Strategies for the rapid characterization of metals and organic pollutants in solid wastes and contaminated soils by using mass spectrometry. TrAC - Trends Anal. Chem. 17, 263–272. https://doi.org/10.1016/S0165-9936(97)00104-0

Deemer, B.R., Harrison, J.A., Li, S., Beaulieu, J.J., DelSontro, T., Barros, N., Neto,

J.F.B., Powers, S.M., Santos, M.A. dos, Vonk, J.A., 2016. Greenhouse Gas Emissions from Reservoir Water Surfaces: A New Global Synthesis. Bioscience 66, 949–964. https://doi.org/https://doi.org/10.1093/biosci/biw117

DelSontro, T., Beaulieu, J.J., Downing, J.A., 2018. Greenhouse gas emissions from lakes and impoundments: Upscaling in the face of global change. Limnol. Oceanogr. Lett. 3, 64–75. https://doi.org/10.1002/lol2.10073

Di Baldassarre, G., Wanders, N., AghaKouchak, A., Kuil, L., Rangecroft, S., Veldkamp, T.I.E., Garcia, M., van Oel, P.R., Breinl, K., Van Loon, A.F., 2018. Water shortages worsened by reservoir effects. Nat. Sustain. 1, 617–622. https://doi.org/10.1038/s41893-018-0159-0

Eggleton, J., Thomas, K., 2004. A review of factors affecting the release and bioavailability of contaminants during sediment disturbance events. Environ. Int. 30, 973–980. https://doi.org/10.1016/j.envint.2004.03.001

Friedl, G., Wüest, A., 2002. Disrupting biogeochemical cycles – Consequences of damming. Aquat. Sci. 64, 55–65. https://doi.org/10.1016/0025-326x(91)90729-c

Grill, G., Lehner, B., Lumsdon, A.E., Macdonald, G.K., Zarfl, C., Reidy Liermann, C., 2015. An index-based framework for assessing patterns and trends in river fragmentation and flow regulation by global dams at multiple scales. Environ. Res. Lett. 10, 1–15. https://doi.org/10.1088/1748-9326/10/1/015001

Jin, H., Yoon, T.K., Lee, S.-H., Kang, H., Im, J., Park, J.-H., 2016. Enhanced greenhouse gas emission from exposed sediments along a hydroelectric reservoir during an extreme drought event. Environ. Res. Lett. 11, 1–10. https://doi.org/10.1088/1748-

9326/11/12/124003

Josué, I.I.P., Cardoso, S.J., Miranda, M., Mucci, M., Ger, K.A., Roland, F., Marinho, M.M., 2019. Cyanobacteria dominance drives zooplankton functional dispersion. Hydrobiologia 831, 149–161. https://doi.org/10.1007/s10750-018-3710-0

Junior, R.A.M., Mimura, A.M.S., Divino, A.C., Silva, R.F., Silva, J.C.J., Ciminelli, V.S.T., 2014. Levels of Metallic Cations in the Surface Sediments in the Vicinity of the Três Marias Dam Lake (Brazil) Determined by ICP-MS and Microwave Sample Preparation. Soil Sediment Contam. 23, 257–269. https://doi.org/10.1080/15320383.2014.820166

Keller, P.S., Catalán, N., Schiller, D. von, Grossart, H.-P., Koschorreck, M., Obrador, B., Frassl, M.A., Karakaya, N., Barros, N., Howitt, J.A., Mendoza-Lera, C., Pastor, A., Flaim, G., Aben, R., Riis, T., Arce, M.I., Onandia, G., Paranaíba, J.R., Linkhorst, A., Campo, R. del, Amado, A.M., Cauvy-Fraunié, S., Brothers, S., Condon, J., Mendonça, R.F., Reverey, F., Rõõm, E.-I., Datry, T., Roland, F., Laas, A., Obertegger, U., Park, J.-H., Wang, H., Kosten, S., Gómez, R., Feijoó, C., Elosegi, A., Sánchez-Montoya, M.M., Finlayson, C.M., Melita, M., Junior, E.S.O., Muniz, C.C., Gómez-Gener, L., Leigh, C., Zhang, Q., Marcé, R., 2020. Global CO2 emissions from dry inland waters share common drivers across ecosystems. Nat. Commun. 11, 1–8. https://doi.org/10.1038/s41467-020-15929-y

Kosten, S., van den Berg, S., Mendonça, R., Paranaíba, J.R., Roland, F., Sobek, S., Van Den Hoek, J., Barros, N., 2018. Extreme drought boosts CO2 and CH4 emissions from reservoir drawdown areas. Inl. Waters 8, 329–340. https://doi.org/10.1080/20442041.2018.1483126

Maavara, T., Parsons, C.T., Ridenour, C., Stojanovic, S., Dürr, H.H., Powley, H.R., Van Cappellen, P., 2015. Global phosphorus retention by river damming. Proc. Natl. Acad. Sci. 12, 15603–15608. https://doi.org/10.1073/pnas.1511797112

Marcé, R., Obrador, B., Gómez-Gener, L., Catalán, N., Koschorreck, M., Arce, M.I., Singer, G., von Schiller, D., 2019. Emissions from dry inland waters are a blind spot in the global carbon cycle. Earth-Science Rev. 188, 240–248. https://doi.org/10.1016/j.earscirev.2018.11.012

Obrador, B., Von Schiller, D., Marcé, R., Gómez-Gener, L., Koschorreck, M., Borrego, C., Catalán, N., 2018. Dry habitats sustain high CO2 emissions from temporary ponds across seasons. Sci. Rep. 8, 1–12. https://doi.org/10.1038/s41598-018-20969-y

Paranaíba, J.R., Quadra, G., Josué, I.I.P., Almeida, R.M., Mendonça, R., Cardoso, S.J., Silva, J., Kosten, S., Campos, J.M., Almeida, J., Araújo, R.L., Roland, F., Barros, N., 2020. Sediment drying-rewetting cycles enhance greenhouse gas emissions, nutrient and trace element release, and promote water cytogenotoxicity. PLoS One 15, 1–21. https://doi.org/10.1371/journal.pone.0231082

Quadra, G.R., Roland, F., Barros, N., Malm, O., Lino, A.S., Azevedo, G.M., Thomaz, J.R., Andrade-Vieira, L.F., Praça-Fontes, M.M., Almeida, R.M., Mendonça, R.F., Cardoso, S.J., Guida, Y.S., Campos, J.M.S., 2019. Far-reaching cytogenotoxic effects of mine waste from the Fundão dam disaster in Brazil. Chemosphere 215, 753–757. https://doi.org/10.1016/j.chemosphere.2018.10.104

Raymond, P.A., Hartmann, J., Lauerwald, R., Sobek, S., McDonald, C., Hoover, M., Butman, D., Striegl, R., Mayorga, E., Humborg, C., Kortelainen, P., Dürr, H.,

Meybeck, M., Ciais, P., Guth, P., 2013. Global carbon dioxide emissions from inland waters. Nature 503, 355–359. https://doi.org/10.1038/nature12760

Remaili, T.M., Simpson, S.L., Amato, E.D., Spadaro, D.A., Jarolimek, C. V., Jolley, D.F., 2016. The impact of sediment bioturbation by secondary organisms on metal bioavailability, bioaccumulation and toxicity to target organisms in benthic bioassays: Implications for sediment quality assessment. Environ. Pollut. 208, 590–599. https://doi.org/10.1016/j.envpol.2015.10.033

Salomons, W., Forstner, U., 1984. Metals in the hydrocycle., Metals in the hydrocycle. Springer-Verlag Berlin Heidelberg. https://doi.org/10.2307/2403266

Scott, G.R., Sloman, K.A., 2004. The effects of environmental pollutants on complex fish behaviour: Integrating behavioural and physiological indicators of toxicity. Aquat. Toxicol. 68, 369–392. https://doi.org/10.1016/j.aquatox.2004.03.016

St. Louis, V.L., Kelly, C.A., Duchemin, É., Rudd, J.W.M., Rosenberg, D.M., 2000. Reservoir Surfaces as Sources of Greenhouse Gases to the Atmosphere: A Global Estimate. Bioscience 50, 766–775. https://doi.org/10.1641/0006-3568(2000)050[0766:rsasog]2.0.co;2

Stanley, E.H., Casson, N.J., Christel, S.T., Crawford, J.T., Loken, L.C., Oliver, S.K., 2016. The ecology of methane in streams and rivers: patterns, controls, and global significance. Ecol. Monogr. 86, 146–171.

Teodoru, C., Wehrli, B., 2005. Retention of sediments and nutrients in the Iron Gate I Reservoir on the Danube River. Biogeochemistry 76, 539–565. https://doi.org/10.1007/s10533-005-0230-6

Tranvik, L.J., Downing, J.A., Cotner, J.B., Loiselle, S.A., Striegl, R.G., Ballatore, T.J., Dillon, P., Finlay, K., Fortino, K., Knoll, L.B., Kortelainen, P.L., Kutser, T., Larsen, S., Laurion, I., Leech, D.M., Leigh McCallister, S., McKnight, D.M., Melack, J.M., Overholt, E., Porter, J.A., Prairie, Y., Renwick, W.H., Roland, F., Sherman, B.S., Schindler, D.W., Sobek, S., Tremblay, A., Vanni, M.J., Verschoor, A.M., Von Wachenfeldt, E., Weyhenmeyer, G.A., 2009. Lakes and reservoirs as regulators of carbon cycling and climate. Limnol. Oceanogr. 54, 2298–2314. https://doi.org/10.4319/lo.2009.54.6_part_2.2298

Van Cappellen, P., Maavara, T., 2016. Rivers in the Anthropocene: Global scale modifications of riverine nutrient fluxes by damming. Ecohydrol. Hydrobiol. 16, 106–111. https://doi.org/10.1016/j.ecohyd.2016.04.001

von Schiller, D., Marcé, R., Obrador, B., Gómez-Gener, L., Casas-Ruiz, J.P., Acuña, V., Koschorreck, M., 2014. Carbon dioxide emissions from dry watercourses. Inl. Waters 4, 377–382. https://doi.org/10.5268/IW-4.4.746

Vörösmarty, C.J., Sharma, K.P., Fekete, B.M., Copeland, A.H., Holden, J., Marble, J., Lough, J.A., 1997. The storage and aging of continental runoff in large reservoir systems of the world. Ambio 26, 210–219. https://doi.org/10.2307/4314590

Wang, F., Maberly, S.C., Wang, B., Liang, X., 2018. Effects of dams on riverine biogeochemical cycling and ecology. Inl. Waters 8, 130–140. https://doi.org/10.1080/20442041.2018.1469335

Zarfl, C., Lumsdon, A.E., Berlekamp, J., Tydecks, L., Tockner, K., 2015. A global boom in hydropower dam construction. Aquat. Sci. 77, 161–170. https://doi.org/10.1007/s00027-014-0377-0

Contribution to published scientific manuscripts during the Ph.D. studies

- Keller PS, Catalán N, ... ***Paranaíba JR***, ... Marcé R. 2020. Global CO_2 emissions from dry inland waters share common drivers across ecosystems. ***Nature Communications***, 11, 2126, 1-8. **DOI:** 10.1038/s41467-020-15929-y
- Quadra G, Sobek S, ***Paranaíba JR***, Isidorova A, Roland F, do Vale R, Mendonça R. 2020. High organic carbon burial but high potential for methane ebullition in the sediments of an Amazonian reservoir. ***Biogeosciences***, 17, 1495-1505. **DOI:** 10.5194/bg-2019-246
- Silva L, ***Paranaíba JR***, Campo LV, Vieira VA, Sá RC, Guerra MO, Peters VM. 2019. Neonatal development and memory of rat pups treated with *Hypericum perforatum* during pregnancy. ***Journal of Psychiatry and Psychiatric Disorders***, 3, 1-11. **DOI:** 10.26502/jppd.2572-519X0076
- Quadra G, ***Paranaíba JR***, Barros N, Roland F, Amado A. 2019. The limnology challenges in the Anthropocene. ***Acta Limonologica Brasiliensia***, 22, 1-7. **DOI:** 10.1590/S2179-975X5118
- Quadra G, ***Paranaíba JR****, Vilas-Boas J*, Roland F, Amado A, Barros N, Dias R, Cardoso SJ. 2019. A global trend of caffeine consumption over time and related-environmental impacts. ***Environmental Pollution***, 43, 1-6. **contributed equally to the manuscript*. **DOI:** 10.1016/j.envpol.2019.113343
- Quadra G, Silva P, ***Paranaíba JR***, Josué I, Souza H, Costa R, Fernandez M, Vilas-Boas J, Roland F. 2019. Investigation of medicines consumption and disposal in Brazil: A study case in a developing country. ***Science of the Total Environment***, 671, 505-509. **DOI:** 10.1016/j.scitotenv.2019.03.334
- Kosten S, Van den Berg S, Mendonça R, ***Paranaíba JR***, Roland F, Sobek S, Van den Hoek J, Barros N. 2018. Extreme drought boosts CO_2 and CH_4 emissions from

reservoir drawdown areas. ***Inland Waters***, 2, 1-12. **DOI:** 10.1080/20442041.2018.1483126